

HYDRAULICS OF SHALLOW FLOWS OVER STABLE
ERODED SAND SURFACES DEFINED BY AREA SPECTRA

A Thesis

Submitted to the Faculty

of

Purdue University

by

Jack Rider Burney

In Partial Fulfillment of the

Requirements for the Degree

of

Doctor of Philosophy

May 1973

ad. School
rm No. 9
vised

PURDUE UNIVERSITY

Graduate School

This is to certify that the thesis prepared

By Jack Rider Burney

Entitled HYDRAULICS OF SHALLOW FLOWS OVER STABLE ERODED SAND

SURFACES DEFINED BY AREA SPECTRA

Complies with the University regulations and that it meets the accepted standards of the Graduate School with respect to originality and quality

For the degree of:

Doctor of Philosophy

Signed by the final examining committee:

L. J. Higgins, chairman
Louis State

St. Mark

J. W. Keenan

Approved by the head of school or department:

February 2 1973 J. W. Keenan

To the librarian:

~~is~~
This thesis is not to be regarded as confidential

L. J. Higgins
Professor in charge of the thesis

ACKNOWLEDGEMENTS

The author wishes to record his appreciation to the following persons and organizations for their assistance:

Dr. L.F. Huggins for his guidance, encouragement and on many occasions, considerable personal involvement in this project.

Dr. L.J. Cote for assistance in the experimental design and analysis of the data.

Dr. E.J. Monke, Dr. J.W. Delleur and Dr. L.D. Meyer for valuable counsel.

Mr. L. Whaley, electronic technician and Mr. D. Rhine and his workshop staff for assistance in construction of equipment.

Dr. G.W. Isaacs, Head of the Department of Agricultural Engineering for the opportunity to undertake graduate studies at Purdue University.

Professor P.J.C. Vorster, Head of the Department of Agricultural Engineering, Natal University, South Africa for enabling, and the Council of Natal University and the Department of Agricultural Technical Services, South Africa, for granting the necessary period of study leave.

Financial support of this study was provided in part by the United States Department of the Interior as authorized by the Water Resources Act of 1964 and by the Agricultural Experiment Station and the Computer Sciences Center of Purdue University.

TABLE OF CONTENTS

	Page
LIST OF TABLES	v
LIST OF FIGURES	vi
ABSTRACT	viii
CHAPTER I - INTRODUCTION	1
CHAPTER II - HISTORICAL REVIEW	3
Developments in Analysis of Overland Flow	3
Depth-Discharge Relationships	9
Apparatus used in Laboratory Modelling of Overland Flow	13
Micro-relief Measurements	15
CHAPTER III - REVIEW OF THEORY RELATING TO RANDOM SURFACE GEOMETRY	17
Spectral Analysis Model	18
Random Functions of One Variable	18
Random Functions of Two Variables	19
CHAPTER IV - DEVELOPMENT AND USE OF EQUIPMENT	24
Bed Surfaces	24
The Micro-relief Meter	31
Electronic Control of the Micro-relief Meter	34
Error Analysis	36
The Rainfall Simulator	39
Operation of the Rainfall Simulator	41
CHAPTER V - EXPERIMENTAL METHODS, RESULTS AND DISCUSSION	43
Physical Measurements and Area Spectra	43
Collapsed Line Spectra	58
Discussion	59
Hydraulic Tests	66
Hydraulic Regression Model	67
Retention - Slope Relationship	68
Discussion of Recording Errors	68
Discussion of Hydraulic Model	73
CHAPTER VI - SUMMARY AND RECOMMENDATIONS	76

	Page
BIBLIOGRAPHY	78
APPENDICES	85
Appendix A - Calibration of the Micro-relief Meter	85
Voltage-Elevation Calibration of the LVDT	85
Calibration for Effect of Probe Position	88
Appendix B - Operation and Control of the Micro-relief Meter	92
Appendix C - Calibration of the Rainfall Simulator	95
Bed Load Calibration	95
Mass Runoff Calibration	97
Runoff Rate Calibration	99
Appendix D - Rainfall Simulator Logic Control Program	102
Appendix E - Listing of Computer Program Conv	105
Appendix F - Listing of Area Spectral Density Computer Program	111
Appendix G - Digital Computer Program to Analyze Hydraulic Data	121
Program Listing	121
Sample Output	126
VITA	130

LIST OF TABLES

Table	Page
1. Moments of line spectra	63
2. Hydraulic tests standard errors	72
Appendix	
Table	
A-1. Voltage-elevation calibration data for LVDT	86

LIST OF FIGURES

Figura	Page
1. The rainfall simulator, with the areas of Bed 3 sampled by the micro-relief meter marked	25
2. The micro-relief meter shown in operation on the rainfall simulator bed	25
3. Bed 4 shown with areas sampled by the micro-relief meter marked	30
4. The micro-relief meter	30
5. Detailed view of the probe carriage on the micro-relief meter	32
6. Impulse motor drive mechanism for the cross-carriage	32
7. Schematic diagram of electronic switching circuit used in operation of micro-relief meter (one of four identical circuits)	35
8. Schematic diagram of intermediate link between the LVDT and the analog-hybrid computer	35
9. Error distribution from a sample replication of micro-relief meter readings on Bed 4	37
10. Comparison between error and recorded spectra	38
11. Sample area position 6 on Bed 3	44
12. Sample area position 1 on Bed 4	44
13. One quadrant of the filter spectrum	46
14. Contour diagram for spectrum from quadrant 1, position 6 on Bed 3 (upper left-hand quadrant of sample area shown in Figure 11)	48
15. Contour diagram of spectrum from quadrant 2, position 6 on Bed 3 (upper right-hand quadrant of sample area shown in Figure 11)	49
16. Contour diagram of spectrum of quadrant 3, position 6 on Bed 3 (lower left-hand quadrant of sample area shown in Figure 11)	50
17. Contour diagram for spectrum from quadrant 4, position 6 on Bed 3 (lower right-hand quadrant of sample area shown in Figure 11)	51

Figure	Page
18. Contour diagram for average spectrum from position 6 on Bed 3	52
19. Contour diagram for spectrum from quadrant 1, position 1 on Bed 4 (upper left-hand quadrant of sample area shown in Figure 12)	53
20. Contour diagram for spectrum from quadrant 2, position 1 on Bed 4 (upper right-hand quadrant of sample area shown in Figure 12)	54
21. Contour diagram for spectrum from quadrant 3, position 1 on Bed 4 (lower left-hand quadrant of sample area shown in Figure 12)	55
22. Contour diagram for spectrum from quadrant 4, position 1 on Bed 4 (lower right-hand quadrant of sample area shown in Figure 12)	56
23. Contour diagram for average spectrum from position 1 on Bed 4	57
24. Collapsed downslope line spectra for Bed 3 sample areas	60
25. Collapsed cross-slope line spectra for Bed 3 sample areas	61
26. Collapsed line spectra for Bed 4 sample areas	62
27. Hydraulic test data and model fit for Bed 3	69
28. Hydraulic test data and model fit for Bed 4	70
29. Retention-slope relationship on Bed 3	71
30. Retention-slope relationship on Bed 4	71
 Appendix	
Figure	
A-1. Voltage-elevation calibration sets CA01 and CA02	87
A-2. Contour map showing position displacement below a level plane obtained from calibration set GC1	89
A-3. Contour map showing position displacement below a level plane obtained from calibration set GC2	90
B-1. Logic control circuit for operation of, and recording from, the micro-relief meter	93
C-1. Bed load calibrations	96
C-2. Mass runoff calibrations	98
C-3. Differentiator calibrations	100
D-1. Circuit for control, filtering and recording of hydraulic test data	103

ABSTRACT

Burney, Jack Rider. Ph.D., Purdue University, May 1973. Hydraulics of shallow flows over stable eroded sand surfaces defined by area spectra. Major Professor: Dr. L.F. Huggins.

Estimation of the hydraulic response of a land surface to shallow overland flow is of major concern in the design of flood control and dependent structures in small agricultural watersheds. The problem concerns the necessity for selecting the appropriate depth-discharge relationship, based on visual observation of the physical land surface form. The advent of high speed digital computers has made feasible the rapid generation of runoff hydrographs indicating the effects of man-made changes. However, the reliability of the generated hydrographs is limited to the accuracy of the input information and is particularly sensitive to the overland flow depth-discharge relationship used.

The objectives in this project were to develop, test and evaluate instrumentation for recording the physical configuration of a natural, fallow land surface to include both grain and form effects, and to attempt to relate the information to the hydraulic response of the surface.

Two eroded sand surfaces were allowed to form naturally and then stabilized on a 14 ft. by 7 ft. bed of a rainfall simulator. A micro-relief meter reading elevations at .098 inch spacings over a 23.46 inch square grid was designed, calibrated and used to obtain information on the physical form of each surface. Six sample areas were selected on the first surface tested and three sample areas on the second surface. The recorded data were subjected to area spectral analysis.

The hydraulic tests were run as a factorial design with four levels of rainfall application, four levels of upstream flow application and five slope levels. Two separately randomized replications were run on each of the two surfaces.

The first surface formed from a cement-sand mix and sealed with fibreglas was dominated by large rilling down the center of the bed and presented reduced grain roughness. An improved technique was used in stabilizing the second surface. An erosion pattern was allowed to develop in a layer of sand and the pattern then fixed by saturating the sand with diluted fibreglas laminating resin. The surface retained its form and grain roughness.

The derived spectral surfaces reproduced detail which could be related to characteristic patterns observed in photographs of the sampled areas. All area spectra exhibited ridges perpendicular to the flow direction. In order to condense the information, the area spectra were collapsed into line spectra parallel and perpendicular to the surface slope. Within surface variation in the low frequencies was large and associated with the presence or absence of large rills. However the second surface spectra were consistently flatter than those from the first surface tested.

Regression relationships derived from the hydraulic tests were

$$d = 0.0038 Q^{.517} S^{-.530}$$

for the first surface and,

$$d = 0.0037 Q^{.512} S^{-.297}$$

for the second surface, in which d is detention (ft.) and Q is runoff rate (in./hr.) mid-way down a slope of $S(\%)$.

A relationship, suggested by the results and comparison with previous data is

$$d = 0.004 Q^{.5} S^{-x} \quad x > 0.2$$

in which x increases with increasing channelization and decreasing grain roughness.

CHAPTER I

INTRODUCTION

Prediction of the rate and volume of runoff from land surfaces is of fundamental importance in the design of culverts, soil erosion control structures, reservoirs and drainage systems. The confidence associated with the runoff design estimates substantially affects the selection of a suitable safety factor and consequently the cost of the project.

In nature, rainfall in excess of the vegetation storage capacity, soil infiltration capacity and retention storage, progresses downslope following a myriad of interlinked and ever-changing flow paths. The complexity and scope of the flow pattern precludes consideration of a direct deterministic approach to overland flow characterization based on the micro-relief configuration. For this reason overland flow is generally considered in terms of an average depth of flow and a uniform equation of the Chezy type used to relate depth to discharge. However, in spite of these simplifying assumptions, the engineer is still faced with the dilemma of selecting a suitable hydraulic roughness coefficient based on visual observation of the physical surface condition.

Huggins and Monke (1966) found the hydrograph produced by their simulation model to be particularly sensitive to the magnitude of the hydraulic roughness coefficient when using Manning's formula as a depth-discharge relationship. In addition, research has indicated a wide variation in hydraulic roughness to occur on apparently similar physical surfaces.

The above-mentioned simulation model, of Huggins and Monke (1966), is based on the conceptual sub-division of a small agricultural catchment into a grid of rectangular elements. Within each element the factors affecting runoff are assumed to be spatially constant. The present project was designed to examine the nature of the overland flow

phase within an analogous elemental area and thus forms an integral part of the continuing development of the model.

The basic objectives set in this project were:

- (i) The development of a technique whereby an eroded sand bed could be fixed in surface configuration on the bed of a rainfall simulator for later physical and hydraulic characterization.
- (ii) The design and construction of automated instrumentation to measure elevations, over sample areas of the sand bed, at a sufficiently close spacing to enable grain size roughness to be reflected in the readings.
- (iii) The development of a steady state hydraulic model for each bed incorporating the influence of slope and, rainfall and upstream application rate.
- (iv) Examination of the applicability of using area spectral analysis related to the physical surface form, to develop a measure of hydraulic roughness.

CHAPTER II

HISTORICAL REVIEW

Development of modern theory and analysis of overland flow on undeveloped surfaces may be traced back through advances in four distinct fields of endeavour which intertwined but remained essentially distinct due to computational difficulties in relating theory to practice. These fields are studies relating to the solution of the quasi-linear, partial differential equations of unsteady open channel hydraulics attributed to Barre de Saint Venant, fluid mechanics theory relating bed roughness to flow characteristics, simulated rainfall-runoff studies from small field plots and natural rainfall-runoff from small agricultural watersheds. The theoretical key to overland flow studies lay in the model provided by applying the Saint Venant equations to a plane. Stable solutions to these equations were obtained in the mid 1960's and the simpler kinematic wave approximation was vindicated as being applicable to the vast majority of problems involving overland flow hydrographs.

It is proposed briefly to review the developments which led to present-day acceptance of the kinematic wave approximation as relevant to overland flow hydrograph generation and later to examine more closely the relationship between depth and discharge in terms of commonly used formulae. Finally brief descriptions of apparatus used to obtain overland flow hydrographs in the laboratory and surface micro-elevations will be presented.

Developments in Analysis of Overland Flow

The Saint Venant equations, formulated in the latter half of the

19th Century, are generally presented, for a unit width of channel, in the following manner:

$$\frac{\partial y}{\partial t} + \frac{\partial Q}{\partial x} = q - f \quad (2.1)$$

which represents the continuity equation, or mass balance, and

$$\frac{\partial v}{\partial t} + v \frac{\partial v}{\partial x} + g \frac{\partial y}{\partial x} = g (S_0 - S_f) - \frac{qv}{y} \quad (2.2)$$

which represents the conservation of linear momentum. In the above equations y is the local depth of flow, Q the discharge, q and f the lateral inflow and outflow per unit length of channel, v the velocity, g the gravitational acceleration and S_0 and S_f are respectively the bed and friction slopes. Strelkoff (1969) presents a rigorous derivation of the above two equations including a consideration of the implications of assumptions inherent to their formulation. As stated by Liggett and Woolhiser (1967b), the above equations represent "the most complex formulation of the physics of the problem (of unsteady, non-uniform flow) that can be handled conveniently..."

According to Chow (1959), Massau obtained a trial-and-error solution to the continuity and momentum equations at the turn of the Century. However the method was laborious and did not find general acceptance.

The years following the "dust bowl" conditions of the early 1930's witnessed an upsurge of interest in soil conservation practices and concomitant experimentation using rainfall simulators on small field plots. To facilitate analysis of this experimentation, Horton (1938) presented a theoretical analysis of overland flow in which he related runoff rate, q_s , to detention, D_a , by the relationship,

$$q_s = K D_a^m \quad (2.3)$$

where K and m are parameters usually determined from a log-log plot. Assuming tacitly that detention represents uniform flow depth, m is 5/3 in terms of Manning's equation for turbulent flow and 3 for laminar flow. He further derived an equation for the overland flow hydrograph applicable to a 75 per cent turbulent condition. The

relationship given by equation (2.3) was extensively used in analysing natural runoff from small watersheds, notably by Sharp and Holtan (1942) and Horner and Jens (1943). The latter research workers also considered urban drainage problems, as did Hicks (1944) in extending the work along the same lines. Izzard (1942) instituted an extensive program of overland flow experiments under the combined auspices of the U.S. Dept. of Agriculture and the Highway Research Board in order to obtain urgently needed design data in the fields of soil conservation, highway design and airport construction.

Studies on raindrop terminal velocities, notably by Laws (1941), and on raindrop size distributions by Laws and Parsons (1943), had paralleled extensive research into the design of a nozzle which would adequately reproduce the characteristics of natural rainfall (Parsons, 1943). The Type F nozzle used by Izzard was considered the most adequate rainfall simulation device available, although as reported by Meyer (1958) drop impact energy is less than 65 per cent of that of natural rainfall. Detailed review articles on attempts to simulate natural rainfall are presented by Smith and Wischmeier (1962), Mutchler and Hermsmeier (1965) and Hall (1970).

A preliminary analysis of data from a smooth asphalt pavement surface using Horton's (1938) discharge-detention relationship is reported by Izzard and Augustine (1943).

Keulegan (1944) derived the equations of continuity and momentum specifically in terms of overland flow. He also appears to be the first to have considered the overpressure effect created by raindrop impact. By neglecting terms of small magnitude he derived an approximate equation of motion applicable to overland flow. Izzard (1944) applied Keulegan's equation to data obtained from overland flow on three widely varying surfaces classified as smooth and rough pavement, and turf. His analysis yielded surface profiles and also indicated an increase in the product of the resistance coefficient and Reynold's number with increasing application intensity on the paved surfaces. In a later paper, Izzard (1946) presented a dimensionless hydrograph method for determining the hydrograph of

overland flow taking into account the degree and length of slope and the surface roughness. The comprehensive set of basic data obtained by Izzard on slopes ranging from 0.1 to 4 per cent and plot lengths of 12 ft to 72 ft has been utilized by many research workers, including Morgali and Linsley (1965), Abdel-Razaq, Viessman and Hernandez (1967) and Woolhiser and Liggett (1967), to verify analytically-derived overland flow hydrographs.

Semi-graphical solutions to the Saint Venant equations derived by Escoffier (1950) and Lin (1952) greatly facilitated the analysis of flood waves in open channels, particularly in the presence of appreciable backwater effects, but had no practical application in the solution of overland flow problems. Later work by Isaacson, Stoker and Troesch (1958) in successfully applying an explicit finite differencing scheme, based on the method of characteristics of Massau (Chow, 1959), to a flood routing problem on the Ohio River, provided the necessary impetus for renewed interest in applications of the Saint Venant equations. A comprehensive bibliography on methods used to obtain solutions to forms of the Saint Venant equations is presented by Yevjevich (1960).

The general theory of kinematic waves outlined by Lighthill and Whitham (1955) demonstrated the dominance of the forward characteristic, in the absence of backwater effects, and expounded a theoretical justification for the characterization of overland flow solely in terms of the continuity equation and a depth-discharge relationship. This was substantiated by Iwagaki (1955) who found the simplified kinematic wave approach to adequately represent the flow profile in the case of lateral inflow into a steep channel. However no firm criterion for neglecting the acceleration terms in the momentum equation was available and in general research work on overland flow continued to be based on momentum concepts in varying forms of modification.

Woo (1956) employed a modified form of the Type C rainfall simulator, used extensively by Ellison and Pomerene (1944) in soil splash studies, to obtain direct data on unsteady flow profiles.

Theoretical flow profiles, obtained through application of momentum principles and neglecting raindrop impact effects, were compared to profiles obtained from shallow flow over the rough side of masonite board, with and without added sand grain roughness. According to Woolhiser and Liggett (1967), extensive studies on the mechanics of overland flow were conducted at Stanford University, principally by Richey, Behlke and Liggett during the latter half of the 1950's. The approach centered on solutions to the Saint Venant equations by the method of characteristics.

Chen (1962) employed an implicit finite difference scheme to obtain analytical solutions to the Saint Venant equations in which the effects of raindrop impact were included. Further applications of finite difference schemes to solutions of the continuity and momentum equations were developed by Ragan (1965) for channel flow and Harbaugh (1966) in terms of flow over conceptual model watersheds. Harbaugh's contention that local depth and velocity did not depend on forward points in effect amounted to the adoption of a kinematic wave approach. A detailed study of acceptable methods of finite difference solutions of the Saint Venant equations is presented by Liggett and Woolhiser (1967a) and by Strelkoff (1970).

The simplified kinematic approach of Iwagaki (1955) was extended by Ishihara (1964) to the consideration of flow over a steep grassed plane. Yu and McNown (1964) used an order of magnitude analysis to simplify the momentum equation to a depth-discharge relationship. They found good agreement between analysis and experiment, indicating that the kinematic wave approach was relevant to flatter gradients than originally assumed. Henderson and Wooding (1964) and later Wooding (1965) presented detailed analytical treatments of the kinematic method and derived curves illustrating the build-up and decay of flow profiles on a plane surface. They applied the method of characteristics directly to the continuity equation alone. A solution to the kinematic equations based on a backward finite difference scheme was obtained by Brakensiek (1966,1967).

Woolhiser and Liggett (1967) studied the influence exerted on the rising limb of an overland flow hydrograph by the parameters in a dimensionless form of the continuity and momentum equations. They found that no single dimensionless hydrograph exists and that the effect of neglect of the dynamic terms in the momentum equation influences the shape of the rising limb hydrograph to an extent dependent on the value of a single parameter, k , defined as

$$k = \frac{S_0 L_0}{H_0 F_0^2} \quad (2.4)$$

S_0 and L_0 are respectively the degree and length of slope while H_0 and F_0 are the normal depth and Froude number for equilibrium flow at the downstream end of the flow plane. For values of k greater than 10 very little advantage in accuracy is gained by using the full momentum equation in place of a depth-discharge relationship. Since k is generally much greater than 10 in most practical situations, and virtually all agricultural applications, the kinematic wave approximation is an adequate representation of the overland flow hydrograph. This was substantiated by Foster (1968) in analyzing overland flow from artificial rainfall on short field plots.

Morgali (1970), using Izzard's data in normalized form found the kinematic wave approach to accurately predict the rising portion of the hydrograph until the point of inflection, and to provide an accurate representation of the recession limb.

In summary, application of the Saint Venant equations is only warranted when accurate flood routing is required under conditions in which a backwater effect exists at the downstream end of the control reach. The simpler kinematic wave approximation, which utilizes the continuity equation and a depth-discharge relationship, provides adequate accuracy in other practical situations of unsteady flow, and particularly in relation to flow over natural watershed surfaces as stressed by Overton (1971). Eagleson (1970) presents an excellent treatment of the relative importance of the various terms in the continuity and momentum equations in relation to practical applications.

Depth-Discharge Relationships

In terms of any depth-discharge relationship used, expression of the resistance to flow is of major importance. Equations normally used to define the friction slope are the Darcy-Weisbach, Chezy or Manning formulae originally derived for normal flow. The value of the particular friction factor selected often involves the lumping of most of the unknowns into a single invariant parameter (Chery, 1966) analogous in many ways to the coefficient in the Rational Formula. Furthermore, as pointed out by Ragan (1965), analytically derived flow profiles are particularly sensitive to the value of the friction coefficient. Similar sensitivity to the selection of Manning's "n" was found by Huggins and Monke (1966) and Brakensiek and Onstad (1968) in modelling runoff from small watersheds, and by Foster (1968) in applying the kinematic method to erosion plots. In all instances the value of the friction factor could not be predicted with any degree of certainty a priori. Review articles on depth-discharge relationships in open channels are presented by Chow (1959) and the Task Force Report (1963). In all instances one dimensional flow only is considered.

Theoretical fluid mechanics studies are usually confined to uniform distributions of roughness elements in which roughness heights are considerably less than the depth of flow. Rouse (1965) suggested that, in view of the arbitrary nature of Nikuradse's sand grain roughness, and in the light of experimental evidence, the Karmen-Prandtl equation may be written in the more practical form,

$$\frac{1}{\sqrt{f}} = A \log \frac{R}{DhE} + B \quad (2.5)$$

in which A, D and B are parameters, f is the Darcy-Weisbach coefficient, R the hydraulic radius, h the roughness height and E the exposure parameter defined as the ratio of the area of roughness elements normal to the flow, to the plan area of the surface. For values of E greater than 0.15, E is replaced by (1 - E). Morris (1955) illustrated in a practical manner the concept of increasing flow

resistance caused by an increase in the concentration of roughness elements until wake interference occurs. This stage of maximum roughness has been found to occur in the vicinity of an exposure parameter value of 0.15. O'Loughlin and McDonald (1964) found that the semi-logarithmic relation presented by equation (2.5) produced a good fit for experimentally derived data using different concentrations of 6 in. cubes in a flume. However as the depth of flow decreased to that of the height of the cubes, a marked increase in the resistance over that predicted by the semi-logarithmic relationship occurred. Kundu (1971) similarly found that equation (2.5) did not present a good fit for data obtained from tests in which the depth of flow was of the order of the height of the roughness elements. Other reported attempts to relate bed resistance to its geometry by means of this relationship are those of Vanoni and Hwang (1967) and Annambhotla (1969). Both studies concerned relatively deep flow over dune beds and used a method of sub-division of the Darcy-Weisbach equation advocated by Taylor and Brooks (1962) to separate out the effect of bed form roughness from that of grain roughness. Vanoni and Hwang evaluated roughness height by averaging direct measurements on the "frozen" surface. The exposure parameter was obtained by planimetering photographs of the particular surface. Annambhotla applied statistical analyses to data on bed profiles obtained from the Missouri River, near Omaha, in order to evaluate the exposure parameters and roughness heights. Vanoni and Hwang report that the semi-logarithmic relationship presented a reasonably good fit to their flume-derived data, while Annambhotla obtained a linear trend on semi-log paper although considerable scatter was evident.

The inter-relationship between bed forms and resistance to flow in alluvial channels is discussed by Simons and Richardson (1961). They found that resistance to flow increased markedly through the lower flow regime of ripples and dunes and then decreased but tended to vary appreciably as sediment transport increased toward the smooth bed transition regime. Nordin and Algert (1966) applied spectral analysis to describe the properties of elevation-time and elevation-

distance in the development and movement of dunes in alluvial channels. Their contention that the relationship of bed elevation to distance downstream could be expressed by a second-order Markov process was substantiated by Ashida and Tanaka (1967). However Nordin and Richardson (1968) and Annambhotla (1969) found that, in general, the spectral density did not present a distinct characteristic wave number and that wave lengths in general follow an exponential distribution. Nordin (1968), Squarer (1968) and Annambhotla (1969) found bed elevations to be normally distributed for dunes in flumes and rivers. Annambhotla (1969) further suggests that wave lengths, amplitudes and heights be represented in terms of a gamma probability distribution of which the exponential distribution is a special case. He found dune bed configurations in the Missouri River to differ markedly in character from flume-induced dune beds and a comparative study showed that zero-crossing distance and amplitude analysis was better suited to river data than was spectral analysis.

The most common depth-discharge relationship used in applying various forms of the dynamic or kinematic equations is Manning's equation. However, as pointed out by Chow (1959), the value of "n" varies considerably in natural channels. Ragan (1965) found Manning's "n" derived from uniform flow tests to be a reliable value when later incorporated into the momentum equation, as long as lateral inflow did not exceed base flow. The "n" value required to model unsteady flow increased over that of an equivalent uniform flow depth when lateral inflow exceeded base flow. Harbaugh (1966) analyzed the uniform data obtained by Woo (1956) for shallow laminar flow over the rough side of masonite board and deduced a relationship which indicated a tendency for "n" to increase with decreasing depth on a constant bed slope of 1 per cent. Chow (1959) indicated a similar tendency for river data. Morgali (1970) incorporated the concepts of a variable friction factor, dependent on the flow regime, into a kinematic model for overland flow by relating Manning's "n" to the Reynold's number.

The effect of raindrop impact in creating an increase in flow resistance was noted by Izzard and Augustine (1943) in reference to the so-called "pip", i.e. a momentary increase in discharge which often occurs when the simulated rainfall is instantaneously shut-off. Parsons (1949) noted an increase in detention caused by raindrop impact and Woo (1956) noted that raindrop impact tended to markedly increase the resistance to flow particularly on a rough surface and at low flow depths. Kisisel (1971) found that raindrop impact was a major factor influencing the friction factor for flows over smooth and rough beds. The value of the Darcy-Weisbach friction factor was found to increase with rainfall intensity, with the effect being greatest in the laminar range and on steeper slopes.

Research workers in the field of soil erosion have long recognized the importance of raindrop impact in causing soil detachment and creating turbulence in overland flow. Palmer (1965) determined that the maximum drop impact force occurs when the water depth is equal to the drop diameter.

Parsons (1949) derived an equation relating average depth of flow to runoff rate using the results of an extensive series of tests on small natural plots. This equation was

$$D = 0.0057 K r^{1/3} S^{-0.55} \quad (2.6)$$

in which D represents average depth in inches, K is a surface condition factor, r is runoff rate in inches/hour and S the slope in ft/ft.

Harbaugh (1966) suggested that Manning's "n" be used in the form of a conceptual watershed roughness, viz.,

$$N = W y^x \quad (2.7)$$

where W is a coefficient of watershed roughness made up from the additive effects of variation of Manning's "n" with depth, drop characteristics and variation of drop impact effects with flow depth. The flow depth is denoted by y and x is a parameter.

Kundu (1971) presented a depth-discharge relationship obtained by regression analysis on data from a series of simulated rainfall tests on rough surfaces. The surfaces consisted of combinations of three

sizes of stones glued to an aluminium bed, with the largest particles being of the order of 4 mm in diameter. The distribution of particles on the bed conformed to the Poisson distribution for each group of particle sizes. The model presented was

$$D = 0.0084 Q^{0.36} S^{-0.17} E^{0.72} \quad (2.8)$$

where D is the flow depth in feet and Q the discharge in in./hr midway down a slope of S ft/ft on which the exposure parameter is E.

Apparatus used in Laboratory Modelling of Overland Flow

The first attempts at modelling rainfall-induced overland flow, notably those of Izzard (1942), Hicks (1946) and Parsons (1949), employed Type F nozzles designed for outdoor use in soil erosion studies. A wide range of surfaces from smooth concrete to dense grass sod were tested in tilting flumes. Mamisao (according to Grace and Eagleson, 1966) was the first to attempt the modelling of a prototype watershed basin. He designed a rainfall module with drop forming tubes located on 2½ in. centers supplied by gravity flow and capable of intensities of 1 to 16 in./hr. However the smooth mortar bed surface used to create the model basin tended to inflate the scaled peak discharge rate.

Woo (1956) designed a modified Type C rainfall simulator consisting of a cheesecloth mattress, from the underside of which lengths of yarn were suspended. Spray nozzles directed water on to the top of the mattress and, by controlling the rate of application to the mattress, the rate of drop formation at the ends of the yarn and thus rainfall intensity could be controlled. An even spatial distribution of drop sizes of 4.5 mm in diameter was achieved over a 6½ in. wide by 29 ft long flume, having a masonite bed.

Chery (1966) made a fibreglass model of a gauged prototype basin. Rainfall was simulated by a set of eleven modules, each consisting of a central distribution point from which capillary tubing radiated outward to settings on 2 in. centers. Provision was made for both temporal and spatial control of rainfall intensity. Surface tension effects were particularly severe and little or no runoff occurred if an initially dry bed was used.

Grace and Eagleson (1966b) constructed a model of a prototype paved parking lot based on a set of similitude criteria (Grace and Eagleson, 1966a). The model basin consisted of a layer of Masco cement and plastic latex overlying a vermiculite-aggregate concrete. Although water ran readily off the surface, they cite surface tension effects as a probable source of discrepancy between model and prototype hydrographs. The rainfall simulating device consisted of 25 separate modules each of 1 ft square and having drop formers consisting of 0.0125 in. I.D. stainless steel needles set on 1 in. centers. The apparatus was capable of almost instantaneous variation over 15 intensity settings.

Chow and Harbaugh (1965) conducted an extensive investigation into the design requirements for the most realistic and efficient means of producing artificial rainfall in a laboratory, with allowance for controlled variation in spatial and temporal application. Their basic design consisted of a 2 ft square module with 0.023 in. I.D. drop formers set on 1 in. centers and producing water drops of 3.2 mm diameter. Sets of these modules then permit spatial variation in rainfall. Harbaugh (1966) used a portion of the 40 ft square module set (described by Chow, 1967) to determine the influence of basin shape on the time distribution of the discharge hydrograph. Conceptual basin models were constructed from masonite board with the rough side forming the flow surface.

The basic module design outlined by Chow and Harbaugh (1965) has been used by Black (1970) to study geomorphological effects on hydrographs, Kleisel (1970) for studies on flow over a plane and Smith and Woolhiser (1971) for studies on combined overland flow and infiltration into a soil surface. Modules of this type also form the core of the 14 ft square installation available in the Agricultural Engineering Department at Purdue University and which was used by Das (1970) and Kundu (1971) in studies relating to overland flow over plane rough surfaces.

Micro-relief Measurements

Measurements of the micro-relief of land surfaces have been recorded to obtain quantitative data relating to tillage effectiveness, vibration in off-road vehicles, depression storage and overland flow roughness. The spacing of elevation readings has in turn reflected the intended use.

Kuipers (1957) reported the use of a board on which 20 probe needles were mounted at 10 cm. intervals. Manual readings were taken along a number of surface profiles. Interest was focused on characterizing the effects of tillage operations on soil surface condition. Burwell, Allmoras and Amemiya (1963) developed a three dimensional apparatus, with the same purpose in mind, by mounting Kuipers' board arrangement on a horizontal frame. Manual readings of elevations on a 2 inch square spacing over a 40 inch square area were obtained. Currence and Lovely (1970) automated the recording of height readings, thus enabling a far greater number of readings to be made over a much larger area. Their apparatus consisted of a horizontal frame supporting a laterally moving cross-frame. A single probe moved along the cross-frame with elevation values directly recorded on punched digital computer cards. Height readings accurate to 0.05 inch on a 1 inch square grid over an area of 60 by 80 inches were recorded.

Mitchell (1970) constructed a three dimensional automatic micro-relief meter along similar lines to that of Currence and Lovely (1970), although on a smaller laboratory scale. Elevation readings were recorded on a 1 inch grid over a 3 ft. square area and used to relate surface depression storage to depth.

The use of semi-automatic micro-relief meters to relate physical roughness to hydraulic roughness is reported by Heerman, Wenstrom and Evans (1969) and Merva, Brasee, Schwab and Curry (1970). In each case single profiles were recorded at close intervals as required by hydraulic considerations relating to shallow overland flow. Merva et al (1970) obtained readings at 0.79 inch spacings over distances of 9.98 ft. in grassland, while Heerman et al (1969) recorded elevations

at 0.126 inch spacings along 9.5 ft. sections of irrigation furrows.

An interesting variation on micro-relief measurements is the use of sonar to measure channel bed elevation. Squarer (1968) employed an automatic Sonar device to obtain profiles along a sand bed laboratory flume at a data spacing of 0.02 ft., while Annambotla (1969) used a similar device to record profiles along the bed of the Missouri River at spacings of 1 ft. Unfortunately equipment of this nature is not yet sufficiently developed for uses relating to shallow overland flow.

CHAPTER III

REVIEW OF THEORY RELATING TO RANDOM SURFACE GEOMETRY

Land surface topography is generally characterized by a contour map. While such a definition is applicable to, and an essential prerequisite for engineering construction it does not provide a quantitative measure for relating differing land surface configurations. The field of geomorphology is essentially associated with this latter aspect and such physiographic measures as drainage density, relief ratio and elongation ratio have been extensively used as parameters in hydrologic regression models related to catchment runoff. Strahler (1964) presents a review in this context.

As pointed out by Merva et al (1970), however, a considerable difference exists between the macrorelief and the microrelief of land surfaces. When emphasis is placed on the detailed topography of areas of the order of a few square feet the surface configuration is vastly different to that of a small catchment basin defined by a contour map having, say, a two foot contour interval.

Clearly it is impractical and unrealistic to adopt a deterministic approach and for this reason statistical measures have been used to quantify microrelief characteristics. The most commonly used measure is that of the variance of the elevation values.

In the context of microrelief relating to tillage operations Kuipers (1957) proposed the use of the logarithm of the standard error as a roughness index while Burwell et al (1963) suggested that the standard error itself be used as a roughness index. Currence and Lovely (1970), in the same context, considered five such indices based on the standard error associated with the height values, after removal of combinations of row and column effects.

Heerman et al (1969) found the standard deviation of height readings taken down an irrigation furrow provided a "significant" index of hydraulic roughness.

Merva *et al* (1970), in discussing the applicability of the variance as a roughness index, clearly illustrated that specifying the probability distribution of surface heights along a series of parallel lines as a normal distribution and then calculating the variance over the grid is insufficient to define the surface configuration. This may further be emphasized in one dimension by consideration of two pure sine waves having the same amplitude but different frequencies. A measure of association or autocorrelation between adjacent height values is necessary to provide an adequate quantitative description. Such measures are most meaningfully provided by taking the Fourier transform of the autocorrelation function, i.e. through the techniques of spectral analysis.

It is proposed briefly to review the assumptions implicit in the mathematical model on which the technique of spectral analysis is based, and to further consider the analysis of random functions of one and, later two independent variables. Detailed treatments of random functions of one variable are presented by many authors among whom are Jenkins and Watts (1968). Longuet-Higgins (1957,1962), Kosin, Cote and Bogdanoff (1963) and Cote (1966) present the logical extension of the technique to random functions of two independent variables.

Spectral Analysis Model

Random Functions of One Variable

A discrete series of data values, $d(x)$, having zero mean, may be written as a Fourier series of the form,

$$d(x) = \sum_k (a_k \cos 2\pi f_k x + b_k \sin 2\pi f_k x) \quad (3.1)$$

$$= \sum_k c_k \cos (2\pi f_k x + \sigma_k) \quad (3.2)$$

in which the coefficients a_k and b_k are related to the amplitude c_k and phase σ_k by the relationships,

$$c_k = \sqrt{a_k^2 + b_k^2}, \text{ and } \sigma_k = \tan^{-1} (b_k/a_k). \quad (3.3)$$

Arrangement of the squared amplitude values, c_k^2 , according to the magnitude of the associated frequencies, f_k , then forms the frequency spectrum in discrete deterministic form.

However, in considering stochastic series, in which the values $d(x)$, must be viewed as a random sample from the ensemble of possible values, classical Fourier analysis does not lead to convergence of the coefficients in a statistical sense. It is therefore necessary to use the autocovariance function which, under the appropriate assumptions, enables statistical inferences to be made about the underlying frequency spectrum. In using the autocovariance,

$$\gamma_s = E [d(x) d(x + s)], \quad (3.4)$$

an assumption of stationarity of the series, $d(x)$, is necessary, viz., the value of γ_s , the autocovariance at lag s , is independent of the x origin. A more stringent assumption, viz., that of ergodicity, assumes that the sample averages tend to the ensemble average.

The autocovariance and the frequency spectrum may be shown to be linked by the relationship,

$$\gamma_s = E [c_0^2] + \frac{1}{2} \sum_{k=1}^M E [c_k^2] \cos 2\pi f_k s \quad (3.5)$$

in which the coefficients of the series form the spectrum when arranged according to the magnitude of the f_k values.

Random Functions of Two Variables

The extension of the techniques of spectral analysis to the consideration of random functions of two variables is presented in detail by Kosin, Cote and Bogdanoff (1963). In a later publication (Bogdanoff et al., 1966) the above authors presented a digital computer program to obtain the three-dimensional frequency spectrum. A modified version of this program is presented in Appendix F, and it is proposed to confine the theory presented below to that applicable directly to the operation of the computer program.

In terms of both acquisition and analysis of the basic data, it is convenient to have the independent variables arranged in the form of a

rectangular lattice. It will therefore be assumed that the data is in this form with intervals of Δx and Δy in mutually perpendicular directions.

In the previous section it was assumed, for the sake of simplicity, that the set of data values had zero mean. In practice it is necessary to reduce the data set to zero mean prior to the use of spectral analysis. In addition, very low frequency components, e.g. trends, tend to obscure the form of the spectrum. Denoting the basic data set by $h_{x,y}$ (in which $x = 1, 2, \dots, N_x$ and $y = 1, 2, \dots, N_y$) use of a moving average filter transforms the set to one which conforms to the desired properties. Low frequency effects are however destroyed but the effect of the filter on the higher frequency values in the spectrum may later be removed. The precise effects are a property of the filter used. Denoting the moving average filter by $B_{r,s}$, with properties such that,

$$B_{0,0} + 2 \sum_{\substack{r=-f \\ r \neq 0}}^f \sum_{\substack{s=-\sigma \\ s \neq 0}}^{\sigma} B_{r,s} = 0, \text{ and } B_{r,s} = B_{-r,s} = B_{r,-s} = B_{-r,-s} \quad (3.6)$$

the $h_{x,y}$ values are transformed to $H_{x,y}$ values as below.

$$H_{x,y} = \sum_{r=-f}^f \sum_{s=-\sigma}^{\sigma} B_{r,s} h_{x+r+f, y+s+\sigma} \quad \begin{cases} x = 1, \dots, n_x \\ y = 1, \dots, n_y \\ n_x = N_x - 2f + 1 \\ n_y = N_y - 2\sigma + 1 \end{cases} \quad (3.7)$$

$$\text{for which, } E \left[\frac{1}{n_x n_y} \sum_{x,y} H_{x,y} \right] = 0. \quad (3.8)$$

Assuming stationarity, the autocovariance matrix is then defined as,

$$Y_{a,b} = E [H_{x,y} H_{x+a, y+b}] \quad \begin{cases} a = 1, 2, \dots \\ b = 1, 2, \dots \end{cases} \quad (3.9)$$

in which a and b represent the number of lags in the x and y directions respectively. The true measures of the lags are then $\Delta x a$ and $\Delta y b$ in inch units. Further, the autocovariance $Y_{a,b}$ has properties such that,

$$Y_{0,0} = E [H_{x,y}^2] \geq 0.$$

$$\gamma_{-a,-b} = \gamma_{a,b} \quad (3.10)$$

and, $|\gamma_{a,b}| \leq \gamma_{0,0}$

In practice, for discrete data, the autocovariance estimate is calculated as,

$$\gamma_{a,b} = \frac{1}{(n_x - a)(n_y - b)} \sum_{x=0}^{n_x} \sum_{y=0}^{n_y} H_{x,y} H_{x+a,y+b} \quad (3.11)$$

$$-n_x \leq a \leq n_x, \quad -n_y \leq b \leq n_y$$

The value of the autocovariance at specific lag values may then be viewed as an average, the random part of which decreases with an increase in the number of points. The assumption of ergodicity implies a convergence toward the ensemble average.

The values of n_x and n_y , i.e. the maximum number of lags in the x and y directions, requires selection in order to balance the conflicting attributes of fidelity and stability in the spectrum. A large number of lags leads to greater resolution, i.e. a narrower spectral window, to be explained later, at the expense of an increasingly "noisy" spectrum, as the autocovariance estimates at large lag values are based on a decreasing number of points. In practice, the number of lags is generally selected to lie between 10 and 25 per cent of the number of data points in the applicable direction.

In the case of continuous functions the autocovariance and power spectral density functions form Fourier transform pairs. Denoting the continuous spectral density function by $F(u,v)$ and the continuous autocovariance function by $R(x,y)$,

$$F(u,v) = \iint_{-\infty}^{\infty} e^{-2\pi i(xu+yv)} R(x,y) dx dy \quad (3.12)$$

$$\text{and, } R(x,y) = \iint_{-\infty}^{\infty} e^{2\pi i(xu+yv)} F(u,v) du dv \quad (3.13)$$

The spectral density function $F(u,v)$ has the properties,

$$\begin{aligned}
 F(u,v) &= F(-u,-v), \\
 F(u,v) &\geq 0, \\
 \text{and, } \int_{-\infty}^{\infty} \int_{-\infty}^{\infty} F(u,v) du dv &= R(0,0).
 \end{aligned}
 \tag{3.14}$$

As described by Bogdanoff *et al* (1966), the latter two properties denote the division of the total variance into components at the u, v frequency values, in which the frequencies u and v are parallel to the x and y axes respectively. The power at a particular frequency, (u_{α}, v_{β}) , is applied to an elementary cosine wave, $\cos 2\pi(u_{\alpha}x + v_{\beta}y)$, having crests parallel to the line $u_{\alpha}x + v_{\beta}y = 0$ and a wavelength of $(u_{\alpha}^2 + v_{\beta}^2)^{-\frac{1}{2}}$.

In the practical case, in which the autocovariance is discrete and the data limited, transformation to obtain estimates of the power spectrum requires additional considerations. The discrete power spectral estimate, $f_{\alpha,\beta}$ at frequencies α (x direction) and β (y direction) may be written in general form as

$$\begin{aligned}
 E [f_{\alpha,\beta}] &= \sum_{a=-n_x}^{n_x} \sum_{b=-n_y}^{n_y} w(a,b; \alpha,\beta) Y_{a,b} \\
 &= \sum_{a=-n_x}^{n_x} \sum_{b=-n_y}^{n_y} w(a,b; \alpha,\beta) \int_{-\infty}^{\infty} \int_{-\infty}^{\infty} e^{2\pi i(a\alpha x + b\beta y)} F(u,v) du dv
 \end{aligned}
 \tag{3.15}$$

in which $F(u,v)$ is the continuous spectrum. However, since $F(u,v) = F(-u,-v)$, and rearranging,

$$E [f_{\alpha,\beta}] = \sum_{a=-n_x}^{n_x} \sum_{b=-n_y}^{n_y} w(a,b; \alpha,\beta) \cos 2\pi(a\alpha x + b\beta y) F(u,v) du dv
 \tag{3.17}$$

$$\text{in which, } W(\alpha,\beta; u,v) = \sum_{a=-n_x}^{n_x} \sum_{b=-n_y}^{n_y} w(a,b; \alpha,\beta) \cos 2\pi(a\alpha x + b\beta y)
 \tag{3.18}$$

is the spectral window. The estimate therefore tends ideally to a weighted average of spectral power in the region of (α,β) . The weights are the values of the spectral window which, if perfect, would be a Dirac function at (α,β) . The window cannot however conform to a Dirac function and, in fact, is periodic with period $1/\Delta x$ in the x direction

and $1/\Delta y$ in the y direction. Frequencies greater than the Nyquist frequency of $1/2\Delta x$ and $1/2\Delta y$ are therefore aliased back and confounded into the spectral estimates. Data spacing Δx and Δy should therefore be selected such that the spectral power becomes negligible beyond the Nyquist rectangle.

Assuming $w(a,b; \alpha, \beta)$ to conform to the finite part of the Fourier cosine series of the Dirac function (Cote, 1966),

$$\text{i.e., } w(a,b; \alpha, \beta) = \Delta x \Delta y \cos 2\pi(a\Delta x\alpha + b\Delta y\beta) \quad (3.19)$$

then leads to the calculation of a spectral estimate as,

$$f_{\alpha, \beta}^A = \Delta x \Delta y \sum_{a=-n_x}^{n_x} \sum_{b=-n_y}^{n_y} Y_{a,b} \cos 2\pi(a\Delta x\alpha + b\Delta y\beta) \quad (3.20)$$

where,

$$\frac{-n_x}{(2n_x+1)\Delta x} \leq \alpha \leq \frac{n_x}{(2n_x+1)\Delta x} ,$$

and,

$$\frac{-n_y}{(2n_y+1)\Delta y} \leq \beta \leq \frac{n_y}{(2n_y+1)\Delta y} .$$

The window shape has some undesirable features and the spectral estimates may be improved by smoothing the spectrum. The raw spectrum is commonly smoothed by using a running average 3 by 3 matrix $G_{x,y}$, i.e. the two-dimensional form of the Hanning window, in which

$$G_{x,y} = \epsilon_x \epsilon_y ; \quad \epsilon_0 = 0.54 \text{ and } \epsilon_1 = \epsilon_{-1} = 0.23$$

The filter spectrum may be obtained in a similar manner, and the smoothed spectrum divided by the filter spectrum to obtain a final power spectrum in which the higher frequency effects of the filter are removed.

CHAPTER IV

DEVELOPMENT AND USE OF EQUIPMENT

In terms of physical equipment necessary to satisfy the central objective, three particular areas existed. These areas were firstly, the selection of the bed material and the type of bed form configuration; secondly, equipment to quantify this configuration; and finally, means to apply water to, and to quantify the hydraulic response of, the bed surface.

As previously reported in Chapter II, Das (1970) and Kundu (1971) used a 13.85 ft. square-bed laboratory rainfall simulator to study shallow flow over plane surfaces to which stones of varying sizes had been glued. This existing facility was again used in this study. However, due to the large increase in proposed load on the bed surface, the necessity for reaching over all areas of the bed surface and possible expense in forming desired bed forms, the rainfall simulator was partitioned down the center with only one-half used. The rainfall simulator in partitioned form, is shown in Figure 1.

A micro-relief meter constructed to obtain quantitative data on the physical surface configuration of sample areas of each bed surface is presented in Figure 2.

Bed Surfaces

The desired attributes of the bed surfaces studied were:

- (i) The surface have a form which conformed to a natural fallow land surface.
- (ii) The surface be impermeable to prevent confounding of the results with non-accountable components of infiltration and interflow.
- (iii) The grain roughness be retained.
- (iv) Once formed the surface must retain its configuration i.e. be "frozen" in position.

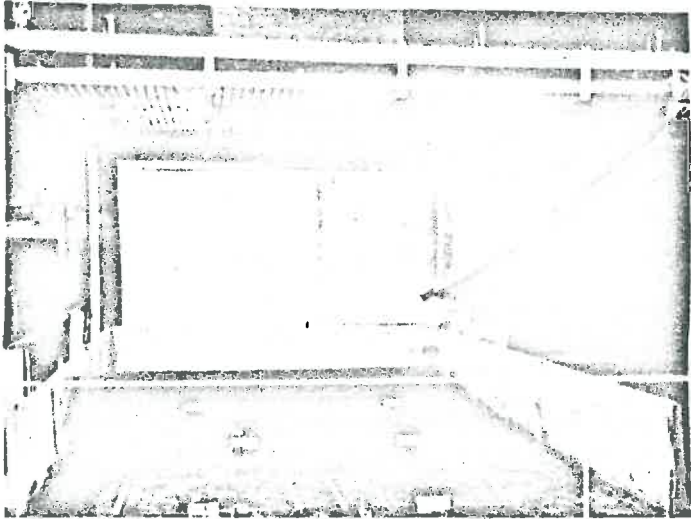


Figure 1. The rainfall simulator, with the areas of Bed 3 sampled by the micro-relief meter marked

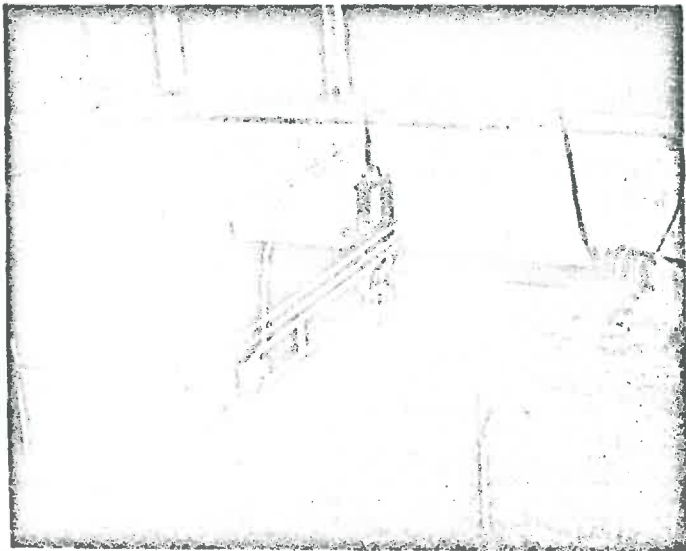


Figure 2. The micro-relief meter shown in operation on the rainfall simulator bed

- (v) It must be possible to reject undesirable surface forms, e.g. rill patterns along a side wall, re-smooth the bed and produce a new bed pattern.
- (vi) It must be possible to obtain the above attributes for a wide range of land forms.
- (vii) The maximum range of bed surface elevations be 1.30 inches. This limitation was imposed by the range of the associated micro-relief meter constructed to map surface elevations and by weight limitations on the bed.

The material selected was a washed sand passing a no. 4 sieve and obtained from Western Indiana Aggregates, West Lafayette, Indiana.

Various methods have been used to fix a soil surface, although generally for different purposes, and no single method appeared directly applicable to the present requirements. Frasier and Myers (1970) used bituminous products to increase runoff from water harvesting catchments while Vanoni and Hwang (1967) used a fufurool polymer to stabilize a sand bed but retain permeability. Fibreglas has been extensively used by Grace and Eagleson (1965), Chery (1966), and Black (1970) among others, to model catchment basins. In general this latter technique has involved the use of a mold over which the fibreglas shell is formed. Foster (1972) has successfully used a similar technique in the field by firstly forming a plaster-of-paris negative over the soil surface and then forming the fibreglas shell from this mold. However grain roughness is generally lost, due to the necessity for using fibreglas mat to strengthen the shell.

In the present study it was considered highly desirable to achieve as natural a surface as was feasible, and to this end a technique was sought whereby the surface could be made both non-erodible and impermeable without unduly disturbing its configuration at the grain size level.

Initial tests considered sample combinations of four water soluble emulsified asphalt products vis. AE-P, AE-60, AE-300 and SS-1 in undiluted, 1:1, 1:2 and 1:6, asphalt: deionised water dilutions. Dilutions of 1:2 of both AE-60 and SS-1 produced good penetration in the sand

material as well as a hard surface. However when subjected to simulated rainfall from a single rainfall module the surface lost its impermeability. A further distinct disadvantage of the emulsified asphalt was the appearance of oil slicks in the applied water and for this reason they were rejected. Two acrylics used extensively in "freezing" soil columns, viz. saran and vinylite exhibited good penetration, dried to hard non-erodible surfaces and appeared relatively impermeable. However as both of these acrylics are only available in powder form and do not readily dissolve in the acetone or methyl-ethyl-keytone solvent there appeared little advantage over using fibreglas diluted with acetone or styrene monomer.

In order to simulate later use, a 1 ft. square tray of wet sand with a form roughened surface was sprayed with a thin coating of surface coat polyester resin, (fibreglas) in a 2:1 (fibreglas:acetone) dilution to fix the surface and prevent slump on drying. After a period of 48 hours, to allow the sand to dry, a mixture of the same solution was applied in bulk to fully saturate the sample. The surface retained its configuration during application, and after 7 days appeared to be both fixed and impermeable. This technique was then accepted and applied to the rainfall simulator bed.

The bed was formed over a layer of polythene sheet used to protect the apparatus from direct contact with the fibreglas additive. The polythene sheet was painted with marine spar varnish and sprinkled with sand to present a rough base. In addition a 1 inch plate was positioned at the downstream end of the bed to retain the sand layer. A $1\frac{1}{2}$ inch layer of sand was carefully levelled and smoothed and both a $6\frac{1}{2}$ in./hr. rainfall and low overland flow rate of approximately 6 in./hr. applied on a 5 per cent slope. However the rainfall tended to distort and obliterate any rill formation which did tend to occur in the short 14 ft. bed length. Consequently the bed was resmoothed and only the overland flow applied. Once a definite rill pattern had developed the whole bed was treated in the manner previously described for the sample. This was designated as Bed 1. Fibreglas tended to pond in certain low areas of rills and slight distortion and cracking

occurred, but not to any great extent. However the bed proved to be highly permeable in places, due to uneven application of fibreglas. Further applications to these areas caused considerable distortion and cracking of the surface and rendered the bed unusable. It was surmised that a single even application of fibreglas was required and a second attempt, Bed 2, was made with careful attention paid to evenness of application and achievement of full saturation. However, after a period of approximately 10 days, considerable uplift occurred in many areas of the bed. The surface top $\frac{1}{8}$ inch cracked and exposed uncured underlying areas.

It appeared that the technique, while eminently successful in a small sample tray, was not possible over a large area, presumably due to a lack of an escape route for the solvent. Since further experimentation obviously required application to the full bed area it was decided to temporarily shelve further attempts at development of this technique.

Bed 3 was produced from a 1:4 mixture of Portland cement : sand mix to obtain a solid bed structure. After a 48 hour drying period, 2 coats of undiluted fibreglas were painted on the surface. An overall view of Bed 3 is presented in Figure 1 and a more detailed illustration of one sampled area (Position 6, in the upper right hand corner) is presented in Figure 12. Bed 3 presented a stable impermeable surface, although finer grain roughness was obliterated. Due to the cement additive the rill formation present prior to first set of the cement had to be accepted. Rill formation tended to be straight up - and - down the slope and the bed was dominated by a relatively large central rill.

Small scale testing to obtain a more desirable method of fixing an erosion pattern in a sand bed continued during the running of tests on Bed 3. A larger, 3 ft. x 4 ft. tray was used to test the techniques which appeared to be promising, since the area-perimeter ratio appeared to be a critical factor. The most promising material still appeared to be a polyester resin (fibreglas) and since clear laminating polyester resin possessed low thixotropic properties, and therefore required less solvent, it was selected for use on Bed 4.

Bed 4 was formed from an initially smooth, 7/8 inch deep, sand layer subjected to an overland flow rate of 6 in./hr. on a 5 per cent slope. An extensive and even diamond shaped rill pattern was obtained and the bed left for 2 hours to drain off excess water. The surface was then sprayed with $\frac{1}{2}$ gal. of a mixture of clear laminating polyester resin and acetone, in the ratio of 2 : 1, following which the bed was left to dry at a 5 per cent slope for a period of 6 days. A mixture of clear laminating polyester resin, diluted with the addition of 5 per cent acetone and 5 per cent styrene monomer plus three times the recommended amount of methyl-ethyl-keytone peroxide hardener was applied at the rate of 1 gallon per 10 sq. ft. to the upper half of the bed. A sprinkling can was used to obtain an even application. The mixture penetrated readily and dried to form a solid mass within 24 hr. As before no perceptible change in surface configuration or grain movement occurred. Some slump and cracking did occur along one edge, evidently due to the added weight on the underlying polythene-sheet which did not fit exactly into the right-angled corner. These cracks were later filled by pouring in a mixture of sand and fibreglas. The remaining lower half of the bed was treated in an identical manner four days later.

Following a further four day drying period the entire bed was sprayed with $\frac{1}{2}$ gallon of surface coat polyester resin having a 5 per cent acetone dilution. Dilution was required in order to obtain flow through the nozzle of the sprayer and also had the advantage of delaying the hardening process sufficiently to enable cleaning of the spray equipment.

Later drilling for insertion of the positioning rods for the micro-relief meter revealed a non-porous crust had formed generally to within about 1/8 in. of the base of the sand layer. Depth of penetration was even but generally less in the finer grained rill material. The bed was not completely impermeable but infiltration, in certain spots where fine cracks may have developed, was extremely slow and not greatly different from the rate of natural evaporation.

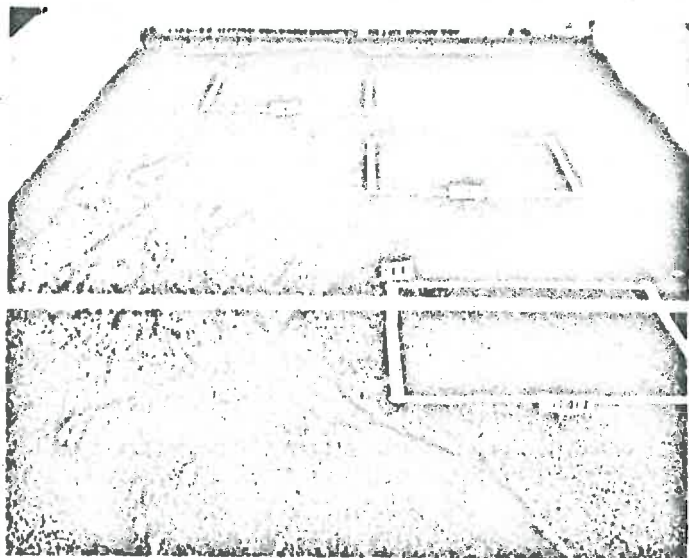


Figure 3. Bed 4 shown with areas sampled by the micro-relief meter marked

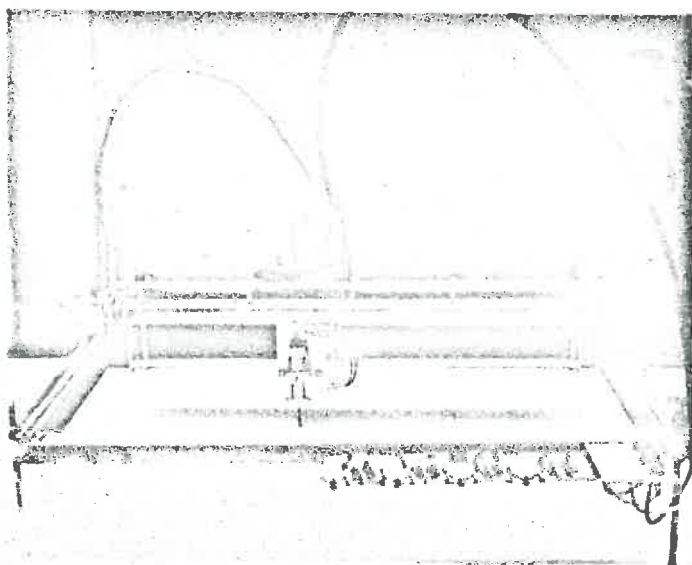


Figure 4. The micro-relief meter

The Micro-relief Meter

The objectives set in the design and construction of the micro-relief meter were the following:

- 1.) The instrument be lightweight for ease of use but sufficiently rugged for possible later outdoor use.
- 2.) The probe be fast acting but provide a minimum of impulse pressure on the surface.
- 3.) Operation and recording be fully automatic with a desired rate of recording of 2 readings per second.

The central sensing mechanism selected was a nominal 1 in. range linear variable differential transformer (LVDT). Basically this instrument consists of a central shaft on which a short iron core is concentrically mounted. A primary coil provides the excitation A.C. voltage which is transmitted by inductance to two secondary coils. The phase difference between the outputs of the secondary coils is proportional to the position of the iron core and, hence the central shaft. This phase shift is transformed into a current output by an ancillary demodulator. Output current is then linearly related to the position of the central shaft over the design range. Response is virtually instantaneous, with continuous resolution.

The method of operation of the LVDT required the instrument to be moved into a vertical position over a level plane with each elevation reading being made by allowing the central shaft to fall under the action of gravity, a reading recorded and provision made for a positive lift prior to moving to the next position. To reduce impulse pressure on the soil surface and to enable a lightweight solenoid to be used for lift, the central shaft of the LVDT was replaced by a 1/8 in., 0.008 in. wall, monel tube. A phonograph needle with a filed down point was silver-soldered into the surface contact end of the tube. The top end of the shaft was then attached, by a slotted lever arm pivoting on a 3/8" O.D., 1/4" I.D. ball bearing on a fixed shaft, to a solenoid. The LVDT, pivot shaft and solenoid were firmly mounted on a 1/8 inch aluminum base plate which formed the probe carriage, shown in Figure 5.

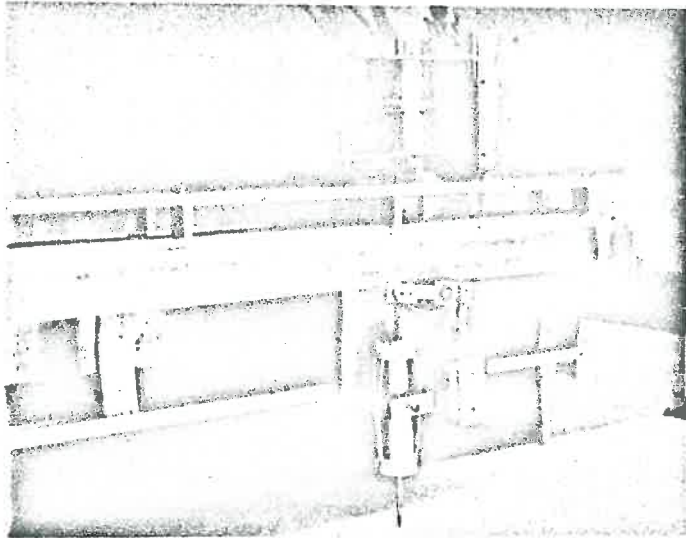


Figure 5. Detailed view of the probe carriage on the micro-relief meter

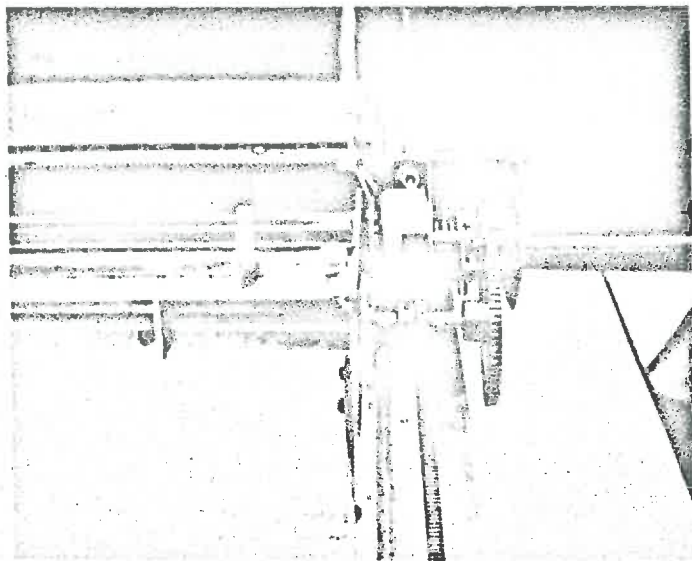


Figure 6, Impulse motor drive mechanism for the cross-carriage

Allowance was made for adjustment of the mechanical advantage by means of slots in the base plate. This enabled a position to be found by trial-and-error in which the probe would fall freely, and positively, under gravity but only produce a light impulse on striking the bed surface. It was further necessary to obtain this fine adjustment as considerations of weight and size necessitated a solenoid with a 1/10 rated duty cycle and a $\frac{1}{2}$ oz. pull at $\frac{1}{2}$ in. extension. Oscilloscope observations indicated the action of the solenoid in retracting the probe from full extension to be the single most limiting restriction on the speed of operation, due to the low duty cycle.

The LVDT mounting plate formed the probe carriage which moved back-and-forth along the cross-carriage. The cross-carriage in turn moved only in one direction, at right-angles to the probe carriage, with a single step movement occurring each time the probe carriage reached an extreme and reversed direction. The cross-carriage was mounted on a square aluminium channel frame, fixed in position by four legs onto the bed surface. The micro-relief meter is presented in Figure 4 and shown in operation in Figure 2.

The cross-carriage consisted of twin back-to-back $1\frac{1}{2}$ x $1\frac{1}{2}$ x $1/8$ inch aluminium angles spaced $\frac{1}{2}$ inch apart through the center of which protruded the LVDT mounting plate, or probe carriage. The probe carriage was supported on the cross-carriage by two $\frac{1}{4}$ in. aluminium axles using $5/8$ in. ball-bearings as wheels. These wheels ran on slotted $\frac{1}{2}$ x $\frac{1}{4}$ in. aluminium flats screwed onto and running the length of the cross-carriage. This provided both vertical and lateral support for the probe carriage. In addition a lower single section of slotted aluminium flat, suspended below the cross-carriage served to hold the probe carriage firmly in position. Cantilever shafts fixed to the bottom of the probe carriage carried $5/8$ in. ball-bearings running in the slotted underside of the suspended section.

A 12-position bi-directional impulse motor was mounted on the top of the probe carriage. The motor shaft was connected to a 32 pitch brass spur gear rack mounted on the cross-carriage by a set of changeable spur-gears. The design gear ratios installed produced a theoretical step of 0.09817 in. per impulse.

The cross-carriage was mounted on the main frame in a similar manner to that previously described for the probe carriage. Again four $5/8$ in. ball-bearings served as wheels and lateral supports. Small teflon blocks attached to the ends and underneath the cross-carriage served to hold the cross-carriage down on the main frame. A 24-position uni-directional impulse motor (shown in Figure 6), mounted at one end of the cross-carriage, served as the stepping mechanism for the cross-carriage. The motor shaft was connected by spur gears, and a drive shaft along the cross-carriage, to spur gear racks attached to the top of the two sides of the main frame. The design gear ratios, which were again changeable, produced a theoretical step of 0.09817 in., i.e. the same spacing as that of the probe carriage.

The main frame itself, consisted of four $1\frac{1}{2}$ x $1\frac{1}{2}$ x $1/8$ in. aluminium angle sections welded to form a 31 in. internal square. The legs were 6 in. lengths of $3/8$ in. aluminium round threaded over the top 3 in. to enable levelling of the micro-relief meter. In later use the legs were replaced by $1/2$ in. stainless steel round to reduce vibration and provide added solidarity.

Detailed procedures used in the calibration of the micro-relief meter are presented in Appendix A.

Electronic Control of the Micro-relief Meter.

Control and operation of the micro-relief meter was effected through direct connection to an analog-hybrid computer. A patched program, presented and described in detail in Appendix B, sequenced and transmitted impulse signals, of 3.6 volts and selected duration, to each of the three impulse motors and the lift solenoid. However, due to the high output impedance of the signal source and the necessity for 24 volt motor operation, the electronic current gain and switching circuit, shown in schematic form in Figure 7, was required as an intermediary between the computer and the motors.

The LVDT primary voltage signal was provided and the output signals converted to a current output by an associated demodulator unit. Conversion of the current output to a floating voltage with low pass filtering was accomplished by the circuit presented in Figure 8. This

voltage signal was conveyed by shielded instrumentation lines to a digital voltmeter in the analog computer and the voltage reading associated with each elevation written on magnetic tape. Each reading consisted of a 6 character field, viz. a sign plus 5 digits representing volts to 4 significant digits. Error analyses associated with the calibration of the micro-relief meter are presented in Appendix A.

Each sampled area consisted of a square grid of 240 by 240 evenly spaced elevation values. The theoretical spacing of individual grid points was 0.09817 inches square giving overall sampled areas of 23.464 inches square.

Error Analysis

Calibration errors associated with measurements obtained by use of the micro-relief meter are presented in Appendix A. However it was also deemed necessary to obtain an estimate of the operational error and to assess its structure.

Following a full test run (position 1 on Bed 4), the cross-carriage was reset in the initial position and the first 20 rows re-recorded. This particular position was selected due to the extreme unevenness of the terrain (as shown in Figure 12), and it was thus considered that such a test would provide an extreme evaluation of recording errors.

Differences between the sets of readings were obtained on a row basis and the average difference, average absolute difference and standard error of the differences associated with each row computed. In addition the sequences of differences from rows 3, 4, 15 and 16 were individually subjected to linear spectral analysis.

The row values obtained are presented graphically in Figure 9 together with the overall values on the ordinate axis. Row standard error values showed no trend and remained close to the overall standard error value of 0.0148 in. The average difference values indicated that the first replication values were generally higher with a slow downward trend occurring through the first ten rows. This effect was probably due to the disturbance of the instrument when manually resetting it prior to running the second replication; it is in the opposite direction to an effect caused by a settling of the instrument.

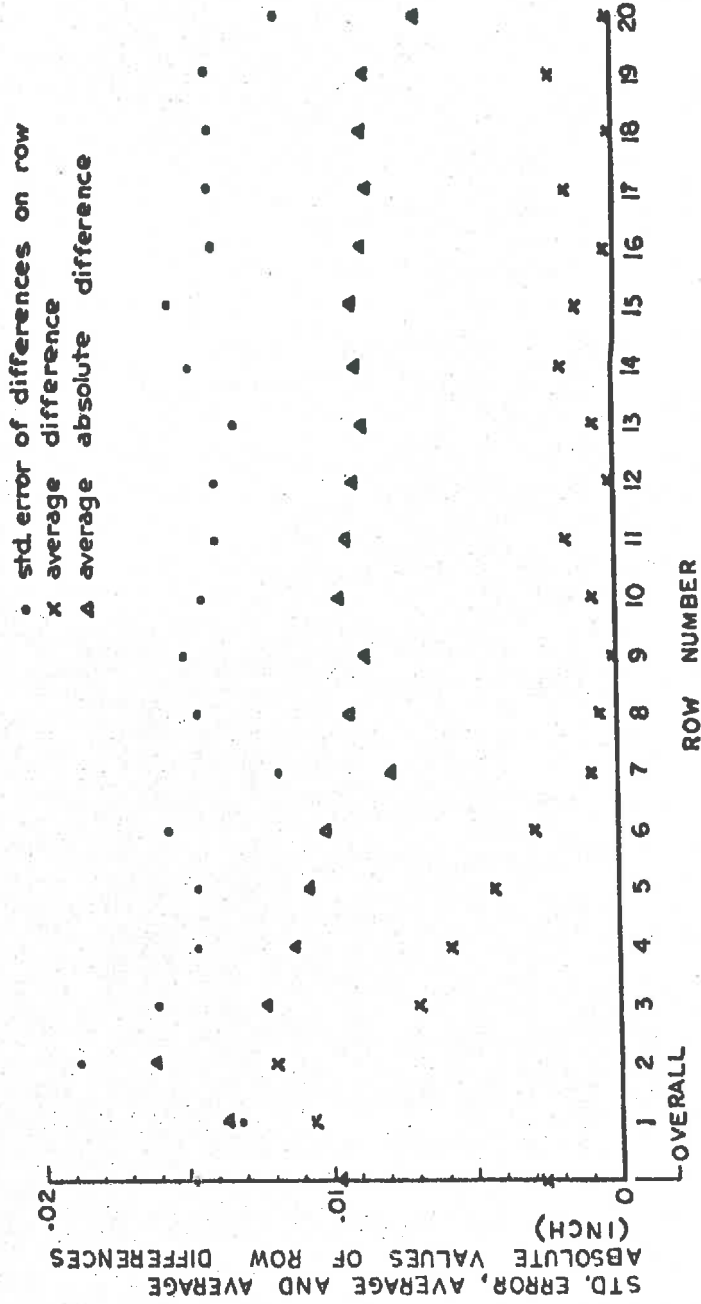


Figure 9. Error distribution from a sample replication of micro-relief meter readings on Bed 4

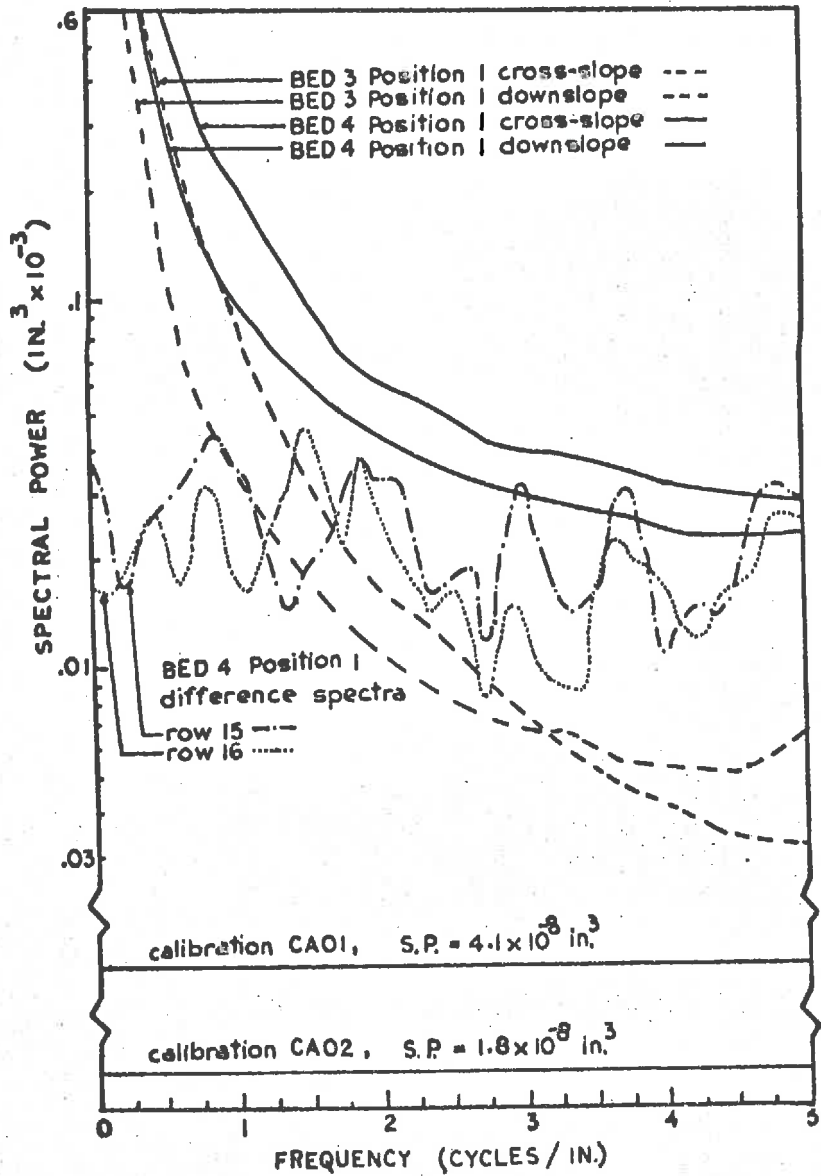


Figure 10. Comparison between error and recorded spectra

or the allowance of an insufficient warm-up period for the demodulator prior to recording.

In general the overall standard error of 0.0148 inches was mainly attributable to the occurrence of a few large difference values of the order of four to six times the standard error. These differences likely occurred in recording on particularly steep-sided sand grains.

Each of the four sampled line spectra exhibited the flat spectrum of a random process and it may safely be assumed that the row difference values possessed no correlations. Recording errors may therefore be assumed to have been evenly distributed over the derived two-dimensional spectra. Two of the four difference spectra are presented in Figure 10. Also presented, for comparison purposes, are the average spectra for Bed 3, position 1, and Bed 4, position 1, collapsed into row spectra.

The Rainfall Simulator

The rainfall simulator has been described in detail by Das (1970) and Kundu (1971) both of whom previously used the same apparatus. For this reason only a brief description of pertinent aspects of the equipment is presented herein.

For the purposes of the present study the 14 ft. square flow bed was divided down the center and only one section (as shown in Figure 1) used. In addition the overland flow pipe, at the upstream end, was sealed off on the unused section and a polythene awning was suspended beneath the rainfall modules to intercept rainfall and return the water directly to the sump.

Basically the rainfall simulator consisted of an outer frame which encompassed, and from which was suspended, a block of rainfall producing modules above a slope adjustable flow bed. A runoff collecting tank was suspended on the outer frame at the downstream end of the flow plane. The block of rainfall modules could be raised, lowered or tilted using four independent electric motors, one of which was located at each corner of the rainfall module frame. The flow plane was suspended from the outer frame on four aluminium rods and could be adjusted to have a

slope of from 0 to .05 ft./ft. Two pairs of strain gauges were mounted on each rod to obtain a temperature-compensated bridge sensitive to axial loads and insensitive to bending. The weighing tank was suspended from the outer frame on two cantilever beams on which pairs of strain gauges were mounted. A constant current power source was used to energise the strain gauges with the Wheatstone bridge network of the flow plane strain gauges serially connected to those of the collecting trough. Two low-level voltage signals were then available, viz. one from the combination of the four flow plane monitoring networks and one from the combined effect of the collecting tank gauges. Each of these two signals were transmitted over shielded lines to instrumentation amplifiers in a remote analog-hybrid computer. The bed load signal was then amplified by a gain factor of 4000 (as shown in the analog section of Figure D-1) and passed through a low-pass filter having a time constant of 1/100 second. The collecting trough signal was amplified by a gain factor of 200 and filtered in the same manner as that of the bed load signal. The above two signals were then available for analog-to-digital conversion on multiplex channels M10 and M8 respectively, and as analog signals on lines 3 and 1 respectively.

The mass runoff signal was also used, after further low-pass filtering through a 1 second time constant filter, as the input to an electronic differentiator. This undesirably heavy filtering was necessitated by the extreme effect of even a small noise-signal ratio in the original signal on its derivative. However, since the main objective was to examine steady-state conditions the time-lag effect created by the filter had little relevance. The derivative, or runoff rate signal, was then available on multiplex channel M9 and Line 2.

Lines 1, 2 and 3 relayed the respective signals back to the laboratory and were used as input to a strip chart recorder. This enabled continuous monitoring during the running of hydraulic tests.

Procedures used in calibrating the bed load, mass runoff and runoff rate signals together with the associated error estimates are presented in Appendix C.

Operation of the Rainfall Simulator

As described in Appendix D, the operation of the rainfall simulator was semi-automatic. Local controls were used to adjust the height of the rainfall modules above the flow plane, change the slope of the flow plane and select the combination of rainfall and overland flow rates pertinent to a particular test.

The computer logic control program which controlled the operation of, and data acquisition from, a particular test is described in detail in Appendix D.

Each of the 49 rainfall modules, of which only half were used in this study, consisted of a 2 ft. square by $1\frac{1}{4}$ in. deep hollow box. Raindrops were formed by 0.023 in. I.D. tubes glued to the underside of each box at $1\frac{1}{4}$ in. centers. The water supply to the boxes was provided from the sump, beneath the rainfall simulator bed via a pump and filter. The supply line then branched into four lines each of which was controlled by a solenoid valve. Each rainfall module was connected to all four supply lines, water entering each module through four nozzles calibrated at 25 lb./sq.in. to produce equivalent intensities of $\frac{1}{2}$, 1, 2 and 4 in./hr. rainfall rates. In addition a non-return valve was located in a corner of each rainfall module with a suction line leading to a vacuum pump. In operation, the rainfall module frame was tilted and air exhausted from the boxes. A particular rainfall rate was selected by activating a combination of the four solenoid valves. Application and cessation of rainfall, controlled by the computer logic program or a local over-ride, was practically instantaneous.

Overland flow was provided by a P.V.C. pipe across the upstream end of the bed and used to simulate an extension of the bed length. Short lengths of $1/8$ in. I.D. brass tubing protruded downwards at 1 in. intervals along the pipe to provide an even application to the upstream end of the flow plane. Water was pumped up to the P.V.C. pipe from the sump. Following the pump, the supply line divided into two branches each of which was controlled by a solenoid valve. Each branch was further controlled by gate valves. One branch contained a single gate

valve while the other branch further sub-divided into two branches, each of which was controlled by a gate valve, one branch having a second gate valve. Selected flow rates of 6, 12 and 18 in./hr. were calibrated using combinations of activating the solenoid valves and fully opening or closing the second gate valve on the one branch line. The remaining three gate valve settings were fixed to give the required flow rates.

CHAPTER V

EXPERIMENTAL METHODS, RESULTS AND DISCUSSION

Physical measurement and hydraulic test data were obtained from each of two bed surfaces, designated Bed 3 (shown in Figure 1) and Bed 4 (shown in Figure 3). As previously indicated (Chapter IV), Bed 3 consisted of an eroded sand-cement bed painted with two coats of surface coat fibreglas. Fine grain roughness was therefore largely obliterated, although as indicated by the sample area presented in Figure 11, the bed surface still retained considerable large grain roughness. Bed 4, made from an eroded sand surface, saturated with fibreglas and sprayed with a light coat of surface coat fibreglas, presented all the roughness features of the original sand surface. A sample area of Bed 4 is presented in Figure 12.

In view of the natural division of the data acquisition and analysis into two sections, viz., the physical characterization and the hydraulic measurements, each section will be considered separately with reference to the inter-relationship.

Physical Measurements and Area Spectra

The micro-relief meter (shown in Figure 2) was run over six sample areas on Bed 3 and three sample areas on Bed 4. The areas sampled on each of the two beds (marked in Figures 1 and 3) were 23.46 inches square with elevation readings taken at intervals of 0.098 inches in two perpendicular directions. All positions, except position 6 on Bed 3, were run with the axes of the sampled grid parallel and perpendicular to the sides of the bed. Position 6 was taken with the cross-carriage of the micro-relief meter at an angle of 45 degrees to the bed slope direction in order to check on the directional influence of errors in recording.

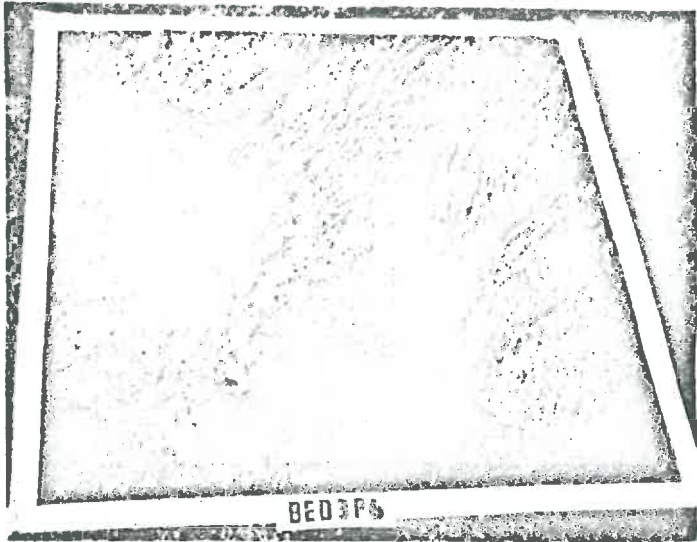


Figure 11. Sample area position 6 on Bed 3

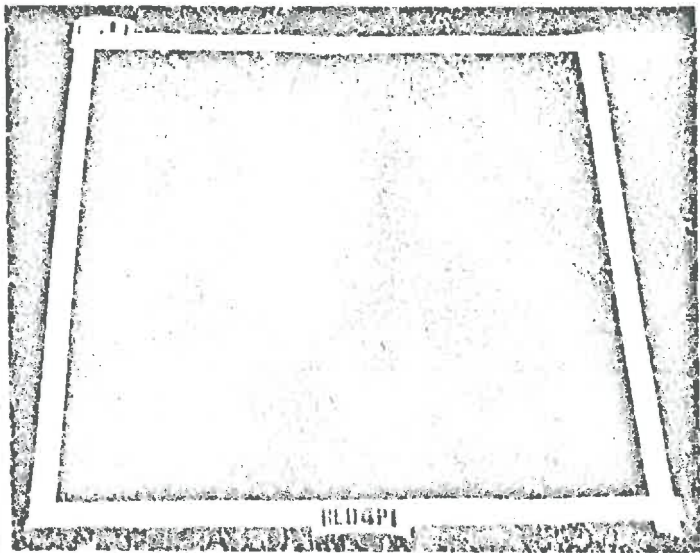


Figure 12. Sample area position 1 on Bed 4

For each sampled area the elevation data was recorded as a voltage reading associated with each grid point, as detailed in Appendix B. The voltage readings were converted to inch readings above an implied level plane using the calibration data presented in Appendix A and a digital computer program, presented in Appendix E. The elevation data were then subjected to area spectral analysis using the digital computer program presented in Appendix F.

In view of the large number of data values collected from each sampled area (57,600 data values in a 240 x 240 matrix, requiring a computer central memory core storage of 176K and a time requirement of approximately 1 hour for executing the program), it was decided to subdivide each sampled area into four (120 x 120) quadrants. The data from each quadrant were separately analyzed and the spectrum of the whole sampled area synthesized by taking an average of the quadrant spectral estimates. In this form each quadrant still required a central memory core allocation of 72K for execution and an execution time of 825 seconds on the Purdue University CDC 6500 digital computer.

A moving average filter (as described in Chapter III) was used to remove trends and limit large-power low-frequency effects in the raw data, and thus decrease round-off errors in the autocovariance matrix computation section of the digital computer program. With reference to equation (3.6) of Chapter III, the selected filter matrix had the properties

$$B_{0,0} = 0.96, B_{r,s} = -0.04 \quad \begin{cases} r = -1, -2, 0, 1, 2 \\ s = -1, -2, 0, 1, 2 \\ r \text{ and } s \text{ not both } 0. \end{cases} \quad (5.1)$$

The spectrum of this filter matrix is symmetrical about the axes. One quadrant of the filter spectrum is presented in Figure 13.

Lag values of $n_x = 20$ and $n_y = 20$ were selected for derivation of all spectra (equation, 3.11).

In accordance with equation (3.20) and the lag selections, a 41 x 41 matrix of spectral estimates was obtained. An approximate degrees of freedom formula for each spectral estimate, presented by Kozin et al (1963), is

$$d.f. = \frac{(n_x - n_x)}{n_x} \frac{(n_y - n_y)}{n_y} \quad (5.2)$$

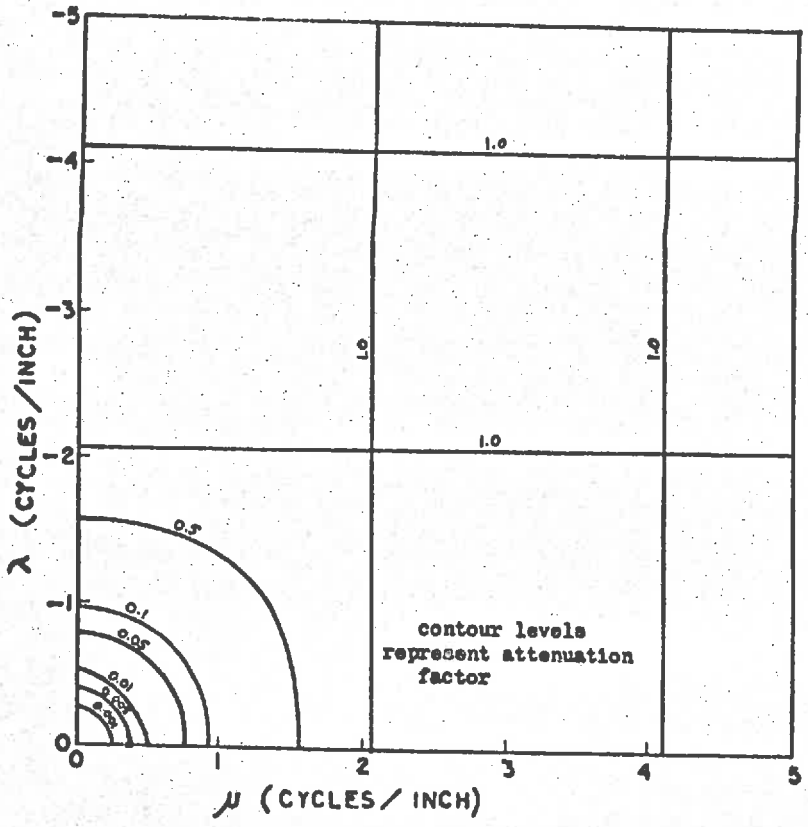


Figure 13. One quadrant of the filter spectrum

where, n_x and n_y are the number of data points in the vertical and horizontal direction in the filtered data matrix. In accordance with equation (3.7), and the magnitude of the filter matrix, n_x and n_y were 117 and the degrees of freedom associated with each spectral estimate of the sample area quadrant spectra was accordingly 23.5.

Confidence limits may be placed on the spectral estimates by use of the relationship of the distribution of the spectral estimates to a χ^2 distribution (Kozin et al, 1963), viz.,

$$P \left[\frac{\nu \bar{f}_{\lambda, \mu}}{\chi^2_{\alpha/2}} < \bar{f}_{\lambda, \mu} < \frac{\nu \bar{f}_{\lambda, \mu}}{\chi^2_{1-\alpha/2}} \right] = 1 - \alpha \quad (5.3)$$

where λ and μ correspond to α and β in Chapter III, α is the probability level and ν is the degrees of freedom. The 95 per cent confidence limits on the individual spectral estimates are accordingly 0.618 and 1.96 times their value. Using the large sample normal distribution approximation to the χ^2 distribution, an averaged area spectral estimate, having 94 degrees of freedom, has 95 per cent confidence limits of 0.875 and 1.17 times its value.

Spectral contour maps were obtained on a Calcomp plotter for each quadrant spectrum and for the average spectrum of each sample area, using a contour mapping program presented by Turner (1969). Sample plots are presented in Figures 14 through 23.

The area spectra obtained from each quadrant of the sampled areas shown in Figures 11 and 12 are presented in Figures 14 through 17 and Figures 19 through 22 respectively. The average spectrum for each position is presented in Figures 18 and 23. In all instances the spectral contour levels shown have units of $\text{in.}^2/(\text{cycle per in.})^2$.

The spectra from all nine sampled areas were generally elliptical in shape in the lower frequencies with the major axes of the ellipses being approximately perpendicular to the flow or bed slope direction indicating a dominance of rilling down the bed slope. In the higher frequencies the effects of instrumentation errors, aliasing and the natural randomness of the grain roughness combined to create nearly circular contours.

SPECTRAL CONTOURS FOR BED3P6Q1

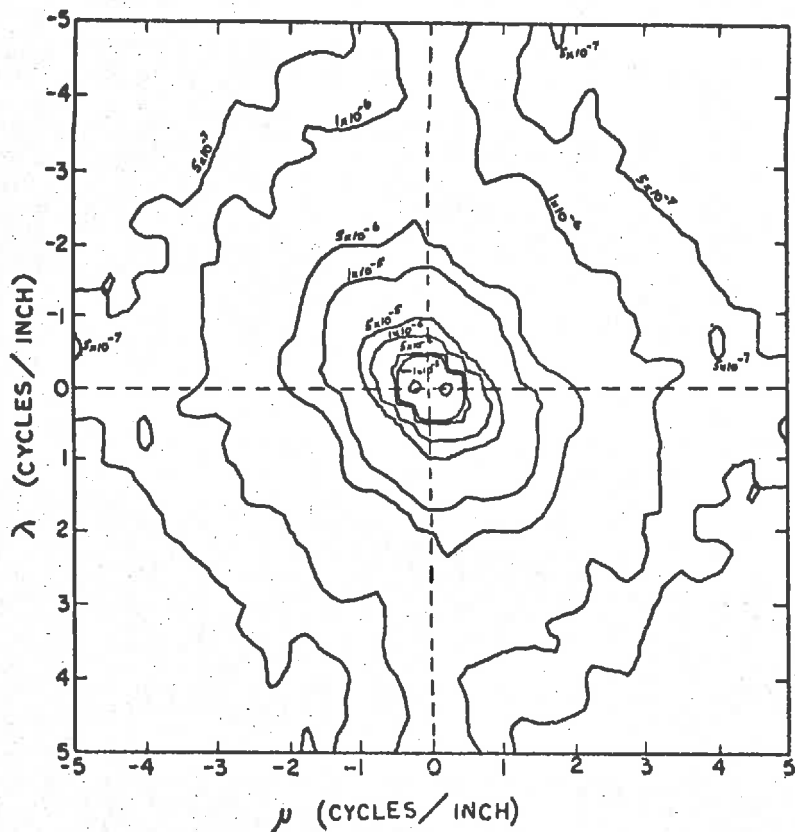


Figure 14. Contour diagram for spectrum from quadrant 1, position 6 on Bed 3 (upper left-hand quadrant of sample area shown in Figure 11)

SPECTRAL CONTOURS FOR BED3P6Q2

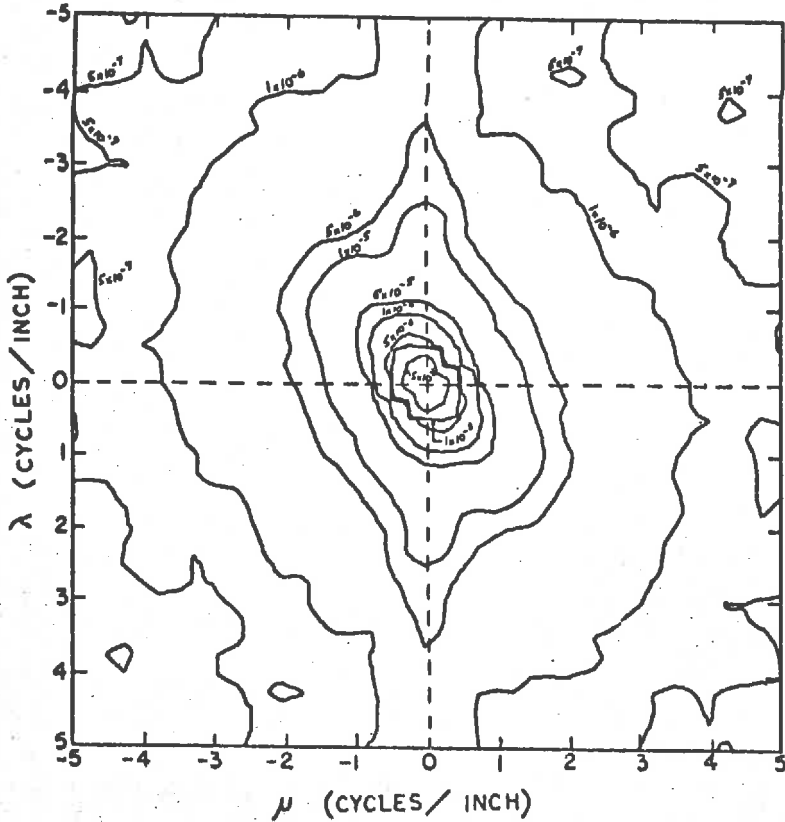


Figure 15. Contour diagram of spectra from quadrant 2, position 6 on Bed 3 (upper right-hand quadrant of sample area shown in Figure 11)

SPECTRAL CONTOURS FOR BED3P6Q3

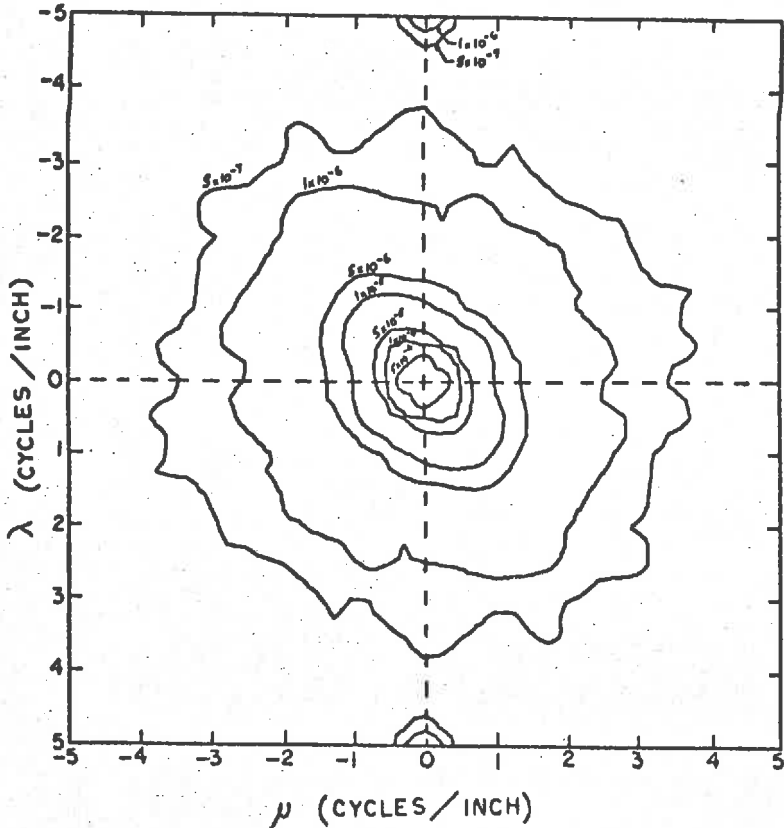


Figure 16. Contour diagram of spectrum of quadrant 3, position 6 on Bed 3 (lower left-hand quadrant of sample area shown in Figure 11)

SPECTRAL CONTOURS FOR BED3P6Q4

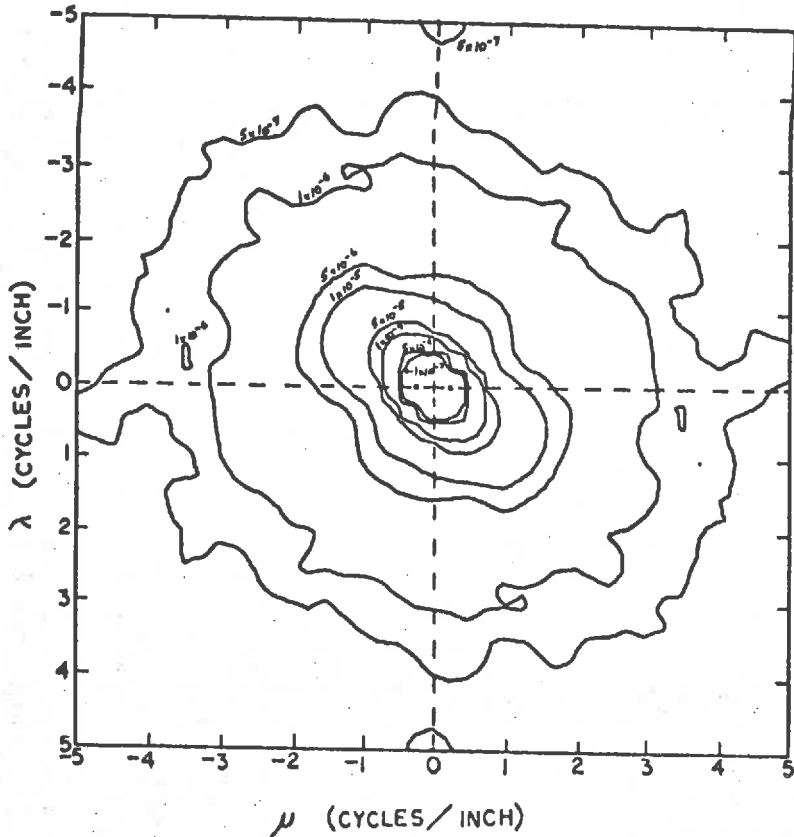


Figure 17. Contour diagram for spectrum from quadrant 4, position 6 on Bed 3 (lower right-hand quadrant of sample area shown in Figure 11)

SPECTRAL CONTOURS FOR BED3P6AV

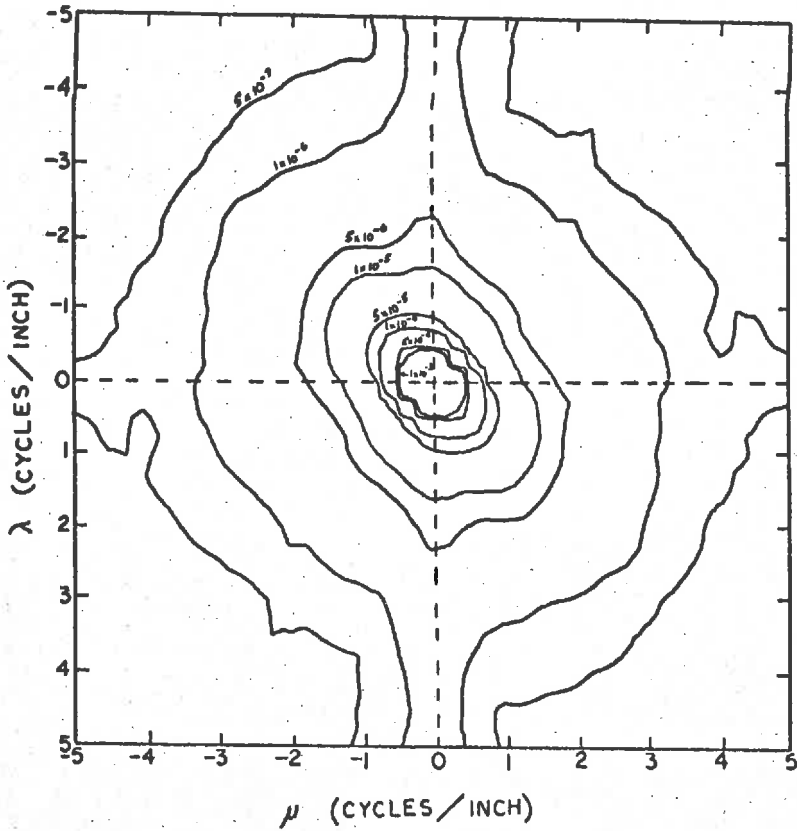


Figure 18. Contour diagram for average spectrum from position 6 on Bed 3

SPECTRAL CONTOURS FOR BED4P1Q1

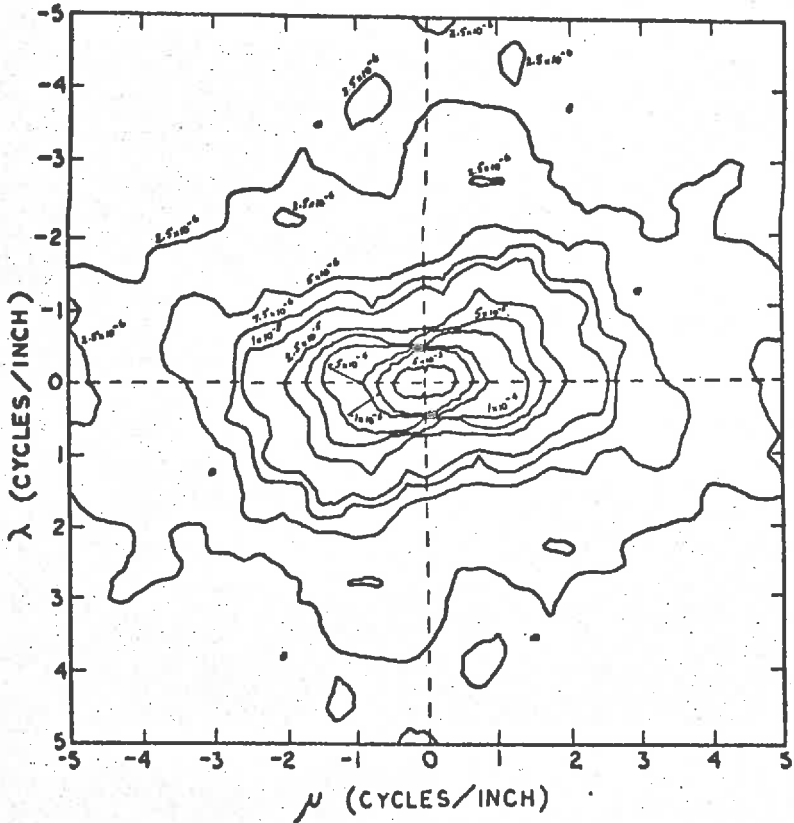


Figure 19. Contour diagram for spectrum from quadrant 1, position 1 on Bed 4 (upper left-hand quadrant of sample area shown in Figure 12)

SPECTRAL CONTOURS FOR BED4P102

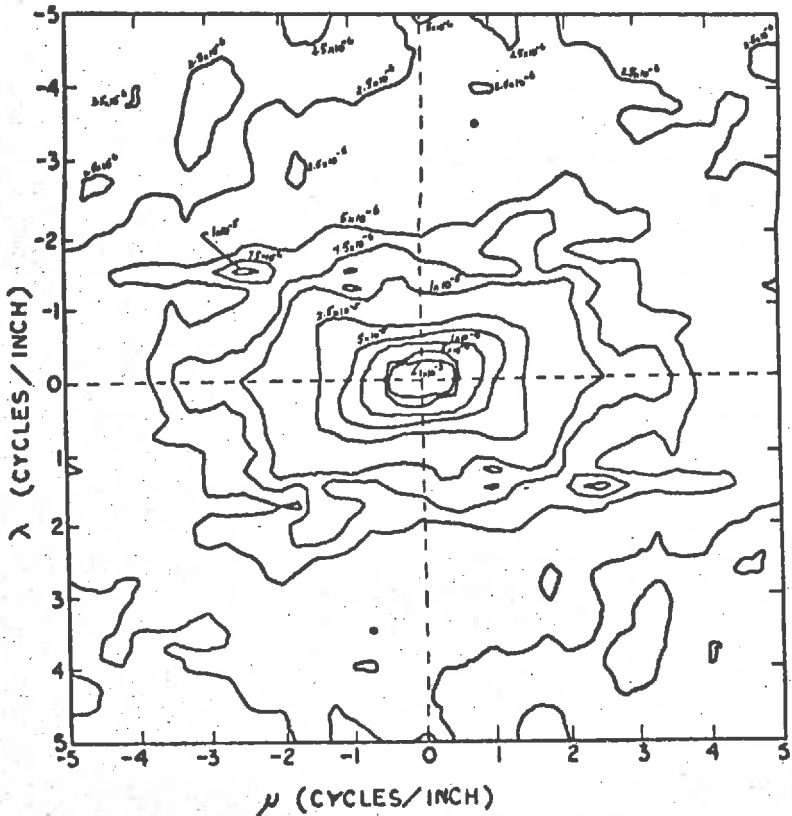


Figure 20. Contour diagram for spectrum from quadrant 2, position 1 on Bed 4 (upper right-hand quadrant of sample area shown in Figure 12)

SPECTRAL CONTOURS FOR BED4P103

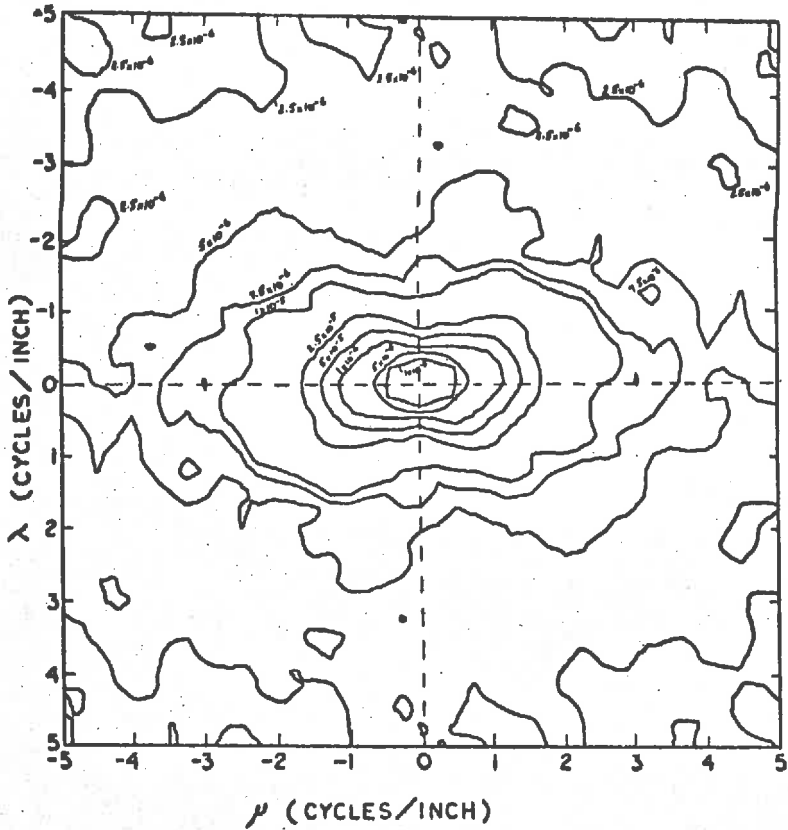


Figure 21. Contour diagram for spectrum from quadrant 3, position 1 on Bed 4 (lower left-hand quadrant of sample area shown in Figure 12)

SPECTRAL CONTOURS FOR BED4P1Q4

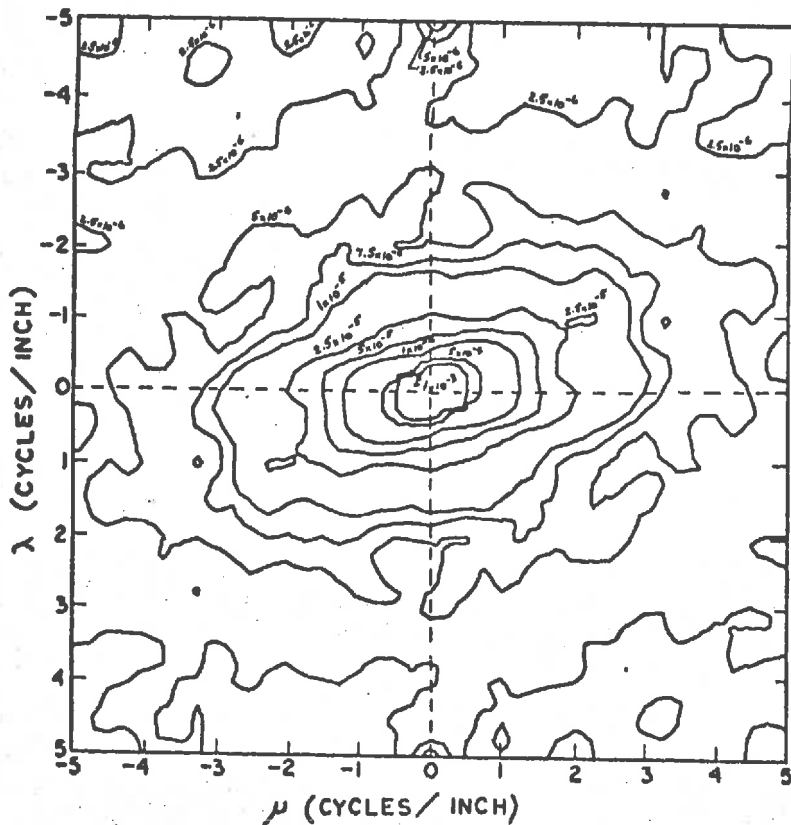


Figure 22. Contour diagram for spectrum from quadrant 4, position 1 on Bed 4 (lower right-hand quadrant of sample area shown in Figure 12)

SPECTRAL CONTOURS FOR BED4P1AV

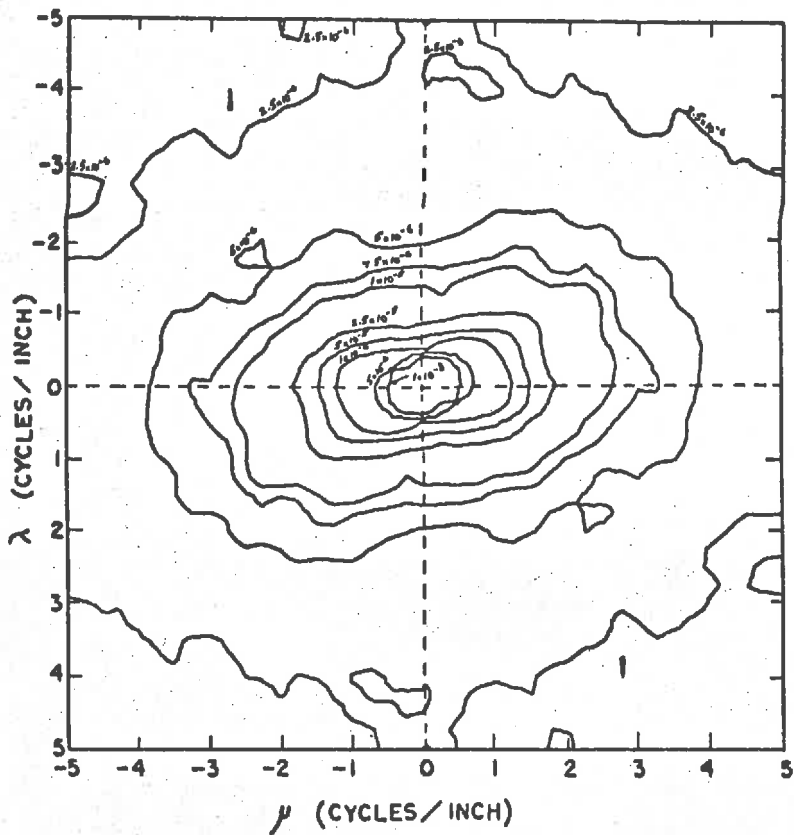


Figure 23. Contour diagram for average spectrum from position 1 on Bed 4

As previously mentioned, position 6 on Bed 3 was recorded with the sides of the grid at 45 degrees to the flow direction, primarily to check on recording errors, and this is reflected in the orientation of the ellipse axes of the spectral contours in Figures 14 through 18. The excess of spectral power on the vertical axis also occurred in some other spectral plots of Bed 3 sampled areas. In general the spectral power in the higher frequencies was exceptionally low and of the order of the instrumentation error, or recording accuracy (as illustrated in Figure 10). These contour extensions are therefore considered to be a reflection of instrument error probably caused by slight vertical movement of the cross-carriage of the micro-relief meter. Prior to running tests on Bed 4 small teflon blocks were added to the ends of the cross-carriage to hold the wheels more firmly down in the guide rails on the outer frame. No spectral plots from sampled areas on Bed 4 exhibited spectral power ridges on the vertical axis. Further consideration of error in recording will be presented in the discussion of the spectra below.

The two peaks on the horizontal axis in Figure 14, at frequencies of $\frac{1}{2}$ cycle/inch, were caused by the necessity for averaging the adjacent recolored spectral estimates to obtain the (0,0) frequency spectral estimate. Theoretically the spectral surface is asymptotic to the vertical (power) axis.

Ridges and troughs in the spectral surfaces may be related back to the presence or absence of waves having a frequency equal to the distance from the origin in the frequency plane and crests perpendicular to the line joining the point in the plane to the origin. In fact, the spectral surfaces contain a great deal of information, the major problem being that of condensing and extracting the relevant information required. For this reason, only the average area spectrum for each position was considered and these area spectra were then collapsed into line spectra parallel to, and perpendicular to, the flow direction.

Collapsed Line Spectra

An area spectrum may be collapsed into a line spectrum using the relationship,

$$f(u) = \int_{-\infty}^{\infty} f(u,v) dv \quad (5.4)$$

where u, v are the perpendicular frequency axes. In discrete form, in practice, the line spectra may be collapsed onto the horizontal or vertical frequency axes of the area spectrum by use of the formula

$$\psi = \lambda \left[\frac{1}{2} (f_{\lambda_{-m}\mu} + f_{\lambda_m\mu}) + \sum_{\lambda=\lambda_{-m+1}}^{\lambda_m-1} f_{\lambda,\mu} \right] \quad (5.5)$$

where λ_m is the Nyquist frequency or $m_x / (2m_x + 1) \Delta x$ in conformity with equation (3.20). Interchange of λ and μ and, m_x and m_y enables collapse of the area spectrum onto the other axis. Similarly collapse onto any other axis through the frequency origin may be accomplished, although the degrees of freedom for each spectral estimate will then decrease with increasing frequency and the computation, except along the 45° lines, becomes considerably more difficult.

Collapsed line spectra for Bed 3 are presented in Figure 24 (down-slope) and Figure 25 (across the slope). Bed 4 line spectra are presented in Figure 26.

Confidence limits placed on the line spectra, in a similar manner to the area spectra, discussed above, had 385/4 degrees of freedom associated with each spectral estimate from the averaged area spectra. For this reason the curves were exceptionally smooth. The 95% confidence limits are 0.978 and 1.023 times the spectral estimate.

Discussion

A commonly used measure to parameterise a line spectrum is that of an "average" wavelength obtained by division of the zero moment (Mom_0) of the positive frequency section of the spectrum by the first moment (Mom_1). For the line spectra presented in Figures 24 to 26 the analysis leads to the data presented in Table 1.

In terms of the area spectra the values in Table 1 reflect the moments of the spectral surface about the horizontal and vertical axes. The zero moment is the volume beneath the spectral surface on a half-plane of the frequency domain, i.e. one-half of the variance of the filtered data matrix. The first moment of the line spectrum on the

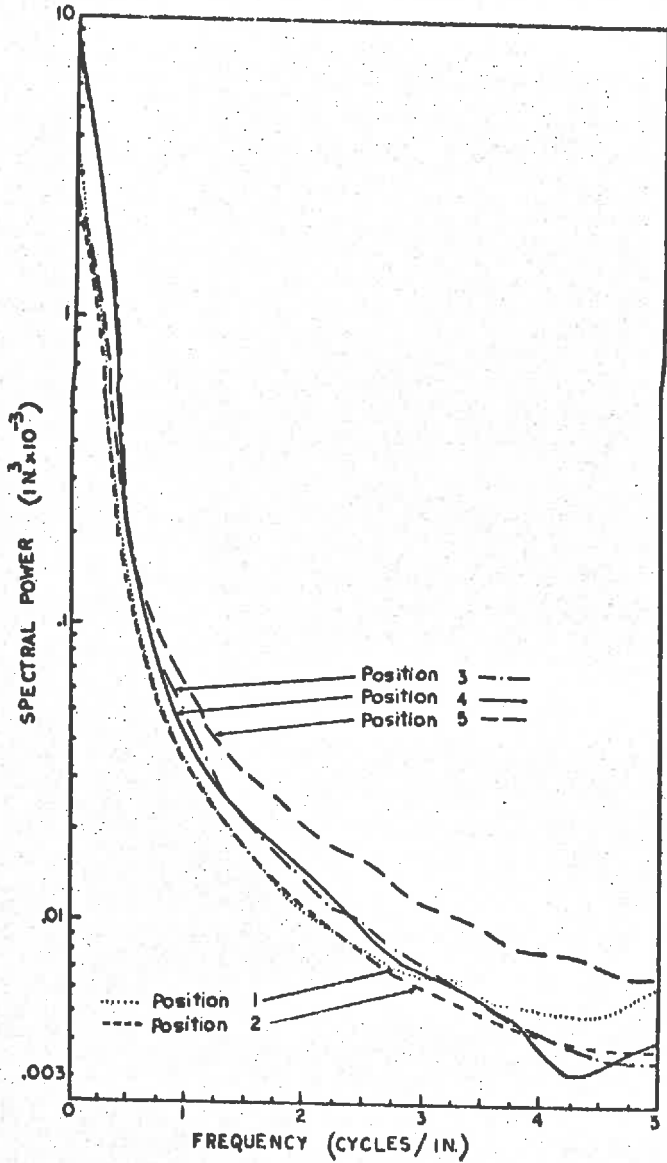


Figure 24. Collapsed downslope line spectra for Bed 3 sample areas

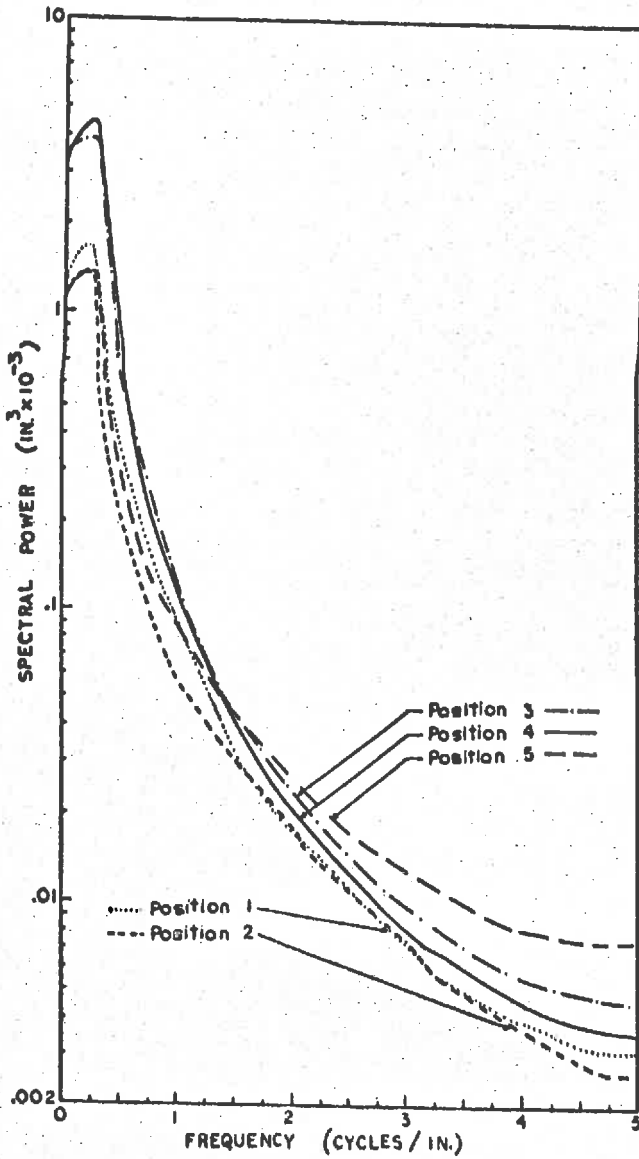


Figure 25. Collapsed cross-slope line spectra for Bed 3 sample areas

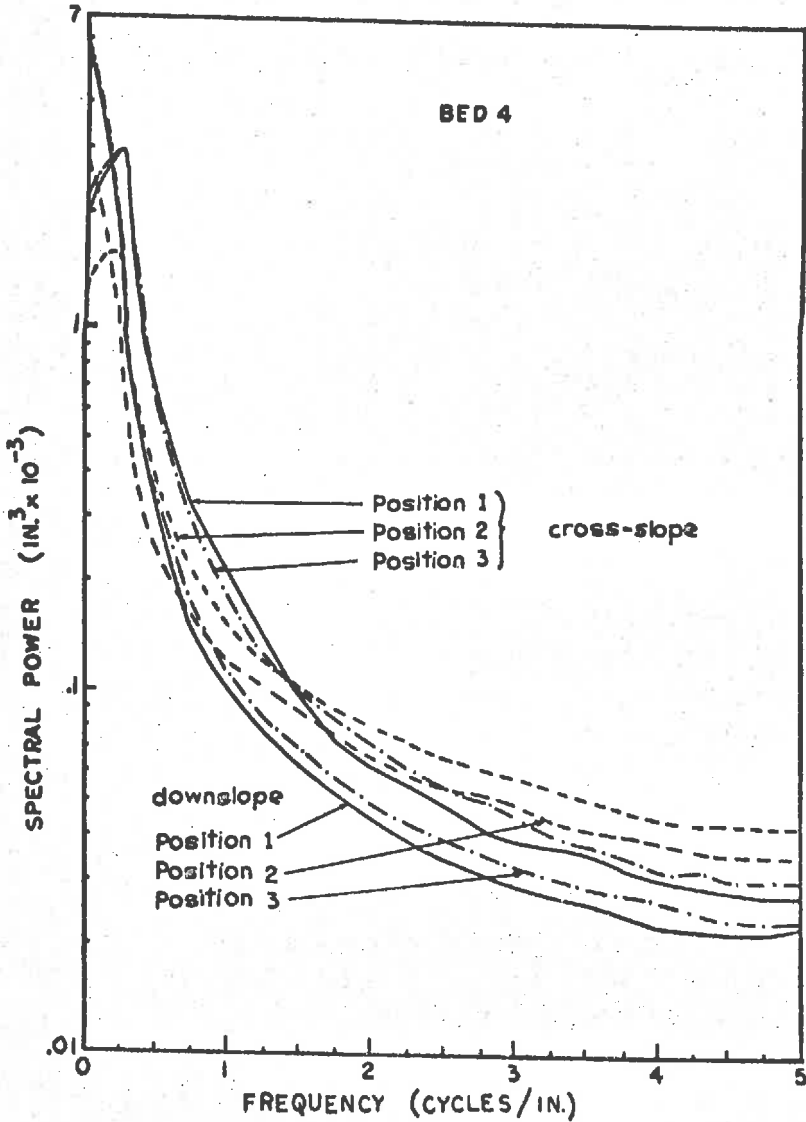


Figure 26. Collapsed line spectra for Bed 4 sample areas

vertical axis is identical to the first moment of the spectral surface in the upper half-plane about the horizontal axis, and vice versa for the horizontal axis line spectrum. Longuet-Higgins (1957) presents an extension of the moment concept to the theoretical derivation of measures of ellipticity or long-crestedness of area spectral surfaces.

Table 1. Moments of line spectra

Bed Surface	Position	Vertical Axis*			Horis. Axis*	
		Mon ₀ (in. ² x 10 ⁻⁴)	Mon ₁ (in. x 10 ⁻⁴)	"Average" wave- length (in.)	Mon ₁ (in. x 10 ⁻⁴)	"Average" wave- length (in.)
Bed 3	1	7.63	2.37	3.22	3.26	2.34
Bed 3	2	6.10	2.03	3.00	2.57	2.38
Bed 3	3	17.40	4.30	4.05	6.06	3.14
Bed 3	4	18.07	4.15	4.24	6.03	3.00
Bed 3	5	7.01	3.02	2.33	3.62	1.96
Bed 4	1	14.42	6.46	2.22	8.94	1.61
Bed 4	2	9.61	7.58	1.27	8.98	1.07
Bed 4	3	14.95	7.04	2.13	9.46	1.58

* Vertical axis refers to downslope spectra while horizontal axis refers to cross-slope spectra.

However in considering the usefulness of the moment concepts, or any other parametric description of spectra, a number of practical problems associated with the data acquisition and analysis merit attention. In practice the basic data is acquired in the form of discrete sampled points. The necessity for using a high-pass filter on the basic data matrix (as discussed in Chapter III) results in a loss of information in the immediate vicinity of the frequency origin. Kowin *et al* (1968) estimated for their data using a similar filter, that spectral estimates in the lower 12 per cent of the frequency axis are unreliable due to round-off errors in computation in recoloring the spectrum. The value of the area spectral estimate at the (0,0) frequency level is therefore somewhat arbitrary as reflected by the declination of the horizontal axis line spectra toward the spectral power axis. Since the "average" wavelength determined by moments is

of low frequency, its value is strongly dependent on the filter selection and the handling of round-off errors in the computation.

Additional influences on the spectral estimates are those of recording errors in acquiring the basic data, and aliasing. Recording errors arise from two sources viz., the error in the reading itself and errors in placement of the recording probe. Aliasing reflects the power of frequencies higher than the Nyquist frequency which are folded back into the spectrum in the form of added power and is essentially caused by the need to record at discrete intervals, whereas the ground surface contains frequencies higher than the Nyquist frequency.

Discussion of the relevance of Figure 10 (page 38) was deferred until the present in order that it may be viewed in terms of the derived spectral estimates. The calibration error, assumed random, is essentially that of instrument non-reproducibility, neglecting placement errors. The calibration data, presented in Appendix A, may be related to the line spectral plots by assuming random spectral power in the Nyquist interval. The calibration data then plot as lines of constant spectral power at one-tenth of the variance, viz., $.041 \times 10^{-6}$ in.³ for CA01 and $.018 \times 10^{-6}$ in.³ for CA02. The difference spectra, obtained by re-running a section of a sampled area on Bed 4, reflect an estimation of the reading and placement error. These spectra are essentially level and independent of frequency indicating random errors, and having average spectral power of 24×10^{-6} in.³ and 19×10^{-6} in.³. However these spectral estimates are considerably inflated due to aliasing. The true spectrum for the differences, if the aliasing could be removed, or folded-out, would be much lower and likely indicate increasing power with frequency to well beyond the Nyquist frequency. Placement error due to deflections of the recording probe is considered to account for the large increase in power in the difference spectra over the calibration error spectra.

Bed 4 contained considerably more grain roughness than Bed 3 (as illustrated in Figures 11 and 12). Probe deflection is therefore considered to have been less severe on Bed 3 and a difference spectrum may be expected to have been much lower than those obtained on Bed 4.

The Bed 3 line spectra are therefore not constrained to lie above the Bed 4 difference spectra.

Of primary concern, however, is the power of the difference spectra which is of the order of the recorded spectra at the Nyquist frequency. The spectral estimates therefore are markedly influenced by recording error in this region. The higher spectral power at the Nyquist frequency for Bed 4, over that of Bed 3, is attributable to increased grain roughness in association with the instrument recording error.

Fitting a suitable descriptive parametric model to the area spectra would be a major undertaking and was not attempted in this study. However certain pertinent features exhibited by the area spectra are worthy of note. The spectral contours were elliptical in the lower frequencies with the major axes of the ellipses generally aligned perpendicular to the bed slope. In the line spectra this is evidenced by a more rapid declination of the vertical axis spectra. In addition the line spectra for each bed surface tended to bunch with the Bed 4 line spectra having a lesser slope. With reference to Table 1, the above variance or zero spectral moment appears to be indicative of the existence of large deep rills. Positions 3 and 4 in the center of Bed 3 (shown in Figure 1) each included a large deep rill while positions 1, and 5 in the lower section of the bed surface and 2 and 6 in the upstream section were relatively free of large rills. No large dominant rills existed on Bed 4 and positions 1 and 3 (shown in Figure 3) were generally representative of the bed surface. Position 2 on Bed 4, selected specifically for its lack of rilling in any discernable form, exhibited a lower variance than either of positions 1 or 3.

No positive conclusions can be made concerning the information obtained from the spectra. However, bearing in mind the limitations imposed by the recording accuracy and the filter characteristics, the following general comments appear worthy of note, with reference to the data presented in Table 1:

- (1) Larger variance or zero moment (M_{00}) values were associated with the occurrence of both large rills and increased grain roughness.

- (ii) Within bed variation in variance was large and strongly dependent on the position of the sample area. The zero moment values from Bed 4 sample areas fall within the range of the Bed 3 values. As expected, variance alone does not indicate the nature of the surface roughness in terms of hydraulic considerations. Grain and form roughness combine in influencing the variance.
- (iii) The ratio of the "average" wavelengths of the cross-slope to downslope directions lay in a range of 0.70 to 0.84 with the Bed 4 values again lying within the range of the Bed 3 values. Presence or absence of rilling was not marked in its effect on this ratio, for the two surfaces tested.
- (iv) The only marked difference between the sets of line spectra from Bed 3 and Bed 4 were in the slopes of the spectra. This is evidenced, by the weighting effect in the first moment, as shown by differences in Bed 3 and Bed 4 line spectra M_{01} values in Table 1. A similar effect could have been obtained in the slope coefficient of a linear relationship between the logarithm of spectral power and the logarithm of frequency as suggested by Kozin et al (1968).

Hydraulic Tests

A randomized factorial design was used in running the hydraulic tests on each of Bed 3 and Bed 4. Two sequential replications were run on each surface at four levels of rainfall rate (0,2,4 and 6 in/hr), four levels of upstream flow rate (0,6,12 and 18 in/hr.) and five slope levels (1,2,3,4 and 5 ft/ft). Treatments were separately randomized within each replication.

The rainfall and upstream flow rates were calibrated and each hydraulic test run under control of an analog-hybrid computer, as described in Appendix D. Prior to each test the surface retention was satisfied and an averaged bed weight then used as a base for calculating detention storage. Three voltage levels representing mass

runoff, runoff rate and detention, calibrated as described in Appendix G, were recorded at 1 second intervals. For treatment levels which included both upstream flow and rainfall, a second steady state condition with rainfall or overland flow alone was used to separate out the component values of rainfall and upstream flow for that particular test. A digital computer program, used to analyze the data from each test, together with a sample print is presented in Appendix G.

Hydraulic Regression Model

The hydraulic regression model used was of the same form as used previously by Kundu (1971) and assumes a simplified trapezoidal shape water profile, viz.,

$$D = a s^b Q^c \quad (5.6)$$

where, D = detention (in.)

S = slope (ft/ft)

Q = discharge mid-way down the surface slope (in./hr.)
= (I/2 + Qu)

I = rainfall rate (in./hr.)

Qu = upstream flow rate (in./hr.)

and, a, b, c = fitted parameters.

The form of the model conforms to that of the commonly used uniform flow equations of Chezy and Manning, generally assumed in relating depth to discharge in applying the kinematic wave method. Detention alone is used as a dependent variable since the addition of retention storage would invalidate the model under zero flow conditions.

Two estimates for rainfall rate and upstream flow rate were available from the analysis of each test, viz., those of the averaged value of the analog differentiator signal and the least square slope of the digitised mass runoff signal. The computer program presented in Appendix G calculated both values over 20 steady state readings. The standard errors associated with each estimate of the runoff rate, as presented in the sample print in Appendix G, were those of the individual data values for the averaged runoff rate signal and the slope of

the regression line for the least square fit value. The averaged runoff rate signal was used in the regression model since its calculation incorporated Chauvenet's criterion (Holman, according to Kundu, 1971) which rejected spuriously high or low data values. The detention values at steady state were similarly subjected to this criterion.

A non-linear regression analysis, using the full set of data from both replications, to fit the model of equation (5.6) resulted in the relationships,

$$D = 0.00397 Q^{.517} S^{-.530} \quad (5.7)$$

with an R^2 value of 0.992 for Bed 3 data, and

$$D = 0.0114 Q^{.512} S^{-.297} \quad (5.8)$$

with an R^2 value of .978 for Bed 4 data. A graphical presentation of the data values and regression relationships is given in Figures 27 and 28.

Retention - Slope Relationship

Values of surface retention at .005 ft/ft increments of slope between .01 and .05 ft/ft were obtained from averaged bed load readings and the mass of water collected in the runoff trough. Two sets of readings were taken for each surface and exponential decay model relationships fitted by non-linear regression analysis. The fitted regression equations for retention in inches and slope in ft/ft were,

$$\text{Retention} = 0.249 e^{-160S} \quad (5.9)$$

for Bed 3, having an R^2 value of .986, and

$$\text{Retention} = .057 e^{-51S} \quad (5.10)$$

for Bed 4, with an R^2 value of .935. The data values and regression lines are presented in Figures 29 and 30.

Discussion of Recording Errors

The regression equations obtained slapy represented a least square fit of the data and any statistical inferences concerning the variables in the regression equations would require an assumption of homoscedasticity, i.e. homogeneous variance, of the errors. A set of correlation tests, run separately for each replication within surfaces,

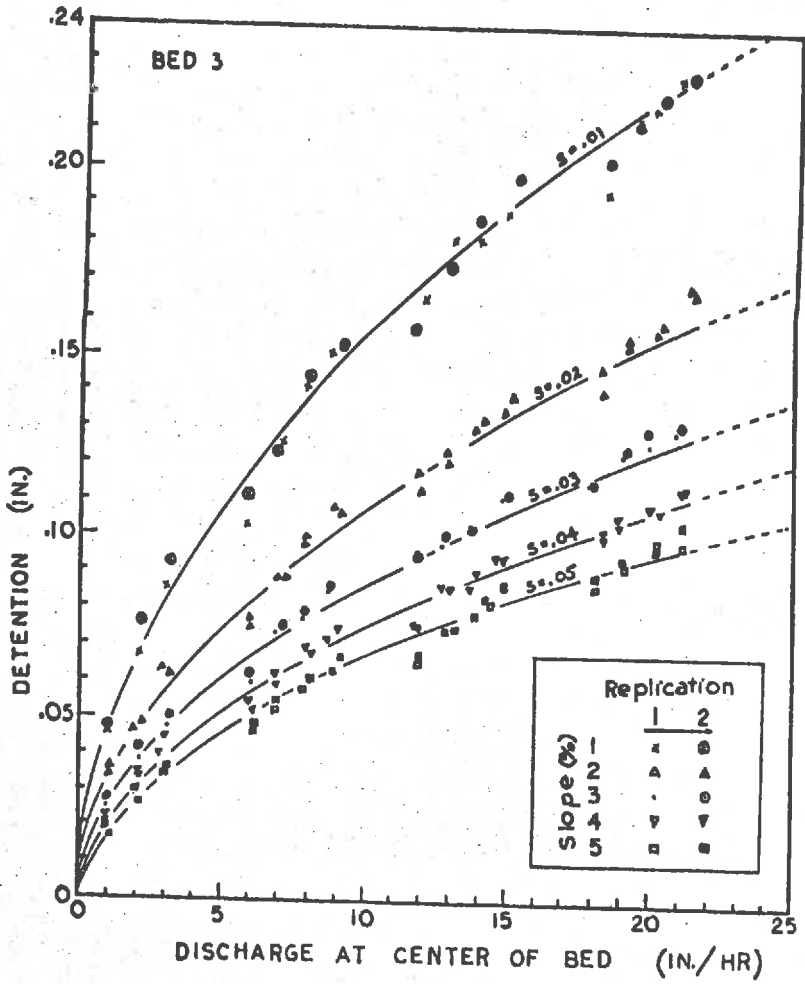


Figure 27. Hydraulic test data and model fit for Bed 3

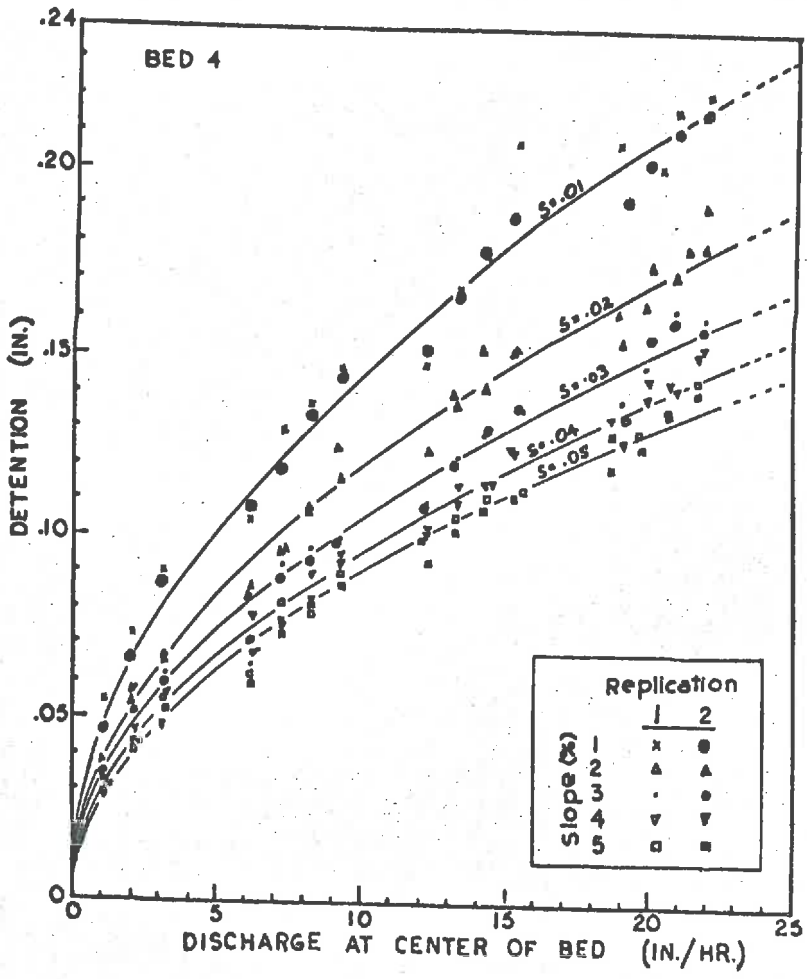


Figure 28. Hydraulic test data and model fit for Bed 4

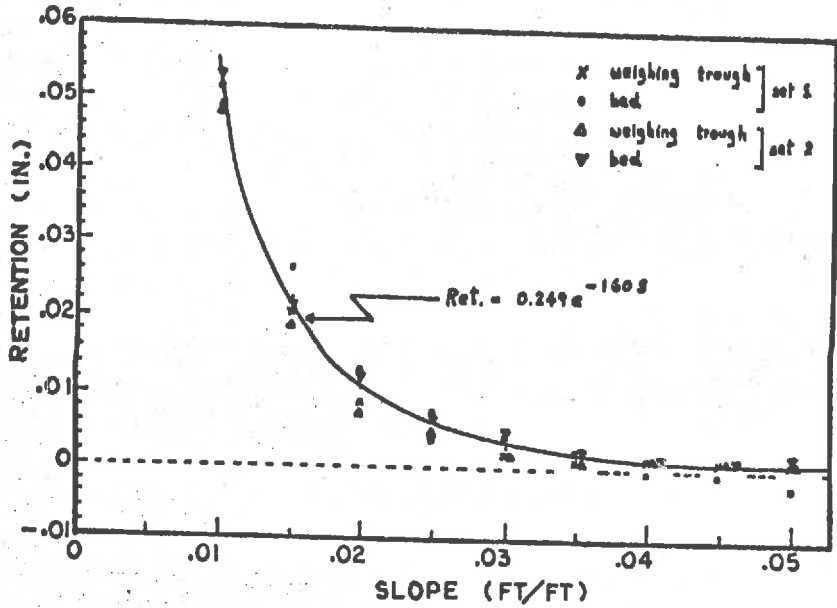


Figure 29. Retention-slope relationship on Bed 3

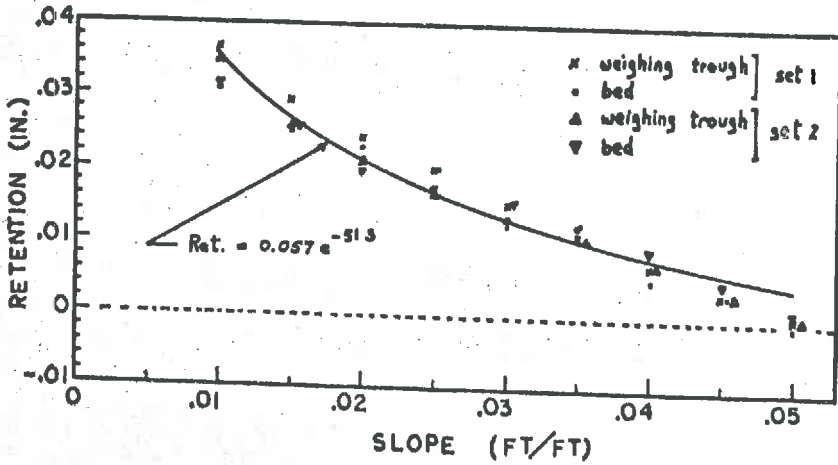


Figure 30. Retention-slope relationship on Bed 4

indicated a highly significant (1% level) positive correlation to exist between the variance of the runoff rate values as recorded and the values themselves for all four data sets. Similar tests on the detention values indicated a highly significant (1% level) positive correlation to exist between the detention values and the variance of their estimate for both replications on Bed 3. Bed 4 values were not significant. Due to these correlations between the magnitude of the values and the variance of their estimate, no attempt is made to postulate the distribution of the runoff rate and detention recording errors. Table 2 presents the median and maximum values for the standard error of the runoff rate and detention values as obtained from the mean of 20 steady state values from each test. The exact number of spurious high or low values rejected according to Chauvenet's criterion out of each set of 20 values is unknown, but could not have been more than one, or two at most, in some sets and is therefore ignored. The effect of the calibration coefficient errors are relatively insignificant.

Additional errors not included in Table 2 were those due to the added forces created by rainfall impact on the rainfall simulator bed and runoff into the weighing tank. However, as reported by Das (1970), these errors are small. Errors of more consequence in these tests, however, are considered to have been created by the necessity for assuming a base level from which to calculate detention storage. It was not possible, in running the tests, to wait until the drip rate dropped to zero and the detention values may therefore be expected to have been slightly underestimated with the major effect being at the flatter slope values.

Table 2. Hydraulic tests standard errors

Surface	Replication	Runoff Rates (in./hr.)		Detention (in.)	
		Median	Maximum	Median	Maximum
Bed 3	1	.019	.049	.00018	.00040
Bed 3	2	.018	.086	.00030	.00047
Bed 4	1	.020	.072	.00043	.00076
Bed 4	2	.018	.067	.00045	.00070

Discussion of Hydraulic Model

The assumption of a trapezoidal average depth of flow profile down the surface slope is not true in terms of the kinematic wave analysis and is considered a possible cause of the cyclic trends exhibited by the data values in Figures 27 and 28. Each cycle was associated with a fixed level of upstream flow application. Similar cycles occurred in the data presented by Kundu (1971) using the same model. It is considered these cycles are due to a combination of added flow resistance due to raindrop impact and a shift in the average depth location.

The regression model is postulated in the form of a uniform flow equation of the type,

$$q = \alpha y^m \quad (5.11)$$

in which q is the discharge in cusecs per ft. width, y the flow depth in ft., and α and m are parameters. Written with depth as the dependent variable Chezy's equation for turbulent flow in a wide rectangular channel is,

$$y = \frac{Q_s^{.66} L^{.66}}{C^{.66} S^{.33}} \quad \text{or,} \quad \frac{0.157 Q_s^{.66} L^{.66} f^{.33}}{g^{.33}} \quad (5.12)$$

where, y is flow depth (ft.), Q_s the discharge (ft./sec.), L the length of flow plane (ft.), S the slope (ft./ft.), and C and f are the Chezy and Darcy-Weisbach friction factors. Under laminar flow assumptions equation (5.11) is

$$y = 0.0102 Q_s^{.33} L^{.33} S^{-.33} \quad (5.13)$$

On a comparative basis equations (5.7) and (5.8), the derived regression equations, become

$$d = 0.0825 Q_s^{.517} S^{-.530} \quad (5.14)$$

for Bed 3, where d is detention in feet and Q_s and S are as given above, and

$$d = 0.219 Q_s^{.512} S^{-.297} \quad (5.15)$$

for Bed 4.

The two regression relationships for Bed 3 and Bed 4 exhibited a close similarity in the discharge index, which in terms of equation (5.11) results in a value of m approximately equal to 2.

In terms of the laminar and turbulent flow equations (equations 5.12 and 5.13) and assuming y is a linear function of d , this represents

conditions lying between laminar and turbulent flows. A value of $n = 2$ is commonly used in applications of the kinematic wave theory, based in part on simplicity of use and partly on research results.

The large value departure of the slope index for the Bed 3 regression relationship, equation (5.14), is not explainable in terms of the laminar and turbulent flow equations given above, in both of which the slope exponent is 0.33. The slope index for Manning's equation is 0.30. However as presented in Chapter II, Parsons (1949) reported a slope exponent of 0.55.

Further consideration of the basic assumptions concerning the relationship between d (the average flow depth defined on a volume per unit area basis) and y (the actual flow depth), indicates that d and y are equivalent only if flow depth is constant over the area. A simple model of a plane surface having all flow confined to a single triangular channel results in d proportional to y^2 . Thus variation in the Q and S exponents from the laminar and turbulent flow exponents may be expected, since d is a function of a power series of y values.

Converting both equations (5.7) and (5.8) to units of slope S_p , in per cent, results in

$$d = .0038 Q^{.517} S_p^{-.530} \quad (5.16)$$

for Bed 3, and

$$d = .0037 Q^{.512} S_p^{-.297} \quad (5.17)$$

for Bed 4, indicating a virtually identical detention-discharge relationship at the 1 per cent slope level. Kundu (1971) included an extra variable, viz., the exposure parameter, E , in his hydraulic model for shallow flow over rough plane surfaces. It was therefore not possible to remove the effect of the E value from the general model presented in Chapter II, in which detention is also defined differently. However an approximation for his first surface model, in which E was small and therefore often constant, yielded the relationship,

$$d = 0.0050 Q^{.48} S_p^{-.23} \quad (5.18)$$

No positive conclusions can be presented, in the absence of re-running the data obtained by Kundu (1971), to exclude the E parameter.

However some general observations appear worthy of note:

- (i) A comparison of equations (5.16), (5.17) and (5.18) indicates a relatively constant exponent on the Q value.
- (ii) The effect of hydraulic roughness appeared in the exponent on the slope variable.
- (iii) The slope exponent appears to increase in absolute value with decreasing grain roughness and increasing form, i.e. greater channel efficiency.

It has not been possible to obtain a simple hydraulic model to theoretically explain the above observations, and in the absence of more extensive data no definite conclusions can be presented. However a general model of the form,

$$d = .004 Q^{.5} s_p^{-x} \quad (5.19)$$

is suggested, in which x is a function of grain and form roughness, increasing with an increase in hydraulic efficiency. In terms of the discussion of the area spectra, in the previous section of this Chapter, a suggested form for x is

$$x = x \left[\frac{Mo_{s_0}^{\frac{1}{2}}}{L_h} \right] \quad (5.20)$$

in which L_h is the "average" wavelength perpendicular to the flow direction. The suggested form for x is therefore analogous to the exposure parameter, K , discussed in Chapter II. The $Mo_{s_0}^{\frac{1}{2}}$ value reflects a measure of grain roughness, while L_h reflects a measure of the distribution of the roughness effect.

The cross-slope "average" wavelength is suggested in preference to the downslope value in spite of the lack of any discernable variation in their ratios between Bed 3 and Bed 4 data. The reason for the choice of the cross-slope direction is that it more logically presents a measure of form effects and thus relates directly to the discussion above concerning the relationship between d and y .

CHAPTER VI

SUMMARY AND RECOMMENDATIONS

A technique was developed for stabilising an eroded sand surface on the bed of a rainfall simulator for later study of the physical characteristics relating to hydraulic roughness. Laminating resin fibreglas was used to fix the sand layer and surface coat fibreglas sprayed on the surface to ensure impermeability.

Two eroded sand surfaces were tested, viz., Bed 3 made from a sand-cement mix and Bed 4 using the technique described above.

A micro-relief meter was constructed to operate under control of an analog-hybrid computer and record surface elevations on the stabilised beds at 0.098 in. spacings over 23.46 in. square sample areas. Area spectral analysis was applied to the elevation readings. Differences between the surfaces was evidenced mainly in the gradient of the spectral surfaces.

Hydraulic tests on each surface were run in two separately randomized replications of a factorial design. Four levels each of rainfall and upstream flow rate and five levels of slope were applied. Regression equations were obtained, in terms of a uniform flow model, from steady-state conditions on each surface. The difference in hydraulic behaviour of the two surfaces was evidenced only in the exponent on the slope term in the regression equation.

The following recommendations are presented in relation to future study:

- (1) The area spectral analysis computations require a considerable time allocation on a digital computer. It is suggested that for future use the program be re-written to utilise the Fast Fourier Transform Technique.

- (ii) In relation to hydraulic roughness of eroded surfaces it is suggested that single cross-slope line spectra be recorded at close spacing with low tolerance on probe placement. Longer lines may economically be analyzed and undesirable filtering effects decreased.
- (iii) An improved hydraulic model incorporating a non-linear water surface profile and subsequent determination of the average depth position should be developed.

BIBLIOGRAPHY

BIBLIOGRAPHY

- ABDEL-RAZAK, A.Y., VIESSMAN, W. & HERNANDEZ, J.W., 1967. A solution to the surface runoff problem. Jour. Hyd. Div. ASCE 93(HY6); 335-352.
- ANNAMBHOTLA, V.S.S., 1969. Statistical properties of bed forms in alluvial channels in relation to flow resistances. Ph.D. Dissertation, Univ. of Iowa, Iowa City, Iowa.
- ASHIDA, K. & TANAKA, Y., 1967. A statistical study of sand waves. Proc. 12th Congress, Inter. Assoc. Hydraulic Res. 2; 103-110.
- BLACK, P.E., 1970. Runoff from watershed models. Water Resources Res. 6(2); 465-477.
- BOGDANOFF, J.L., KOZIN, F. & COTE, L.J., 1966. Atlas of off-road ground roughness P.S.D.'s and report on data acquisition technique. Tech. Rep. No. 9387 (LL 109) Land Locomotion Lab., U.S.Army-Tank Automotive Center, Warren, Mich.
- BRAKENSIEK, D.L., 1966. Storage flood routing without coefficients. USDA, ARS Paper No. 41-122.
- BRAKENSIEK, D.L., 1967. Kinematic flood routing. Trans. Am. Soc. Agr. Eng. 10(3); 340-343.
- BRAKENSIEK, D.L. & ONSTAD, C.A., 1968. The synthesis of distributed inputs for hydrograph prediction. Water Resources Res. 4(1); 79-85.
- BURWELL, R.E., ALLMARAS, R.R. & AMEMIYA, M., 1963. A field measurement of total porosity and surface microrelief of soils. Proc. Soil Sci. Soc. Amer. 27; 697-700.
- CARNAHAN, B., LUTHER, H.A. & WILKES, J.O., 1969. Applied numerical methods. John Wiley & Sons, Inc.; New York.
- CHEN, C., 1962. An analysis of overland flow. Ph.D. Dissertation, Michigan State Univ., East Lansing, Mich.
- CHERY, D.L., 1966. Design and tests of a physical watershed model. Jour. of Hydrol. 4; 224-235.
- CHOW, V.T., 1959. Open channel hydraulics. McGraw-Hill; New York.

- CHOW, V.T. & HARBAUGH, T.E., 1965. Raindrop production for laboratory watershed experimentation. *Jour. of Geophys. Res.* 70(24); 6111-6119.
- CHOW, V.T., 1967. Laboratory study of watershed hydrology. *Intern. Hydrol. Symposium, Proc. 1, Fort Collins, Colo.*; 194-202.
- COTE, L.J., 1966. Two dimensional spectral analysis. Mimeograph Series No. 83, Dept. of Statistics, Purdue University, Lafayette, Indiana.
- CURRENCE, H.D. & LOVELY, W.C., 1970. The analysis of soil surface roughness. *Trans. ASAE* 13(6); 710-714.
- DAS, K.C., 1970. Laboratory modelling and overland flow analysis. Ph.D. Dissertation, Purdue Univ., Lafayette, Ind.
- EAGLESON, P.S.; 1970. *Dynamic hydrology.* McGraw-Hill; New York.
- ELLISON, W.D. & POMERENE, W.H., 1944. A rainfall applicator. *Agr. Eng.* 25(6); 220.
- ESCOFFIER, F.F., 1950. A graphical method for investigating the stability of flow in open channels or closed conduits flowing partly full. *Trans. Am. Geophys. Un.* 31(4); 583-586.
- FOSTER, G.R., 1968. Analysis of overland flow on short erosion plots. M.S. Thesis, Purdue Univ., Lafayette, Ind.
- FOSTER, G.R., 1972. Personal communication.
- FRASIER, G.W. & MYERS, L.E., 1970. Protective spray coatings for water harvesting catchments, *Trans. ASAE* 13(3); 292-294.
- GRACE, R.A. & EAGLESON, P.S., 1966a. The modelling of overland flow. *Water Resources Res.* 2(3); 393-403.
- GRACE, R.A. & EAGLESON, P.S., 1966b. Construction and use of a physical model of the rainfall-runoff process. *Mass. Inst. of Tech., Hydrodynamics Tech. Note No. 11, 85pp.*
- HALL, M.J., 1970. A critique of methods of simulating rainfall. *Water Resources Res.* 6(4); 1104-1114.
- HARBAUGH, T.E., 1966. Time distribution of runoff from watersheds. Ph.D. Dissertation, Univ. of Ill., Urbana, Ill.
- X HEERMAN, D.F., WENSTROM, R.J. & EVANS, N.A., 1969. Prediction of flow resistance in furrows from soil roughness. *Trans. ASAE* 12(4); 482-485, 489.

- HENDERSON, F.M. & WOODING, R.A., 1964. Overland flow and ground water flow from a steady rainfall of finite duration. *Jour. of Geophys. Res.* 69(8); 1531-1540.
- HICKS, W.I., 1944. A method of computing urban runoff. *Trans. Am. Soc. Civil Eng.* 109; 1217-1268.
- HICKS, W.I., 1946. Discussion on "Hydraulics of runoff from developed surfaces" by G.F. Izzard. *Proc. Highway Res. Bd.* 26; 146-150.
- HORNER, W.W. & JENS, S.W., 1943. Surface runoff determination from rainfall without using coefficients. *Trans. Am. Soc. Civil Eng.* 107; 1039-1117.
- HORTON, R.E., 1938. The interpretation and application of runoff plot experiments with reference to soil erosion problems. *Soil Sci. Soc. Am. Proc.* 3; 340-349.
- HUGGINS, L.F. & MONKE, E.J., 1966. The mathematical simulation of the hydrology of small watersheds. *Water Resources Res. Center Tech. Rep. No. 1, Purdue Univ., Lafayette, Ind.*
- ISAACSON, E., STOKER, J.J. & TROESCH, A., 1958. Numerical solution of flow problems in rivers. *Jour. of Hyd. Div. ASCE* 84(HY5); Paper 1810.
- ISHIHARA, Y., 1964. Hydraulic mechanism of runoff. *Proc. Conf. on Hydraulics and Fluid Mech., Univ. of Western Australia*; 173-189.
- IWAGAKI, Y., 1955. Fundamental studies on the runoff analysis by characteristics. *Disaster Prevention Res. Inst. Bull. No. 10, Kyoto Univ., Japan*; 25pp.
- IZZARD, C.F., 1942. Runoff from flight strips. *Proc. Highway Res. Bd.* 22; 94-99.
- IZZARD, C.F. & AUGUSTINE, M.T., 1943. Preliminary report on analysis of runoff resulting from simulated rainfall on a paved plot. *Trans. Am. Geophys. Un.* 24; 499-509.
- IZZARD, C.F., 1944. The surface-profile of overland flow. *Trans. Am. Geophys. Un.* 25; 959-968.
- IZZARD, C.F., 1946. Hydraulics of runoff from developed surfaces. *Proc. Highway Res. Bd.* 26; 129-146.
- JENKINS, G.M. & WATTS, D.G., 1968. Spectral analysis and its applications. Holden-Day; San Francisco.
- KEULEGAN, G.H., 1944. Spatially variable discharge over a sloping plane. *Trans. Am. Geophys. Un.* 25; 956-959.

- KISISEL, I.T., 1971. An experimental investigation of the effect of rainfall on the turbulence characteristics of shallow water flow. Ph.D. Dissertation, Purdue Univ., Lafayette, Ind.
- KOZIN, F., COTE, L.J. & BOGDANOFF, J.L., 1963. Statistical studies of stable ground roughness. Tech. Rep. No. 8391 (LL95), Land Locomotion Lab., U.S. Army-Tank Automotive Center, Warren, Mich.
- KOZIN, F., COTE, L.J. & BOGDANOFF, J.L., 1968. Supplement to the atlas report of off-road ground roughness. Tech. Rep. No. 10316 (LL130) Land Locomotion Lab., U.S. Army-Tank Automotive Center, Warren, Mich.
- KUIPERS, H., 1957. A relief meter for soil cultivation studies. Netherlands Jour. of Agr. Sci. 5; 255-262.
- KUNDU, P.S., 1971. Mechanics of flow over very rough surfaces. Ph.D. Dissertation, Purdue Univ., Lafayette, Ind.
- LAWS, J.O., 1941. Measurements of the fall velocities of water drops and raindrops. Trans. Am. Geophys. Un. 22; 709-721.
- LAWS, J.O. & PARSONS, D.A., 1943. The relation of raindrop size to intensity. Trans. Am. Geophys. Un. 24; 452-460.
- LIGGETT, J.A. & WOOLHISER, D.A., 1967a. Difference solutions of the shallow-water equations. Jour. Eng. Mech. Div. ASCE 93(EM2); 39-71.
- LIGGETT, J.A. & WOOLHISER, D.A., 1967b. The use of shallow water equations in runoff computation. Proc. of the 3rd Annual Am. Water Res. Conf., San Francisco, Calif.
- LIGHTHILL, M.J. & WHITHAM, G.B., 1955. On kinematic waves 1. Proc. Royal Soc., London, Series A, Vol. 229; 281-316.
- LIN, P., 1952. Numerical analysis of continuous unsteady flow in open channels. Trans. Am. Geophys. Un. 33(2); 227-234.
- LONGUET-HIGGINS, M.S., 1957. The statistical analysis of a random moving surface. Phil. Trans. Royal Soc. of London Ser. A. 249; 321-387.
- LONGUET-HIGGINS, M.S., 1962. The statistical geometry of random surfaces. Proc. of Symposium in App. Math. 13; 105-143.
- X MERRA, G.E., BRAZIER, R.D., SCHWAB, G.O. & CURRY, R.B., 1970. Theoretical considerations of watershed surface description. Trans. ASAE 13(4); 462-465.

- MEYER, L.D., 1958. An investigation of methods of simulating rainfall on standard runoff plots and a study of the drop size velocity, and kinetic energy of selected spray nozzles. USDA, ARS Spec. Rpt. No. 81.
- MITCHELL, J.K., 1970. Micro-relief surface depression storage. Ph.D. Dissertation, Univ. of Ill., Urbana, Ill.
- MORGALI, J.R. & LINSLEY, R.K., 1965. Computer analysis of overland flow. Jour. Hyd. Div. ASCE 91(HY3); 81-100.
- MORGALI, J.R., 1970. Laminar and turbulent overland flow hydrographs. Jour. Hyd. Div. ASCE. 96(HY2); 441-460.
- MORRIS, H.M., 1955. A new concept of flow in rough conduits. Trans. Am. Soc. Civil Eng. 120; 373-398.
- MUTCHLER, C.K. & HERMSMEIER, L.F., 1965. A review of rainfall simulators. Trans. Am. Soc. Agr. Eng. 8(1); 67-68.
- NORDIN, C.F. & ALGERT, J.H., 1966. Spectral analysis of sand waves. Jour. Hyd. Div. ASCE 92(HY5); 95-114.
- NORDIN, C.F., 1968. Statistical properties of dune profiles. Ph.D. Dissertation, Colo. State Univ., Fort Collins, Colo.
- NORDIN, C.F. & RICHARDSON, E.V., 1968. Statistical descriptions of sand waves from streambed profiles. Bull. IASH 13(3); 25-32.
- O'LOUGHLIN, E.M. & McDONALD, E.G., 1964. Some roughness-concentration effects on boundary resistance. La Houille Blanche No. 7.
- OSTLE, B., 1966. Statistics in research. Iowa State Univ. Press, Ames, Iowa.
- OVERTON, D.E., 1971. Modelling watershed surface water flow systems. 3rd Intern. Seminar Hydrol. Prof., Purdue Univ., Lafayette, Ind.
- PALMER, R.S., 1965. Water drop impact forces. Trans. Am. Soc. Agr. Eng. 8(1); 69-70, 72.
- PARSONS, D.A., 1943. Discussion on "The application and measurement of artificial rainfall in types FA and F infiltrimeters", by H.G. Wilm. Trans. Am. Geophys. Un. 24; 485-487.
- PARSONS, D.A., 1949. Depths of overland flow. USDA, SCS Tech. Paper No. 82, 33pp.
- RAGAN, R.M., 1965. Synthesis of hydrographs and water surface profiles for unsteady open channel flow with lateral inflows. Ph.D. Dissertation, Cornell Univ., Ithaca, New York.

- ROUSE, H., 1965. Critical analysis of open-channel resistance. Jour. Hyd. Div. ASCE 91(HY4); 1-25.
- SHARP, A.L. & HOLTAN, H.N., 1942. Extension of graphic of analysis of sprinkled-plot hydrographs to the analysis of hydrographs of control-plots and small homogeneous watersheds. Trans. Am. Geophys. Un. 23; 578-593.
- SIMONS, D.B. & RICHARDSON, E.V., 1961. Forms of bed roughness in alluvial channels. Jour. Hyd. Div. ASCE 87(HY3); 87-105.
- SMITH, D.D. & WISCHMEIER, W.H., 1962. Rainfall erosion. Advances in Agron. 14; 109-148.
- SMITH, R.E. & WOOLHISER, D.A., 1971. Overland flow on an infiltrating surface. Water Resources Res. 7(4); 899-913.
- SQUAKER, D., 1968. An analysis of relationships between flow conditions and statistical measures of bed configurations in straight and curved alluvial channels. Ph.D. Dissertation, Univ. of Iowa, Iowa City, Iowa.
- STRAHLER, A.N., 1964. Quantitative geomorphology of drainage basins and channel networks. (In Handbook of Applied Hydrology; V.T. Chow, Editor). McGraw-Hill; New York.
- STRELKOFF, T., 1969. One-dimensional equations of open channel flow. Jour. Hyd. Div. ASCE 95(HY3); 861-876.
- STRELKOFF, T., 1970. Numerical solution of St. Venant equations. Jour. Hyd. Div. ASCE 96(HY1); 223-252.
- TASK FORCE REPORT, 1963. Friction factors in open channels. Jour. Hyd. Div. ASCE 89(HY2); 97-143.
- TAYLOR, R.H. & BROOKS, N.H., 1961. Discussion on "Resistance to flow in alluvial channels" by D.B. Simons and E.V. Richardson. Jour. Hyd. Div. ASCE 87(HY1); 246-257.
- TURNER, A.K., 1969. The GCARS system Fortran IV programmers manual. Part C - programs for contour mapping. Joint Highway Research Project, Purdue University, Lafayette, Indiana.
- VANONI, V.A. & HWANG, L., 1967. Relation between bed forms and friction in streams. Jour. Hyd. Div. ASCE 93(HY3); 121-144.
- WOO, D., 1956. Study of overland flow. Ph.D. Dissertation, Univ. of Mich., Ann Arbor, Mich.

- WOODING, H.A., 1965. A hydraulic model for the catchment-stream problem. 1 Kinematic wave theory. Jour. of Hydrol. (Holland) 3; 254-267.
- WOOLHISER, D.A. & LICGETT, J.A., 1967. Unsteady one-dimensional flow over a plane - the rising hydrograph. Water Resources Res. 3(3); 753-771.
- YEVDJEVICH, V.M., 1960. Bibliography and discussion of flood routing methods and unsteady flow in channels. Geol. Sur. Water Supply Paper No. 1690.
- YU, Y.S. & McNOWN, J.S., 1964. Runoff from impervious surfaces. Jour. of Hydrol. Res. 2(1); 3-24.

APPENDICES

APPENDIX A

CALIBRATION OF THE MICRO-RELIEF METER

The micro-relief meter described and presented in Chapter IV was calibrated on a level block of polished marble. Calibrations were carried out prior to use on each of Bed 3 and Bed 4. These calibrations established the relationship between position on the LVDT probe and voltage output from the demodulator circuit (shown in Figure 8), and the position correction required due to imperfections and deflections in the component support members. In addition adjustments to the micro-relief meter were carried out prior to calibration and at regular intervals between periods of use to ensure the components parts were in correct alignment.

Voltage-Elevation Calibration of the LVDT

The micro-relief meter was levelled in a position such that the tip of the probe, in fully extended position, remained above the level of the table. A milled plexiglas step block with step heights of 1/10 in. ($\pm 5 \times 10^{-3}$ in.) was then used to obtain 10 sets of voltage-elevation calibration data values by reading alternately in increasing and decreasing elevation directions. The probe carriage remained in position and the step block was moved to preclude confounding with position variation.

Two sets of calibration data (coded CA01 and CA02) taken prior to use of the instrument on Bed 3 and Bed 4 respectively, are presented in summary form in Table A-1. A four-digit DVM was used to record the voltage values.

The lack-of-fit standard error, obtained from the pooled sum of the variances, rejecting the extreme value beyond -2.5 volts in each of CA01 and CA02, was .00064 in. for data set CA01 and .00042 in. for data set CA02. The decreased range evidenced by set CA02 was due to modifications to the equipment which improved reliability performance at

the expense of limiting the available range.

Table A-1. Voltage-elevation calibration data for LVDT

Elevation above table (in.)	GAO1			GAO2		
	Voltage (10 sets)			Voltage (10 sets)		
	Average	Standard Error Volts	in.	Average	Standard Error Volts	in.
.530	2.187	.0018	.0009			
.630	1.981	.0022	.0010			
.730	1.760	.0015	.0006	1.717	.0007	.0002
.830	1.476	.0008	.0003	1.423	.0012	.0004
.930	1.133	.0011	.0003	1.086	.0011	.0003
1.030	0.772	.0006	.0002	.6451	.0006	.0002
1.130	.4033	.0015	.0004	.2435	.0011	.0003
1.230	.0383	.0007	.0002	-.1631	.0012	.0003
1.330	-.3378	.0012	.0003	-.5892	.0010	.0002
1.430	-.7191	.0041	.0010	-1.071	.0019	.0004
1.530	-1.129	.0022	.0005	-1.447	.0027	.0007
1.630	-1.530	.0010	.0003	-1.808	.0014	.0004
1.730	-1.891	.0013	.0004	-2.113	.0019	.0007
1.830	-2.184	.0015	.0005	-2.370	.0015	.0006
1.930	-2.439	.0022	.0013	-2.577	.0052	.0025
2.030	-2.513	.0064	.0086			

The conversion of standard error in volts to equivalent inches was made by use of numerical differentiation on the data set. The two sets of calibration data are illustrated in Figure A-1. The difference in slope between the two calibration curves is due to a difference in settings on the demodulator unit.

Calibration results indicated an inherent non-linear behaviour in the LVDT which was particularly marked beyond the nominal 1 in. range. Since it was desirable to extend the usable range beyond 1 in., and no simple equation could be found to accurately fit the calibration set, conversion of recorded data (program CCNV - Appendix E refers) was accomplished by linear interpolation.

The extreme values of data set GAO1 indicated a marked quadratic effect and an error analysis was made to determine the maximum difference obtained by conversion using linear interpolation as against the use of a quadratic equation fitted through each set of three extreme

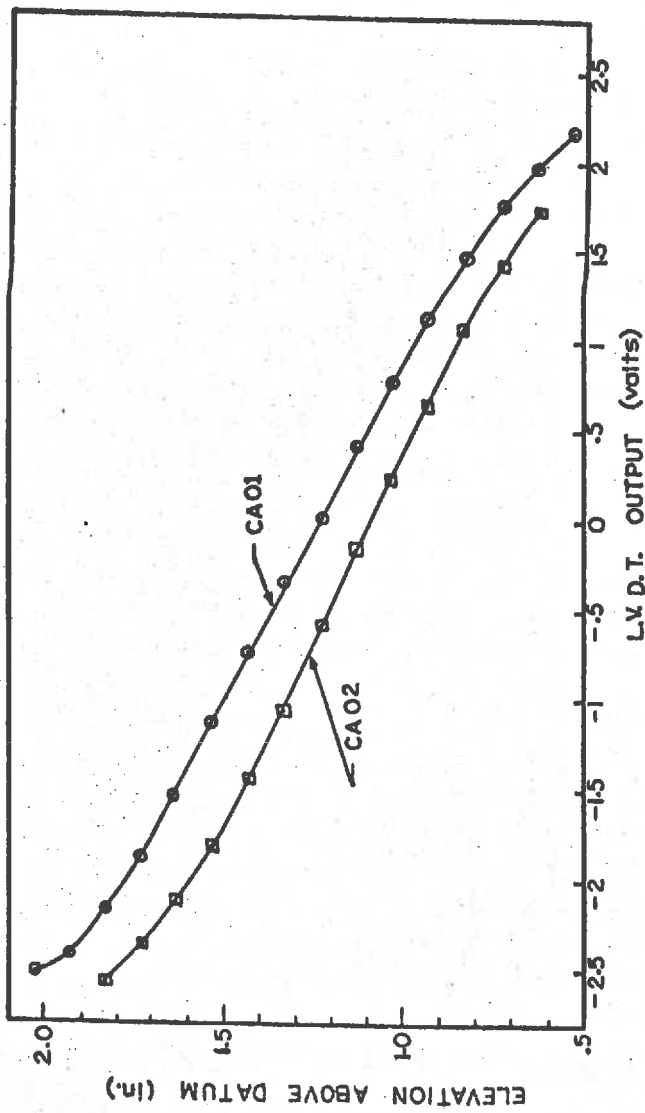


Figure A-1. Voltage-elevation calibration sets CA01 and CA02

points. The analysis is presented below using the technique of Lagrange interpolating polynomials (Carnahan, Luther and Wilkes, 1969):

- (i) For the data set (V, E_1) of (1.760 , 0.730), (1.981 , 0.630) (2.187 , 0.530) the interpolating polynomial is

$$E_1 = 1.238 - 0.1437 V - 0.08228 V^2. \quad (A.1)$$

A linear equation fitted to the two extreme (latter) points gave,

$$E_1 = 1.594 - 0.4866 V. \quad (A.2)$$

By subtraction, deviation

$$\Delta E_1 = 0.08228 V^2 + 0.3429 V - 0.3565, \quad (A.3)$$

and equating $\frac{d}{dV} (\Delta E_1) = 0.1646 V + .3429,$

to zero gave the maximum difference at $V = 2.084$. From equation (A.3)

$$\Delta E_1 = .00078 \text{ in.}$$

This value was close to the estimated error of calibration and a linear interpolation was therefore considered adequate.

- (ii) In a similar manner, for data at the other extreme of the range, the maximum difference between a quadratic equation through the extreme points and a linear interpolation on the two extreme points was 0.004 in. In terms of an estimate of overall accuracy, discussed below, this value was relatively high and for this reason, readings between -2.439 volts and -2.513 volts were converted to inches by use of a quadratic equation through the three extreme points.

Calibration set CA02 exhibited a smaller non-linear effect at the extremes and the use of fitted quadratic equations was not warranted. Linear interpolation was however again employed in using this calibration set.

Calibration for Effect of Probe Position

The micro-relief meter was levelled in a position such that the LVDT probe was in close proximity to its null position. This was to ensure the most linear response. A set of readings was then taken at

SAB CONTOURS GRID CALIBRATION GC1

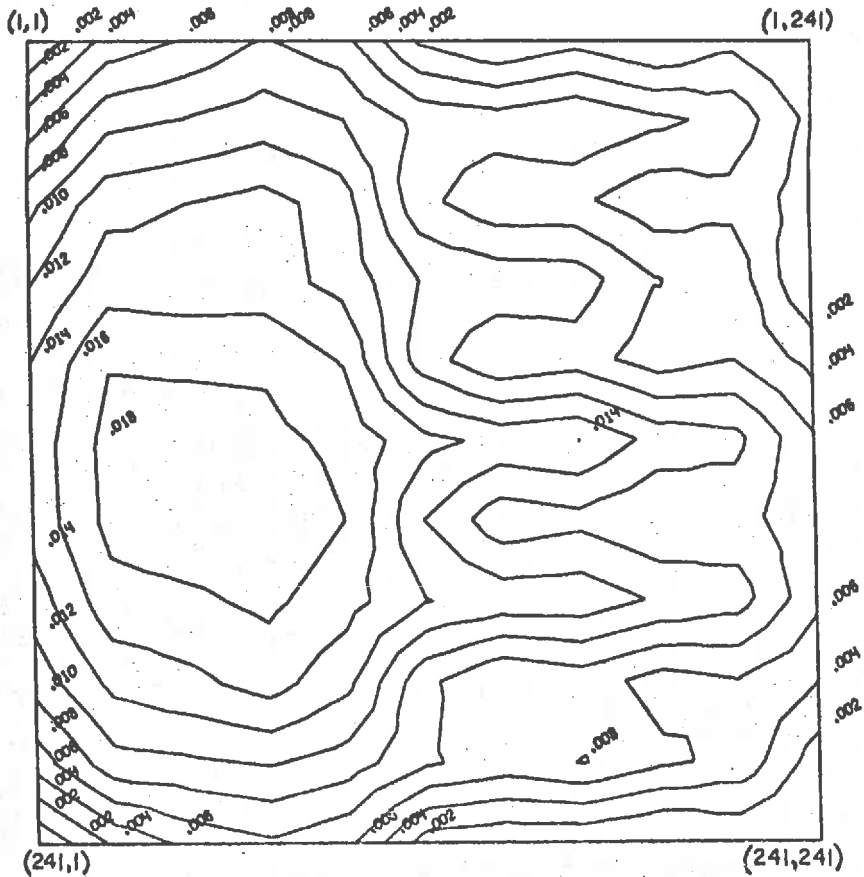


Figure A-2. Contour map showing position displacement below a level plane obtained from calibration set GC1

SAB CONTOURS GRID CALIBRATION GC2

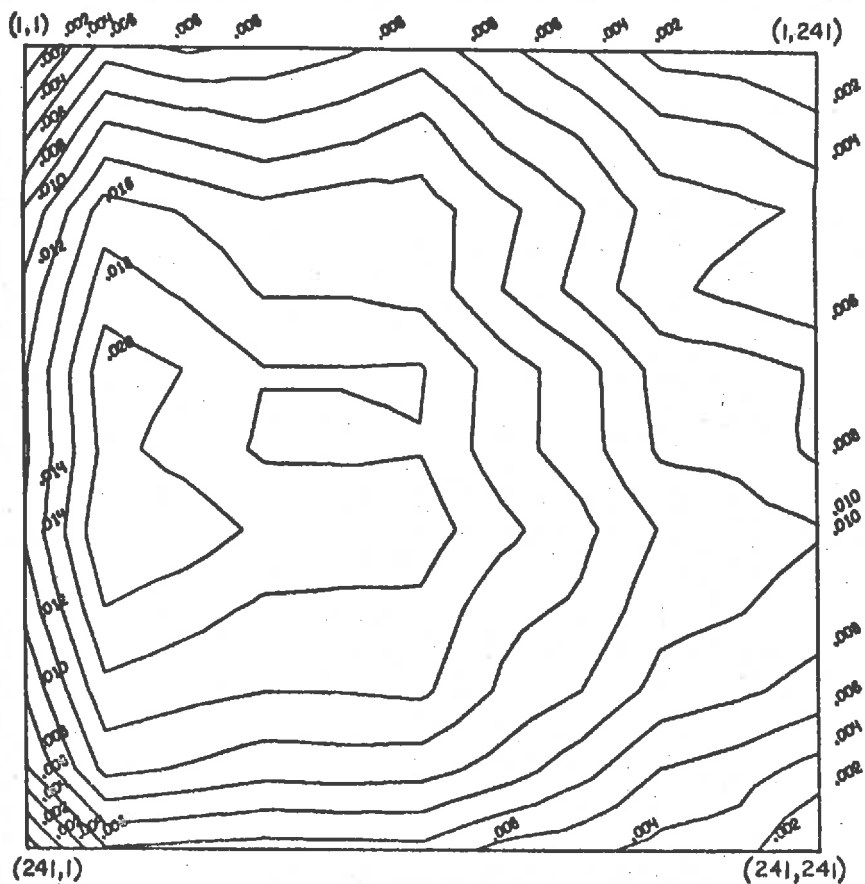


Figure A-3. Contour map showing position displacement below a level plane obtained from calibration set GC2

each 24th position (spacing of 24×0.098 in.) along and perpendicular to the cross-carriage. An 11×11 matrix set of position effect readings then sampled the possible set of 241×241 data reading positions.

The micro-relief meter was 'broken-up', re-levelled and a second set of readings taken at the same positions.

In analyzing the data the reading at the starting position (1,1) was subtracted from all other values for each set, average values obtained for each position, and an associated standard error calculated.

The above procedure was carried out prior to use on each of Bed 3 and Bed 4. The standard error associated with the grid calibration used for analysis of data obtained on Bed 3 was 0.0016 in. This calibration set was denoted as GC1, and is illustrated in contour form in Figure A-2. A position calibration was again carried out prior to recording data on Bed 4. This set was denoted as GC2, had an associated standard error of 0.0013 in. and is illustrated in contour form in Figure A-3. These values included the effects of error due to instrument repeatability, which however was relatively negligible at the null point. These position calibration errors then reflect a measure of the ability to level the instrument.

Position effects tended to be relatively large in relation to the range and error of recording and were removed from a recorded data set by using two-way linear interpolation.

APPENDIX B

OPERATION AND CONTROL OF THE MICRO-RELIEF METER

Prior to the use of the micro-relief meter, the rainfall simulator bed was levelled and the instrument was set up over the area to be mapped. The position of each of the four legs was marked on the bed and holes were drilled in the center of each of these markings. A 1 in. length of 1/8 in. brass rod was glued in each hole leaving a short section protruding above the bed surface. The micro-relief meter was then later set up over the protrusions, each of which fitted into a hole in the underside of a leg and served to steady the instrument by preventing lateral movement. The micro-relief meter was levelled and the probe set in position (1,1).

The micro-relief meter operated under fully automatic control of the Digital Expansion System of an analog-hybrid computer. The logic circuit, designed to operate on a clock frequency of 1 Kc/sec, is presented in Figure B-1 and its operation described below.

The logic control program, started by depressing push-button D, recorded the voltage (on multiplex channel MX1) corresponding to the probe elevation at position (1,1), on magnetic tape as a 6 character field representing a sign plus 5 digits (volts $\times 10^3$). Multiplex channel MX1 was only addressed for sufficient time to enable the ADC conversion to be made and transferred to the data buffer. A high signal on BBY (buffer busy) indicated the completion of this operation when associated with an acknowledge (ACK) high indicating reference to the front patch panel. A write complete (WC) blip in association with ACK high indicated the transfer of the reading to the magnetic tape and provided the signal initiating movement of the probe to the next position. In general print time, between ADC and WC blips, occupied about 12ms. but could take up to 600ms. depending upon the timing and nature of requests from priority interrupt users of the time-shared computer system.

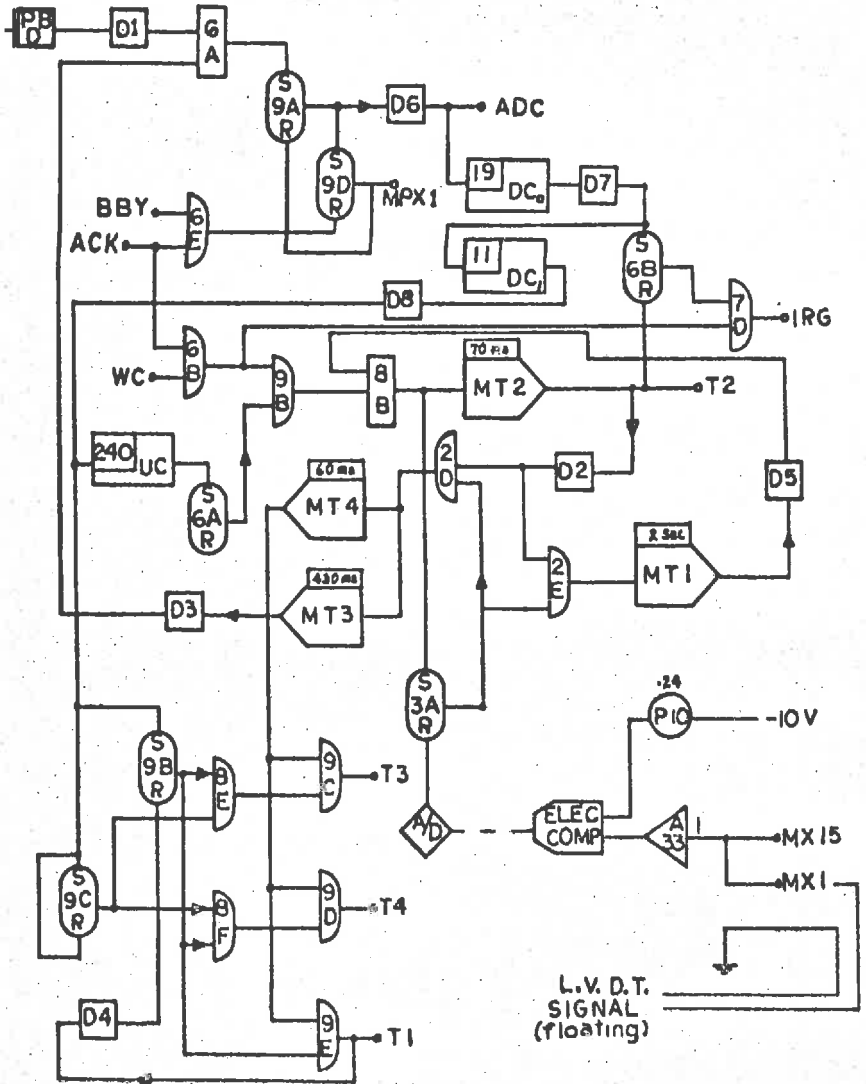


Figure B-1. Logic control circuit for operation of, and recording from, the micro-relief meter

The WC blip activated monotime 2 (MT2) and a 70 ms. pulse was transmitted over trunk line T2 energizing the solenoid to lift the probe. During this period the LVDT signal was monitored, using an electronic comparator, to ensure the probe had lifted above a pre-selected elevation. This precaution prevented damage to the probe by precluding movement of the probe carriage, or cross-carriage, with the probe still in the down position. A negative response resulted in a 2 sec. time delay, to allow cooling of the power transistor, and was followed by a second 70 ms. pulse to the probe solenoid. Repetition occurred until a positive response was obtained. The trailing edge of the pulse on T2 activated monotime MT3 and MT4, with the latter transmitting a 60 ms. pulse over trunk line T4 enabling the probe carriage to move one position along the cross-carriage.

Monotime MT3 controlled the time delay following the trailing edge of the pulse energizing the probe solenoid until the following request for an ADC conversion. This time period included the time required for the probe to fall to the surface under the action of gravity in position (1,2) and for transients in the signal to fade. From oscilloscope observations a time period of 430 ms. was selected. A second reading was then recorded and the probe moved on to the next position (1,3) as described above. An inter-record gap (IRG), occupying 250 ms., was inserted after each 20 readings.

Following the 240th recording along the cross-carriage, the next pulse activating position movement was transmitted along T1 to the cross-carriage. The following sequence of 240 pulses were then transmitted along T3 causing the probe carriage to reverse direction along the cross-carriage.

The above sequence continued until the probe carriage had moved back-and-forth along the cross-carriage covering 240 positions of the cross-carriage. The control program then automatically stopped on the setting of flip-flop 6A.

APPENDIX C

CALIBRATION OF THE RAINFALL SIMULATOR

Three separate calibrations were carried out on the rainfall simulator. These consisted of the calibration of the bed weight signal, the weighing trough or mass runoff signal, and the electronic differentiator, used to obtain the runoff rate signal. In calibrating the former two signals known weights were added to the bed and weighing trough in increasing and decreasing magnitude to incorporate hysteresis effects. In the latter case, i.e. the differentiator, a known ramp input signal was used directly on the analog computer patch panel.

The patch panel electronic circuit, shown in Figure D-1, was used with the logic circuit changed to cause a teletype print of the value of the required signal each time a push button was depressed. In this way random values were obtained.

Bed Load Calibration

Known weights were suspended beneath the bed and on the centerline of the section used. Prior trials had shown no apparent relationship between load placement and recording obtained from the summed output of the strain-gauges mounted on the four supporting rods. However, even placement on the centerline was considered to be the most realistic procedure.

Two sets of readings were obtained, each consisting of an increasing and decreasing weight sequence. Starting with a zero load, 10 readings were recorded for each load value. A total of 40 readings were then associated with each weight, and all readings were used in fitting a regression line relating load in pounds weight to the sampled recorded output of amplifier A32 (shown in Figure D-1).

Separate calibrations were carried out prior to running hydraulic tests on each of Bed 3 and Bed 4 and the applicable regression equation

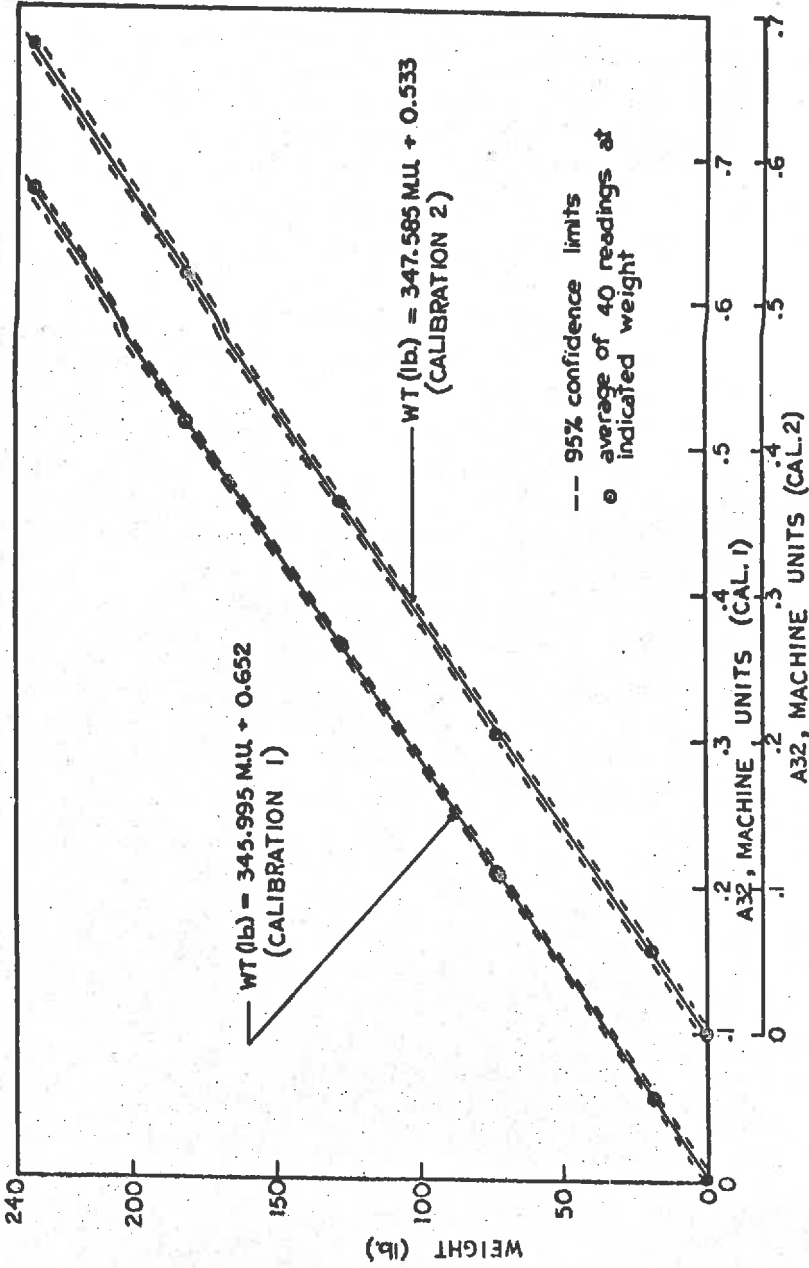


Figure C-1. Bed load calibrations

was used in the analysis of each hydraulic data set. Since only the slope of the regression line was of relevance, the regression equations may be presented as:

$$\text{Weight (lb.)} = 346.0 \text{ Machine Units} \quad (\text{C.1})$$

for Bed 3, and

$$\text{Weight (lb.)} = 347.6 \text{ Machine Units} \quad (\text{C.2})$$

for Bed 4. These regression relationships together with the average reading at each selected weight are presented in Figure C-1.

The former relationship (equation C-1) had an associated standard error of 0.67 lb. and the latter (equation C-2) 1.55 lb. As presented in Figure D-1, however, the basic signal is amplified by a factor of 4000 and is thus subject to considerable noise. A check calibration following the tests on Bed 4 produced a standard error of 1.13 lb. which is considered to be a more realistic average error estimate.

The bed area measured 13.854 ft. by 6.867 ft. or 95.135 sq.ft. The standard error value of 1.13 lb. then converts to an average depth value of 0.00193 in. of water over the bed surface.

Mass Runoff Calibration

The weighing trough at the lower end of the flow plane was supported by two aluminium cantilever beams on each of which a pair of strain gauges were mounted. The output signal reflected the combined effect of both sets of strain gauges, and was monitored as the output of amplifier A28, shown in Figure D-1.

In a similar manner to that described above, for calibrating the bed load, known weights were added to, and removed from, the weighing trough. Again two sets of increasing and decreasing load values were used with 10 random readings taken for each load value, i.e. a total of 40 readings was associated with each weight.

The above calibration procedure was carried out prior to running hydraulic tests on each of Bed 3 and Bed 4. The resultant regression lines are presented in Figure C-2. Only the slopes of the regression lines were of relevance, the first calibration yielding

$$\text{Weight (lb.)} = 509.4 \text{ Machine Units} \quad (\text{C.3})$$

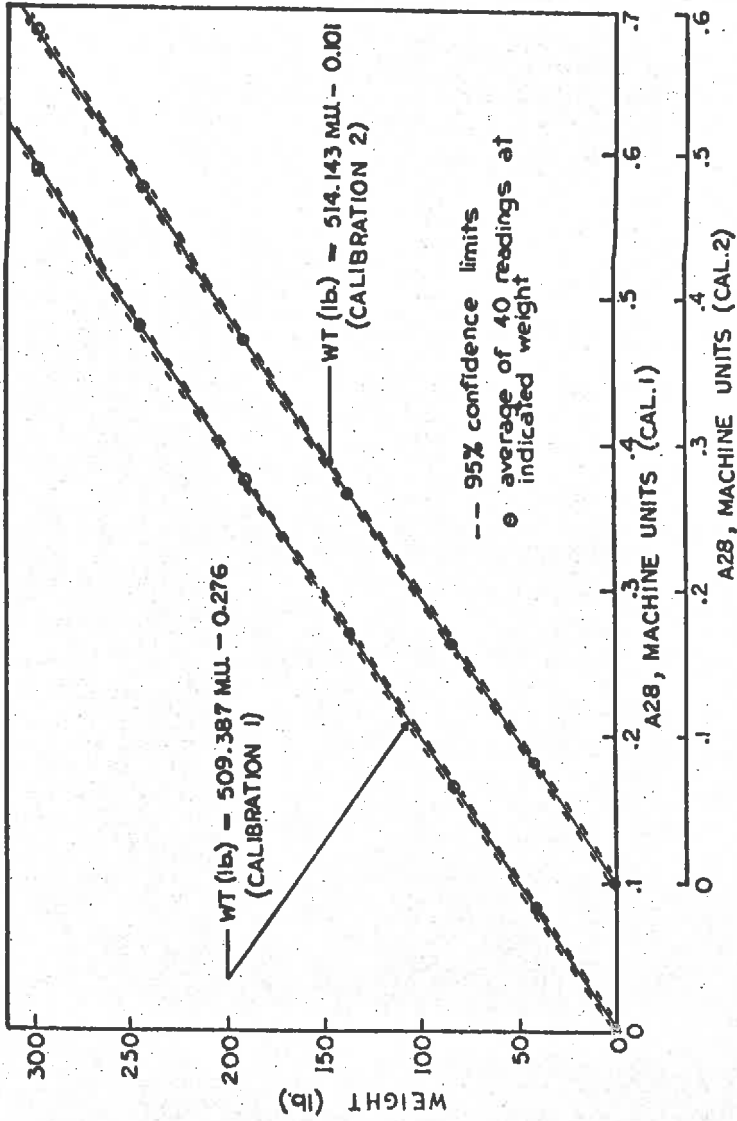


Figure C-2. Mass runoff calibrations

with a standard error of 0.67 lb. and was used in the analysis of data for the hydraulic tests on Bed 3. The second calibration, prior to the running of hydraulic tests on Bed 4, and used in the data analysis, yielded

$$\text{Weight (lb.)} = 514.1 \text{ Machine Units} \quad (\text{C.4})$$

with a standard error of 0.65 lb.

Changes in the calibration coefficient was due to realignment and adjustments made to the cantilever beams.

Combining the error variances, and converting to average depth of water on the bed, yields an estimate of error of 0.00133 in. water.

Runoff Rate Calibration

The differentiator circuit, associated with amplifier A6 in Figure D-1, was calibrated using a ramp input to amplifier A18. The ramp input was obtained by integration of a preset voltage and a relationship then obtained between the voltage setting (or ramp slope) and the differentiator output. Four voltage settings were selected and ten random readings taken at each setting with the procedure repeated twice in increasing and decreasing directions for each calibration. The resultant regression equations are presented in Figure C-3. The first calibration, used in the analysis of data from Bed 3 produced the regression relationship,

$$\begin{aligned} \text{Ramp input slope (M.U.)} &= 0.0270 \text{ Differentiator} \\ &\text{output (M.U.)} \end{aligned} \quad (\text{C.5})$$

with a standard error of 0.000068 M.U.

In conjunction with the mass runoff relationship (equation C-3),

$$\text{Runoff rate} = 0.0270 \times 509.4 \text{ (lb./sec.)/M.U.}$$

or, in in./hr. units,

$$\begin{aligned} \text{Runoff rate} &= \frac{0.0270 \times 509.4 \times 43200}{95.135 \times 62.4} \\ &= 100.2 \text{ (in./hr.)/M.U.} \end{aligned} \quad (\text{C.6})$$

Similarly, the second calibration, prior to the hydraulic tests on Bed 4 yielded a regression equation

$$\begin{aligned} \text{Ramp input slope (M.U.)} &= 0.0275 \text{ Differentiator} \\ &\text{output (M.U.)} \end{aligned} \quad (\text{C.7})$$

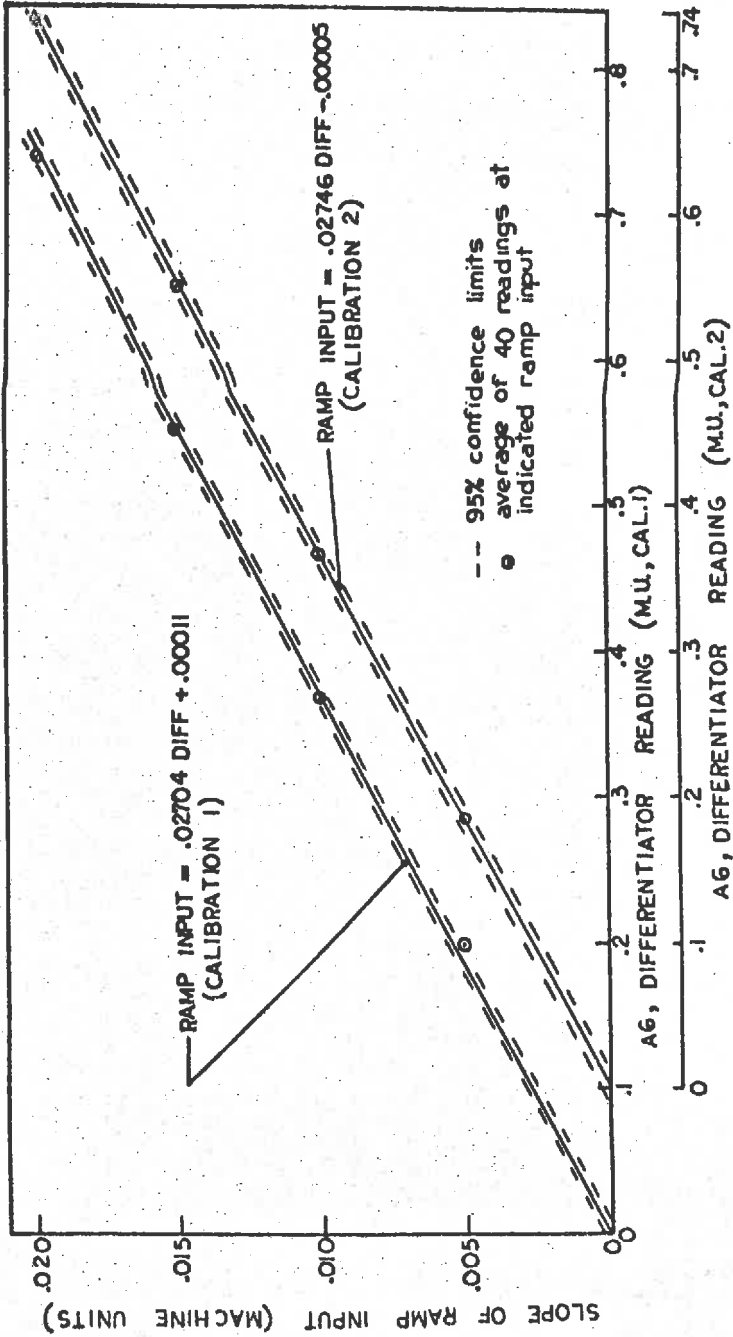


Figure C-3. Differentiator calibrations

with a standard error of 0.000057 M.U.

The runoff rate relationship, in conjunction with equation C-4, was therefore

$$\text{Runoff rate} = 102.7 \text{ (in./hr.)}/\text{M.U.} \quad (\text{C.8})$$

APPENDIX D

RAINFALL SIMULATOR LOGIC CONTROL PROGRAM

The rainfall simulator operated in a semi-automatic mode, in that local controls could be used to over-ride the rainfall and overland flow controls. This over-ride was used in applying rainfall or overland flow alone following a combined application.

The control program, which operated on a clock frequency of 1 Kc/sec., is presented in Figure D-1 together with the analog gain and filter circuit. Activation of this program was accomplished by pressing either push-button D at the patch-panel or a push-button in the laboratory. In practice the latter was used, push-button D being used only in checking out the operation of the control program. Flip-flop 3A set, followed by the on-clock setting of flip-flop 3C and the sequential printing on magnetic tape of the mass flow signal (M8), the runoff rate signal (M9) and the bed weight signal (M10). Each of these signals was stored at the on-clock values (at 1 c/sec. frequency) in track-hold amplifiers until completion of the print operation, to obtain on-clock readings at 1 second intervals even if requests by priority interrupt users delayed acknowledgement of the print requests by up to 600ms. The second and third ADC requests followed immediately upon completion of the prior request (signalled by a high blip from WC, write complete) to prevent other slower users of lower priority from intervening. Multiplex channels were readdressed on the BBY (buffer busy) blip which signalled the completion of the storage of the requested analog to digital conversion in the data buffer. The third BBY blip in each print sequence reset flip-flop 3C and the WC blip following caused the insertion of an inter-record gap (IRG) on the magnetic tape. Each data value consisted of a 6 character field (sign plus 5 digits representing volts $\times 10^3$ or machine units $\times 10^4$). Each

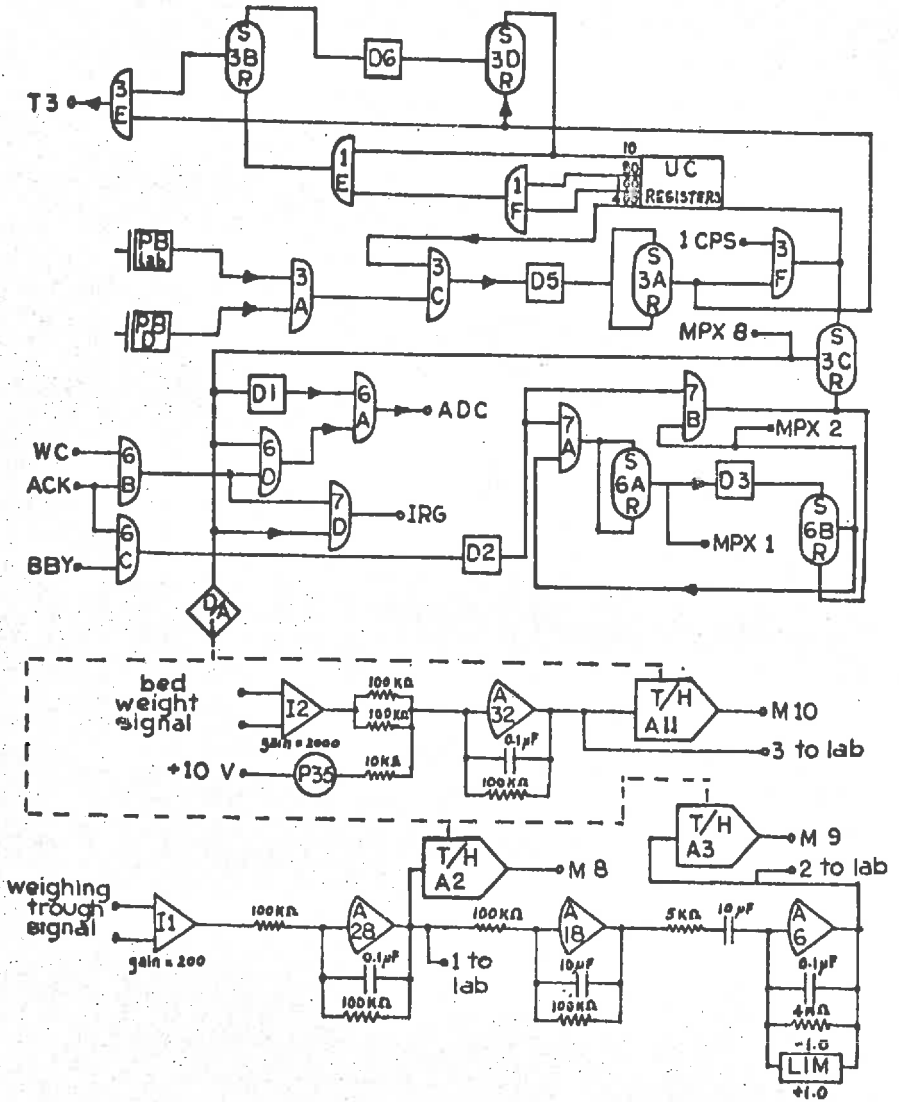


Figure D-1. Circuit for control, filtering and recording of hydraulic test data

record contained only 18 characters with a resultant inefficient usage of magnetic tape storage. However this system was preferred as a safeguard against a large block loss of information (generally 1 PRU) caused by occasional tape imperfections and resultant parity errors.

Flip-flop 3A provided the central memory control and, while set, enabled sequential sets of 3 data values to be recorded per second. A test run could be aborted at any stage by again pressing one of the push-buttons and causing flip-flop 3A to reset.

Ten sets of initial data values were recorded (as selected on the up-counter registers) prior to activation of rainfall and/or overland flow via a signal on trunk line T3. Trunk line T3 went low (+3.6 v) during rainfall and/or overland flow application and remained in this condition until a time period, generally 130 or 190 seconds after depressing the push-button, and pre-selected on the up-counter, had elapsed. Trunk line T3 then went high (0 v) causing the rainfall and/or overland flow to stop. Recording of the 3 analog signals continued until the up-counter registered a count of 400 data sets. Flip-flop 3A then reset, signalling the end of the test run.

APPENDIX B

LISTING OF COMPUTER PROGRAM CONV

PROGRAM CONV (INPUT, OUTPUT, TAPES=INPUT, TAPE6=OUTPUT, TAPE1, TAPE2)

CONVERSION OF ELEVATION MATRIX IN MACHINE UNITS TO ELEVATIONS
IN HEIGHT ABOVE IMPLIED DATUM PLANE

OUTPUT DATA FROM THE L.V.D.T. ON THE MICRO RELIEF METER IS RECORDED AS MACHINE UNITS (1 M.U. = 10 VOLTS) IN BCD FORM ON DIGITAL MAGNETIC TAPE. PROGRAM CONV SEQUENTIALLY READS BLOCKS OF UP TO 24 ROWS (TO PRECLUDE THE NECESSITY FOR A LARGE BLOCK OF CENTRAL MEMORY CORE STORAGE). EACH VALUE IS CONVERTED TO INCHES BY LINEAR INTERPOLATION ON THE L.V.D.T. CALIBRATION SET. TWO-WAY LINEAR INTERPOLATION IS THEN PERFORMED ON A MATRIX OF POSITION CALIBRATION VALUES READ ON 24 COLUMN AND 24 ROW SPACINGS. EACH RECORDED VALUE IS THEN CORRECTED FOR POSITION.

OPTIONS

THE FOLLOWING INPUT-OUTPUT OPTIONS ARE AVAILABLE,

- (A) INPUT DATA MAY BE READ FROM CARDS OR 9CD TAPE (FORMAT 109)
- (B) OUTPUT OF THE FINAL DATA MATRIX MAY BE RECORDED IN BCD FORM (FORMAT 115), OR IN UNFORMATTED FORM RECORDING TWO ROWS PER P.R.U.
- (C) LINE PRINTER OPTIONS INCLUDE PRINTS OF THE FOLLOWING,
 - (1) THE VOLTAGE-ELEVATION CALIBRATION DATA READ AS INPUT
 - (2) THE POSITION CORRECTION CALIBRATION MATRIX READ AS INPUT
 - (3) A SECTION OF THE RAW DATA MATRIX IN VOLTS. THIS SECTION MUST BE SELECTED WHOLLY FROM WITHIN ONE OF THE 24 ROW BLOCKS.
 - (4) THE SAME SECTION SELECTED ABOVE, APPLIED TO THE RAW DATA MATRIX IN INCHES
 - (5) THE SAME SECTION OF THE FINAL CALIBRATED MATRIX.

INPUT CARDS

(A = ALPHANUMERIC, I = INTEGER, F = FLOATING POINT, PUNCH DECIMAL)
CARD 1
COLUMNS

1-5

NX = NUMBER OF ROWS IN RAW DATA MATRIX

(1)

C 6-10 NY = NUMBER OF COLUMNS IN RAW DATA MATRIX (I)
 C 11-15 IC = NUMBER OF VOLTS-INCHES CALIBRATION POINTS (I)
 C 16-20 IKG = NUMBER OF READINGS PER P.R.U. ON INTAPE (I)
 C 21-25 INTAPE = 1 IF UCD TAPE, OR (I)
 C = 5 IF CARDS ARE USED FOR INPUT (I)
 C 26-30 IOUTAP = 2 IF UCD OR BINARY TAPE, OR (I)
 C = 7 IF PUNCHED CARDS ARE DESIRED AS OUTPUT (I)
 C 31-35 IWT = NUMBER OF VALUES PER P.R.U. ON IOUTAP (I)
 C 36-40 C = IDENTIFICATION FOR VOLTS-INCHES CALIBRATION DATA (A)
 C USED
 C 41-45 G = IDENTIFICATION FOR POSITION CALIBRATION DATA (A)
 C USED
 C 46-50 IPT(1) = 00000 FOR NO PRINT OF VOLTS-INCHES CALIBRATION (I)
 C DATA USED (I)
 C 51-55 IPT(2) = 00000 FOR NO PRINT OF THE POSITION CALIBRATION (I)
 C DATA USED (I)
 C 56-60 IPT(3) = 00000 FOR NO PRINT OF SECTION OF RAW DATA MATRIX (I)
 C IN VLTS (I)
 C 61-65 IPT(4) = 00000 FOR NO PRINT OF SECTION OF RAW DATA MATRIX (I)
 C IN INCHES (I)
 C 66-70 IPT(5) = 00000 FOR NO PRINT OF SECTION OF FINAL MATRIX (I)
 C 71-75 NTO = 1 FOR NO CARD OR TAPE OUTPUT, (I)
 C = 2 FOR UCD TAPE OR CARD OUTPUT, (I)
 C = 3 FOR BINARY TAPE OUTPUT. (I)

CARD 2

(NOTE, COLUMNS 1 THROUGH 25 REFER TO OUTPUT OPTION B (3))

ABOVE AND MAY BE BLANK IF IPT(3,4,5) ARE ALL = 0)

C 1-5 N1 = FIRST MATRIX SECTION COLUMN PRINTED (I)
 C 6-10 N2 = LAST MATRIX COLUMN PRINTED (I)
 C 11-15 N3 = FIRST MATRIX ROW PRINTED (I)
 C 16-20 N4 = LAST MATRIX ROW PRINTED (I)
 C 21-25 MK = BLOCK NUMBER WHERE PRINT REQUESTED (I)
 C 26-30 POS = POSITION IDENTIFICATION NUMBER ON SURFACE (I)
 C 31-35 FILE = FILE NUMBER ON IOUTAP (I)
 C 36-40 SUR = SURFACE IDENTIFICATION (A)
 C 41-45 TAPE = IOUTAP IDENTIFICATION (A)

CARD 3

VOLTAGE READINGS FOR VOLTAGE-ELEVATION CALIBRATION DATA (PLUS TO MINUS SEQUENCE). FORMAT 101 APPLIES. (F)

CARD 4

ELEVATION VALUES CORRESPONDING TO VOLTAGE VALUES ON CARD 3 ALSO ACCORDING TO FORMAT 101. REPEAT CARDS 3 AND 4 AS REQUIRED. (F)

CARD 5

POSITION CALIBRATION DATA READ IN AS ONE ROW PER CARD ACCORDING TO FORMAT 115. REPEAT CARDS AS REQUIRED. (F)

CARD 6

RAW DATA MATRIX IF INPUT ON CARDS. FORMAT 109 APPLIES. (F)

 COMMON M(24,24), SC(11,11), PA
 DIMENSION V(23), CH(24), IPT(5), EN(24,24), SH(24,24), REJ(1,24)
 EQUIVALENCE(M(1,1), FH(1,1), SH(1,1))

.....READ IN WITH CHECK OUTPUT.....

READ(5,100) NX,NY,IC,IRG,INTAPE,IOUTAP,IWT,C,G,(IPT(I),I=1,5),NTO
 READ(5,100) N1, N2, N3, N4, MK, POS, FILE, SUR, TAPE
 WRITE(6,117) SUR, POS
 WRITE(6,116) N4,NY,C,G,INTAPE,IOUTAP,IRG,IWT,FILE,TAPE
 DO 10 I=1,IC,4

```

11 = I+7
READ(5,101) (V(J), J=I,11)
10 READ(5,101) (C(I,J), J=I,11)
IF(IPT(1).EQ.0) GO TO 12
WRITE(6,102)
DO 11 I=1,IC,1)
II = I+9
IF(II.GT.IC) II=IC
WRITE(6,103) (V(J),J=I,11)
11 WRITE(6,104) (C(I,J), J=I,11)
12 READ(5,105) ((IC(I,J), J=1,11), I=1,11)
IF(IPT(2).EQ.0) GO TO 13
WRITE(6,106)
CALL W(ITER(1,1,11,1,11))
13 NA = (IX-1)/24 + 1

```

CCCCTREAT RAW DATA MATRIX IN BLOCKS OF 24 ROWS MAXIMUM.....

```

DC 45 MA=1,NA
NB = NY - (MA-1)*24
IF(NB.GT.24) N3=24
DO 14 I=1,NB
DO 14 J=1,NY,IC
JJ = J+IC-1
IF(JJ.GT.NY) JJ=NY
14 READ(I,TAPE,103) (H(I,JL), JL=J,JJ)
.....REVERSE ORDER ON ALTERNATE ROWS.....
DO 20 I=2,NB,2
DO 21 J=1,NY
21 REJ(I,J) = H(I,J)
DO 20 J=1,NY
K = NY + 1 - J
20 H(I,J) = REJ(I,K)
IF(IPT(3).EQ.0.OR.PK.NE.MA) GO TO 15
WRITE(6,105)
CALL W(ITER(2,1,1,N2,N3,N4))

```

CCCCCHECK FOR READINGS OUTSIDE CALIBRATION RANGE.....

```

15 I = (MA-1)*24 + 1
J = I + NB - 1
WRITE(6,107) I, J
IT = 0
DO 17 I=1,NB
DO 17 J=1,NY
IF(H(I,J).LE.V(1).AND.H(I,J).GE.V(IC)) GO TO 17
IT = 1
IX = (MA-1)*24 + I
WRITE(6,111) IX, J, H(I,J)
IF(IJ.NE.1) GO TO 34
J1 = 2
GO TO 35
34 J1 = J-1
IF(IJ.NE.NY) GO TO 35
J2 = NY-1
GO TO 36
35 J2 = J+1
36 H(I,J) = (H(I,J1)+H(I,J2))/2.
IF(H(I,J).LE.V(1).AND.H(I,J).GE.V(IC)) GO TO 37
IF(H(I,J).GT.V(1)) EH(I,J) = V(1)
IF(H(I,J).LT.V(IC)) EH(I,J) = V(IC)

```

```

WRITE(6,111) E4(I,J)
GO TO 17
37 WRITE(6,112) 4(I,J)
17 CONTINUE
IF(IIT.EQ.0) WRITE(6,110)

```

C
C
C

.....LINEAR INTERPOLATION H.U. TO HEIGHT.....

```

DO 30 I=1,NB
DO 30 J=1,NY
DO 18 L=2,IC
IF(M(I,J).GT.V(L)) GO TO 38
18 CONTINUE
38 L1 = L-1
EH(I,J) = (H(L1)-(CM(L1)-CH(L1))*(H(I,J)-V(L1))/(V(L1)-V(L1)))
20 CONTINUE
IF(IPT(4).EQ.0.OR.PK.NE.MA) GO TO 40
WRITE(6,113)
CALL WRITER(2,N1,N2,N3,N4)

```

C
C
C

.....CORRECTION FOR ERROR IN P.M.D. BY 2-WAY LINEAR INTERPOLATION.

```

40 I1 = MA+1
DO 43 I=1,NB
DO 43 J=1,NY
J1 = (J-1)/24 + 1
J2 = J1-1
J3 = J1+1
A = SC(MA,J1) + FLCAT(I-1)*(SC(I1,J1)-SC(MA,J1))/24.
B = SC(MA,J3) + FLCAT(I-1)*(SC(I1,J3)-SC(MA,J3))/24.
43 SH(I,J) = EH(I,J)+FLOAT(J-1-24*J2)*(B-A)/24.*A
IF(IPT(5).EQ.0.OR.PK.NE.MA) GO TO 50
WRITE(6,114)
CALL WRITER(2,N1,N2,N3,N4)
50 GO TO (45,46,47) NTO

```

C
C
C

.....FORMATTED OUTPUT ON TAPE.....

```

46 DO 44 I=1,NB
DO 44 J=1,NY,I4T
JJ = J+INT-1
IF(IJ.GT.NY) JJ=NY
44 WRITE(IOUTAP,115) (SH(I,JL), JL=J,JJ)
GO TO 45

```

C
C
C

.....UNFORMATTED OUTPUT ON TAPE.....

```

47 DO 48 I=1,NB,2
II = I + 1
48 WRITE(IOUTAP) ((SH(L,J), J=1,NY), L=I,II)
45 CONTINUE
130 FORMAT(7I5,2A5,6I5)
101 FORMAT(8F10.4)
102 FORMAT(10X,#TIME VOLTAGE-HEIGHT CALIBRATION DATA#)
103 FORMAT(2X,#VOLTAGE#,1CF10.4)
104 FORMAT(2X,#HEIGHT#,1CF10.3)
105 FORMAT(11F7.4)
106 FORMAT(//10X,#TIME SAG GRID IN INCHES#)
107 FORMAT(//10X,#DATA VALUES OUTSIDE CALIBRATION RANGE IN ROWS#,I4,
# 10F,14/ )
108 FORMAT(//10X,#SECTION OF RAW DATA MATRIX IN VOLTS#)

```



```

109 FORMAT(2G6.3)
110 FORMAT(10X, #ENDING I =#, I3, # J =#, I3, # IS OUT OF RANGE AT #, F9.4)
111 FORMAT(10X, #CALIBRATION LIMIT VALUE#, F9.4, # VOLTS ASSUMED##)
112 FORMAT(10X, #SMOOTHED TO #, F8.4, # VOLTS##)
113 FORMAT(///10X, #SECTION OF DATA MATRIX CONVERTED TO INCHES##)
114 FORMAT(///10X, #SECTION OF FINAL ELEVATION MATRIX##)
115 FORMAT(2G6.3)
116 FORMAT(10X, #ELEVATION MATRIX HAS#, I4, # ROWS AND#, I4, # COLUMNS#
#10X, #CALIBRATION DATA SET#, A5, # GRID#, A5/10X, #INPUT ON TAPE#, I3, #
#WITH OUTPUT ON TAPE#, I3/10X, #NUMBER OF DATA POINTS BETWEEN IRGS IS
#, I3, # ON INPUT AND#, I4, # ON OUTPUT FILE #, I4, # OF TAPE #, A5 /)
117 FORMAT(1M1, 20X, #CONVERSION OF L.V.C.T. READINGS TO ELEVATIONS ABOVE
#E AN IMPLIED DATUM PLANE## 10X, #SURFACE #, A5, # POSITION #, I3)
118 FORMAT(//10X, #NIL#)
END

```

C
C

```

SUBROUTINE WRITER (IM, I1, I2, I3, I4)
COMMON M(24, 24), SC(11, 11), MA
DIMENSION LAP(15)
IA = 1
N3 = 0
N = 1
N1 = I2 - I1 + 1
N2 = N1
M = I4 - I3 + 1
42 IF (N1.GT.12) G3 TO 40
IA = 0
NN = N1 + N3
GO TO 41
40 NN = N3 + 12
41 DO 31 L=N, NN
IL = L - N + 1
31 LAB(IL) = L + I1 - 1
WRITE(6, 100) (LAB(L), L=1, IL)
N4 = N + I1 - 1
N5 = NN + I1 - 1
GO TO (32, 33) IM
32 DO 21 I=1, M
II = I + I3 - 1
21 WRITE(6, 101) II, (SC(II, J), J=N4, N5)
GO TO 34
33 DO 20 I=1, M
II = I + I3 - 1
IJ = II + (MA - 1) * 24
20 WRITE(6, 101) II, (M(II, J), J=N4, N5)
34 IF (IA.EQ.0) RETURN
N1 = N2 - NN
N3 = NN
N = NN + 1
GO TO 42
100 FORMAT(//2X, 3H//Y, I7, 11Y //)
101 FORMAT(2X, I3, 13F9.4)
END

```

SAMPLE DATA

240	243	13	20	1	2	480	CA02	GC02	1	1	1	1	1	3
10	36	10	20	3	1	157	BED	4	1421					

APPENDIX F

LISTING OF AREA SPECTRAL DENSITY COMPUTER PROGRAM

PROGRAM SPEC (INPUT, OUTPUT, PUNCH, TAPE5=INPUT, TAPE6=OUTPUT, TAPE1, TAPE2, TAPE7=PUNCH)

THREE-DIMENSIONAL POWER SPECTRAL DENSITY PROGRAM

THIS PROGRAM IS A MODIFIED VERSION OF THE ORIGINAL PROGRAM WRITTEN BY BOGDANOFF, KIZIN AND COTE (1966). SUBROUTINE PSGRID IS ESSENTIALLY UNCHANGED WHILE THE MAIN PROGRAM (SPEC) AND SUBROUTINE WRITER HAVE BEEN RE-WRITTEN.

THE PROGRAM IS DESIGNED TO ACCEPT AN INPUT MATRIX ON CARDS (FORMAT 102), BINARY TAPE (2 ROWS PER P.R.U.) OR BCD TAPE (FORMAT 101, 1 ROW PER P.R.U.). A SPECIFIC PORTION OF THIS MATRIX MUST THEN BE SELECTED FOR ANALYSIS BY SPECIFYING THE STARTING ROW AND COLUMN (REFERENCED TO THE INPUT MATRIX) AND DESIGNATING WHETHER EVERY 1, 2, ..., N ROW AND 1, 2, ..., M COLUMN IS TO BE READ. THE SELECTED MATRIX IS RE-INDEXED, IF NECESSARY, WITH ROWS AND COLUMNS RUNNING 1, 2, ...

FORM OF INPUT-OUTPUT

THE INPUT MATRIX IS EXPECTED IN THE FORM GIVEN BELOW (OUTPUT IS IDENTICALLY PRESENTED).

			Y (J)		
		(1,1)	(1,C)	
		
X (I)		(I, J)	
		
		(R,1)	(R,C)	

THE VERTICAL AXIS IS POSITIVE DOWNWARDS AND IS DESIGNATED BY X VARIABLE, AND I SUBSCRIPTS. THE HORIZONTAL AXIS IS POSITIVE TO THE RIGHT AND DESIGNATED BY Y VARIABLES AND J SUBSCRIPTS. FOR EXAMPLE, M(I, J) REFERS TO ROW I POSITIVE DOWNWARDS, COLUMN J POSITIVE TO THE RIGHT.

OPTIONS

- IN ADDITION TO INPUT OPTIONS OTHER OPTIONS INCLUDE,
- (A) THE USE OF A FILTER MATRIX.
- (B) OUTPUT ON A LINE PRINTER TO INCLUDE OR EXCLUDE ANY OF THE FOLLOWING
- (1) THE SPECTRAL SMOOTHING MATRIX.
 - (2) THE FILTER MATRIX.
 - (3) A SPECIFIED SECTION OF THE RE-INDEXED SELECTED MATRIX.
(NOTE - THE SELECTED MATRIX IS RE-INDEXED ON INPUT)
 - (4) A SPECIFIED SECTION OF THE FILTERED, OR PRE-WHITENED, MATRIX.
 - (5) THE COVARIANCE MATRIX.
 - (6) THE RAW SPECTRUM.
 - (7) THE SMOOTHED SPECTRUM.
 - (8) THE LAGGED PRODUCTS OF THE SMOOTHING COEFFICIENTS.
 - (9) THE FOURIER TRANSFORMS OF THE L.P.S.C.
 - (10) THE RE-COLORED SPECTRUM.
- (C) PUNCHED OUTPUT OF THE RE-COLORED SPECTRUM IN ROW FORM ACCORDING TO AN 8E10.1 FORMAT. ONLY THE UPPER HALF-PLANE, X NEGATIVE, IS PUNCHED.

INPUT CARDS

(A = ALPHANUMERIC, I = INTEGER, F = FLOATING POINT, PUNCH DECIMAL)

CARD 1

COLUMNS

1-6	N =	START OR ANYTHING OTHER THAN SPINIS	(A)
7-9	INTAPE =	01 IF INPUT ON BINARY TAPE,	(F)
		02 FOR BCD TAPE, (FORMAT 101 APPLIES),	(F)
		05 FOR CARDS, (FORMAT 102 APPLIES)	(F)
9-10	IPT (1) =	00 IF NO PRINT OF SPECTRAL SMOOTHING MATRIX	(I)
11-12	IPT (2) =	00 IF NO PRINT OF FILTER MATRIX	(I)
13-14	IPT (3) =	00 IF NO PRINT OF SECTION OF SELECTED MATRIX	(I)
15-16	IPT (4) =	00 IF NO PRINT OF SECTION OF FILTERED MATRIX	(I)
17-18	IPT (5) =	00 IF NO PRINT OF COVARIANCE MATRIX	(I)
19-20	IPT (6) =	00 IF NO PRINT OF RAW SPECTRUM	(I)
21-22	IPT (7) =	00 IF NO PRINT OF SMOOTHED SPECTRUM	(I)
23-24	IPT (8) =	00 IF NO PRINT OF LAGGED PRODUCTS OF SMOOTHING COEFFICIENTS	(I)
25-26	IPT (9) =	00 IF NO PRINT OF GAIN MATRIX OF FILTER	(I)
27-28	IPT (10) =	00 IF NO PRINT OF RE-COLORED SPECTRUM	(I)
29-30	IB =	00 IF NO FILTER MATRIX PROVIDED AND USED (NOTE, IF I3 = 00 NO FILTER MATRIX MUST BE INCLUDED ON INPUT, I.E. LEAVE OUT CARDS 7,....,N)	(I)
31-33	NY1 =	NUMBER OF INPUT MATRIX COLUMNS	(I)
34-36	MA =	INPUT MATRIX COLUMN NUMBER WHICH WILL BECOME COLUMN 1 OF SELECTED MATRIX	(I)
37-39	MC =	SPACING OF COLUMNS (E.G. 002 MEANS READ MA AND EVERY SECOND, I.E. SKIP 1, COLUMN OF INPUT MATRIX)	(I)
40-42	M1 =	INPUT MATRIX ROW NUMBER WHICH WILL BECOME ROW 1 OF THE SELECTED MATRIX	(I)
43-45	M2 =	SPACING OF ROWS (E.G. 001 MEANS READ EVERY ROW FROM AND INCLUDING M1)	(I)
46-48	PUN =	001 IF NO PUNCH OF RE-COLORED SPECTRUM	(I)
73-80	ID =	IDENTIFICATION CODE	(A)

CARD 2

(NOTE, VALUES REFER TO ORIGINAL INPUT MATRIX)

1-10	DX =	DATA INTERVAL AL CN X (VERTICAL) AXIS	(F)
11-20	DY =	DATA INTERVAL ON Y (HORIZONTAL) AXIS	(F)

CARD 3

C 1-10 NX = NUMBER OF ROWS FOR SELECTED MATRIX (I)
 C 11-20 NY = NUMBER OF COLUMNS FOR SELECTED MATRIX (I)
 C 21-30 NBR = NUMBER OF ROWS IN FILTER MATRIX (=0 IF IB = 0) (I)
 C 31-40 NBS = NUMBER OF COLUMNS IN FILTER MATRIX (=0 IF IB=0) (I)
 C 41-50 MX = NUMBER OF LAGS ON ROWS (I)
 C 51-60 MY = NUMBER OF LAGS ON COLUMNS (I)

CARD 4

(NOTE, CARD MAY BE BLANK IF IPT(3) = 0 AND IB = 0 BUT MUST BE INCLUDED)

C 1-10 N1 = FIRST COLUMN OF SECTION OF RE-INDEXED SELECTED RAW
 C DATA MATRIX DESIRED ON OUTPUT PRINT (I)
 C 11-20 N2 = LAST COLUMN OF ABOVE (I)
 C 21-30 N3 = FIRST ROW OF ABOVE (I)
 C 31-40 N4 = LAST ROW OF ABOVE (I)
 C 41-50 N5 = FIRST COLUMN OF SECTION OF FILTERED MATRIX DESIRED
 C ON OUTPUT PRINT (I)
 C 51-60 N6 = LAST COLUMN OF ABOVE (I)
 C 61-70 N7 = FIRST ROW OF ABOVE (I)
 C 71-80 N8 = LAST ROW OF ABOVE (I)

CARDS 5, 6

THE 3*3 SPECTRAL SMOOTHING MATRIX ACCORDING TO AN (6F10.3) FORMAT. THE MATRIX IS EXPECTED IN SEQUENTIAL COLUMN FORM.

CARDS 7, 8,N

THE FILTER MATRIX. NOTE, IF IB = 0 THESE CARDS MUST BE LEFT OUT.

C 1-10 ROW 1, COLUMN (NBS + 1)/2 (F)
 C 11-20 ROW 2, COLUMN (NBS + 1)/2 (F)
 C
 C ROW NBR, COLUMN (NBS + 1)/2 (F)
 C ROW 1, COLUMN ((NBS + 1)/2) + 1 (F)
 C
 C ROW NBR, COLUMN NBS (F)

CARDS N+1,1

RAW DATA MATRIX. REQUIRED IF INPUT ON CARDS, I.E. INTAPE = 05 (FORMAT 102 REFERS, I.E. 6F10.3). READ ENTIRE ROW, I.E. NY1 COLUMNS ON SEQUENTIAL CARDS. START NEW CARD FOR EACH ROW.

CARD N+1

1-6 N = \$FINIS IF NO NEW DATA IS TO BE READ IN AND ANALYSED
 IF NEW ANALYSIS IS TO BE PERFORMED REPEAT CARDS
 1,.....N

 COMMON SH(120,120),PHI(50,25),B(11,11),G(3,3),GA(50,25),F(50,50),
 1FB(50,50), IPT(10), XNO, YNO, FUN
 DIMENSION M(12),120), REJ(1,400)
 EQUIVALENC (M(1,1),SH(1,1)), (REJ(1,1), PHI(1,1))
 DATA IFIN/ 6M\$FINIS/
 1030 READ(5,100) (, INTAPE, (IPT(IJ),IJ=1,10), I9, NY1, MA, MC, M1, M2,
 *PUN,IO

IF (N.EQ.IFIN) GO TO 510

READ(5,102) OX,OY

READ(5,103) NX,NY, NBR, NBS, MX, MY

READ(5,103) N1, N2, N3, N4, N5, N6, N7, N8

READ(5,102) ((I(1,J), I=1,3), J=1,3)

NRMO = (NBR-1)/2

NSIS = (NBS-1)/2

NSMX = NX - 2*IRMO

NSHY = NY - 2*ISIG

NNS = NSIG + 1

DX = OX*FLOAT(12)

```

DY = DY*FLOAT(IC)
NXC = FLOAT(P*IX + 1)*DX
NYC = FLOAT(P*JY + 1)*DY
WRITE (6,14) IJ, NX, NY, NPH, NPS, MX, MY, DX, DY
WRITE (6,106) I1, M1, I2, M2
IF (IPT(1).EQ.1) GO TO 10
WRITE (6,120)
CALL WRITEM (1,1,3,1,3)
10 IF (IR.EQ.1) GO TO 41
C .....READ IN FILTER MATRIX.....
READ (5,102) ((FC(I,J), I=1,NPR), J=NWS,NPS)
DO 3 I=1,NPR
  I1 = NPH + 1 - I
  DO 3 J=1,NSIG
    J1 = NPS + 1 - J
3  B(I,J) = B(I1,J1)
IF (IPT(2).EQ.1) GO TO 41
WRITE (6,121)
CALL WRITEM (2,-NSIG,NSIG,-NRHO,NRHO)
C .....READ IN RAW DATA MATRIX.....
41 L1 = 0
  I = 1
  NY2 = NY1*2
  NY3 = NY1 + 1
22 L1 = L1 + 2
  IF(I.GT.NX) GO TO 40
  IF(INTAPE.EQ.1) GO TO 50
  IF(INTPE.EQ.2) GO TO 52
C .....READ IN DATA FROM CARDS.....
  READ(5,102) (REJ(1,J), J=1,NY1)
  IF(I.EQ.NX) GO TO 51
  READ(5,102) (REJ(1,J), J=NY3,NY2)
  GO TO 51
C .....READ IN DATA FROM BCD TAPE.....
52 READ(2,101) (REJ(1,J), J=1,NY1)
  IF(I.EQ.NX) GO TO 51
  READ(2,101) (REJ(1,J), J=NY3,NY2)
  GO TO 51
C .....READ IN DATA FROM BINARY TAPE.....
70 READ(11,TAPE) ((EJ(1,J), J=1,NY2)
C .....T: NSFEQ REQUIRED DATA TO H MATRIX.....
51 IF(L1.LT.M1) G) TO 22
  IF(L1.EQ.M1) G) TO 24
  DO 25 J=1,NY
    JJ = M1 + (J-1)*HC
25  H(I,J) = REJ(1, JJ)
    M1 = M1 + I2
    I = I + 1
    IF(41.GT.L1) G) TO 22
24 DO 26 J=1,NY
    JJ = M1 + (J-1)*HC + NY1
26  H(I,J) = REJ(1, JJ)
    I = I + 1
    M1 = M1 + H2
    GO TO 22
4  IF (IPT(3).EQ.1) GO TO 43
  WRITE (6,122)
  CALL WRITEM (3,N1,N2,N3,N4)
43 IF (IR.EQ.1) GO TO 60
C .....REMOVE MEVA IF NO FILTER IS USED.....
  SUM = 0.

```

```

00 70 I=1,NX
00 71 J=1,NY
70 SUM = SUM + M(I,J)
  XH = S1/(FLOAT(NX)*FLOAT(NY))
  DO 51 I=1,NX
  DO 50 J=1,NY
91 M(I,J) = M(I,J) - XH
  GO TO 42
C
.....SMOOTH RA4 DATA MATRIX.....
60 DO 6 I=1,NSMX
  DO 6 J=1,NSHY
    SUM = 0.
    DO 5 I1=1,NBR
      I2 = I + I1 - 1
      DO 5 J1 = 1,NB3
        J2 = J + J1 - 1
        5 SUM = SUM + B(I1,J1)*M(I2,J2)
    6 SH(I,J) = SUM
    IF (IPT(4),EQ.1) GO TO 42
    WRITE (6,123)
  42 CALL PSGRID (MX,MY,NBR,NB3,NSMX,NSHY,DX,DY,NRHO,I9)
  GO TO 1000
900 STOP
100 FORMAT(26, 12I2, 6I3, 24X, A8)
111 FORMAT(2LF6.3)
122 FORMAT (8F10.3)
131 FORMAT (8I10)
114 FORMAT(1H1,3JX,4SELECTED MATRIX FOR SURFACE#,5X,A8//10X,#MATRIX HAS
  1S#,I4,# ROWS A10#,I4,# COLUMNS#/10X,#FILTER MATRIX HAS #,
  2 I4,# ROWS A12#,I4,# COLUMNS#/10X,#NUMBER OF LAGS IS#,I4,# ON ROW
  3S A10#,I4,# ON COLUMNS#/10X,#DATA INTERVAL I2,F6.3,# ON ROWS AND#
  4,F6.3,# ON COLUMNS# )
115 FORMAT (5F10.0)
116 FORMAT(//10X,4SELECTED MATRIX STARTS IN ROW#,I4,# COLUMN#,I4,# READ
  *ING EVF-##,I3,# ROW AND#,I3,# COLUMN# )
126 FORMAT (//10X, 32HTHE SPECTRAL SMOOTHING MATRIX IS )
121 FORMAT (//10X, 23HTHE SMOOTHING MATRIX IS )
127 FORMAT (//11X, 13HSECTION OF RAW ELEVATION MATRIX )
123 FORMAT (//10X, 28HSECTION OF SMOOTHED MATRIX )
  END
C
C
SUBROUTINE PSGRID (MX,MY,NBR,NB3,NSMX,NSHY,DX,DY,NRHO,I9)
COMMON /N(120,12),PHI(5,25),P(11,11),G(3,3),GA(50,25),F(50,50),
1FB(50,50), IPT(10), XNO, YNG, PUN
DIMENSION FS(5,50), M(50,25)
EQUIVALENCE (F(1,1),FB(1,1)), (GA(1,1),M(1,1))
PI2 = 2..*3.1415)
.....COMPUTE THE MEAN LARGED PRODUCTS.....
.....A LESS THAN ZERO.....
NGMX = MX + 1
NGMY = MY + 1
NGX = 10MX + 40
DO 127 I0 = 1, IX
K69 = IX + 1 - I0
K67 = 10MX - 40
DO 127 JB = 1, 10HY
K70 = JB + 1
K68 = 10HY - K70
SUM = 0.0

```

```

DO 126 I6 = 1,467
I7 = I6 + 16
DC 176 J7 = 1,463
J8 = J7 + 17
TEMP = SM(I7,J7)*SM(I6,J6)
127 SUM = SUM + TEMP
D = K67*K66
127 GA(I6,J6) = SM(I7)
.....A EQUAL TO AND GREATER THAN ZERO.....
DO 177 I6 = NGIX,NGX
K69 = I6 - MX - 1
K71 = NSHX - K59
DO 177 J6 = 1,IGHY
K73 = J6 - 1
K72 = NSHY - K70
SUM = SUM
DO 176 I7 = 1,K71
I6 = I7 + K69
DC 175 J7 = 1,K72
J6 = J7 + K73
TEMP = SM(I7,J7)*SM(I6,J6)
178 SUM = SUM + TEMP
D = K71*K72
177 GA(I6,J6) = SM(I7)
IF (IPI(5),E7,1) GO TO 60
WRITE(4,23.1)
CALL WRITE(4,J,MY,-MX,MX)
.....RIN SPECTRAL CALCULATIONS.....
60 NFX = 2*MX + 1
NFY = 2*MY + 1
FX = NFX
FY = NFY
LPMX = MX + 1
LPHY = MY + 1
DO 131 I10 = 1,NFX
ALPHA = I10 - LPMX
ALPHA = ALPHA/PI
DO 131 J10 = 1,NFY
BETA = J10 - LPHY
BETA = BETA/PI
SUM = SUM
DO 136 I9 = 1,IGX
A = I9 - LPMX
A = A*ALPHA
DO 132 J9 = 2,IGHY
BE = J9 - 1
ANG1 = PI2*(A + BE*BETA)
TEMP = GA(I9,J10)*COS(ANG1)
137 SUM = SUM + TEMP*2.0
ANG2 = PI2*A
136 SUM = SUM + GA(I9,1)*COS(ANG2)
131 F(I10,I10) = D*NY*SUM
IF (IPI(6),E7,1) GO TO 61
WRITE(4,24.1)
CALL WRITE(4,MY,MY,-MX,MX)
.....3 OTHER SPECTRA.....
A1 NFBX = NFX - 1
NFBY = NFY - 1
DO 140 I13 = 2,NFBX
DO 141 J13 = 2,NFBY
SUM = SUM

```



```

DO 141 I11 = 1,3
I12 = I11 + I11 - 2
DO 141 J11 = 1,3
J12 = J11 + J11 - 2
TEMP = G(I11, I11)*F(I12, J12)
141 SU4 = SUM + TEMP
141 FR(I11, J11) = SUM
DO 142 I13 = 2, NFBX
SUM = 0.0
SUMA = 0.0
DO 143 I14 = 1,3
I15 = I13 + I13 - 2
TEMP = G(I14,1)*F(I15,2) + G(I14,2)*F(I15,1) + G(I14,3)*F(I15,2)
TEMPA = G(I14,1)*F(I15,NFOY) + G(I14,2)*F(I15,NFY) +
IF(I14,3)*F(I15,NFOY)
SUM = SUM + TEMP
143 SUMA = SUMA + TEMPA
FR(I13, 1) = SU4
142 FC(I13, NFY) = SUMA
GO 144 J13= 2, NFBY
SUM = 0.0
SUMA = 0.0
DO 145 J14 = 1,3
J15 = J14 + J11 - 2
TEMP = G(1, J14)*F(2, J15) + G(2, J14)*F(1, J15) + G(3, J14)*F(2, J15)
TEMP2 = G(1, J14)*F(NFBX, J15) + G(2, J14)*F(NFY, J15) +
IG(3, J14)*F(NFBX, J15)
SUM = SUM + TEMP
145 SUMA = SUMA + TEMPA
FR(1, J13) = SU4
144 FR(NFY, J13) = SUMA
K27 = 2
K28 = 1
K29 = 2
K30 = 1
DO 146 L19 = 1,4
SUM = 0.0
K26 = <29
DO 147 L20 = 1,3
TEMP = G(L20,1)*F(K26, K27) + G(L20,2)*F(K26, K28) +
IG(L20, 3)*F(K26, K27)
IF(L20=2) 148, 149, 147
146 K26 = <31
GO TO 147
149 K26 = <29
147 SUM = SUM + TEMP
GO TO (150, 151, 152, 154), L19
150 FR(1, 1) = SUM
K29 = .FLX
K30 = NFX
GO TO 146
151 FR(NFX, 1) = SUM
K29 = 2
K30 = 1
K27 = NFOY
K28 = NFY
GO TO 146
152 FR(1, NFY) = SUM
K29 = NFBX
K30 = NFY
GO TO 146

```

```

154 PH(NFX,IFY) = SUM
144 CONTINUE
IF (IP.(71.EQ.)) GO TO 62
WRITE (6,21)
CALL WITE. (5,-IV,MY,-MX,MX)
97 IF (IB.EQ.7) GO TO 66
C .....COMPUTE CORRECTION COEFFICIENTS.....
C .....U LESS THAN ZERO.....
N2K = 4*MO + NHO
DO 157 I18 = 1,N2R
K36 = N2K + 1 - I18
K40 = NNR - K33
DO 157 J18 = 1,NRS
K39 = J18 - 1
K41 = NRS - K33
SUM = .0
DO 158 I17 = 1,K40
I19 = I17 + K33
DO 158 J19 = 1,K41
J17 = J19 + K33
TEMP = B(I17,J17)*B(I19,J19)
155 SUM = SUM + TEMP
157 W(I18,I16) = SUM
C .....U EQUAL TO OR GREATER THAN ZERO.....
NMX = 4*MX + M2R
DO 159 I18 = 1,N1R,NMX
K42 = I18 - NNR
K40 = NNR - K42
DO 159 J18 = 1,NRS
K39 = J18 - 1
K41 = NRS - K33
SUM = 1.0
DO 163 I17 = 1,K40
I19 = I17 + K42
DO 163 J17 = 1,K41
J19 = J17 + K33
TEMP = B(I17,J17)*B(I19,J19)
155 SUM = SUM + TEMP
159 W(I18,I16) = SUM
IF (LPH.(61.EQ.)) GO TO 63
WRITE (6,23)
CALL WITE. (4,C,NRS-1,-NR+1,NX-NR)
C .....COMPUTE FILTER SPECTRUM.....
63 LPHX = PX + 1
DO 145 J20 = 1,NFX
S = J2 - LPHX
Z = 1/FX
DO 145 J21 = 1,NHXY
T = J21 - 1
T = T/FY
SUM = .0
DO 167 I21 = 1,NXX
U = I21 - 1.0
U = U*
DO 166 J21 = 2,NRS
V = J21 - 1
ANG1 = PI2*(U - V*T)
TEMP = W(I21,J11)*COS(ANG1)
166 SUM = SUM + TEMP*2.0
ANG2 = PI2*U
167 SUM = SUM + W(I21,I1)*COS(ANG2)

```

```

IF(AABS(SUM),LY,0.00001) SUM = SIGN(D.000001,SUM)
164 PHI(I2,J2) = SUM
IF (IPI(4),E9,1) GO TO 64
WRITE (6,2.4)
CALL WRITE (7,0,MY,-4X,HX)
.....RECOLOR SPECTRUM.....
64 DO 164 J22 = 1,NFX
DO 164 J22 = 1,NFY
I23 = I22
J23 = NGHY + 1 - J22
IF (J22.GT.MY) J23 = J22 - MY
169 FS(I22,J22) = DB(I22,J22)/PHI(I23,J23)
K51 = NGHX + 1
K51 = NGHY + 1
FS(NGHX,NGHY) = (FS(IHX,K51) + FS(INGHX,K51) + FS(K50,K51) +
FS(K50,NGHY))/4.0
IF (IPI(13),F9.0) G3 TO 66
WRITE (6,205)
CALL WRITER (6,-MY,MY,-HX,HX)
66 IF(PUN.EQ.1) G3 TO 65
WRITE (7,206) ((FS(I,J), J=1,NFY), I=1,NGHX)
65 RETURN
205 FORMAT (//10X, 29MEAN LAGGED PRODUCTS (COVAR.) )
206 FORMAT (//20X, 14MEAN SPECTRUM (F) )
207 FORMAT (//10X, 15HSMOOTHED SPECTRUM (F-4R) )
208 FORMAT (//10X, 35HLAGGED PRODUCTS OF SMOOTHING COEFF. )
209 FORMAT (//10X, 34HFOURIER TRANSFORMS OF L.P.S.C. )
210 FORMAT (//10X, 27HCORRECTED SPECTRUM (F-STAR) )
211 FORMAT(6E10.3)
END

```

C

```

SUBROUTINE WRITER (I1,I2,I3,I4)
COMMON SH(120,12),PHI(50,25),B(11,11),G(3,3),GA(50,25),F(50,50),
I(5,5),IPI(15),XNO,YNO,PUN
DIMENSION LAB(15),XLAB(15)
IA = 1
N3 = 0
N = 1
N1 = I2 - I1 + 1
N2 = N1
M = I4 - I3 + 1
42 IF (N1.GT.10) GO TO 43
IA = 0
NN = N1 + N3
GO TO 41
41 NN = 10 + N3
43 DO 41 L=N,NN
IL = L - N + 1
44 LAB(IL) = L + I1 - 1
IF (I1.GT.4) GO TO 45
IF(I1.GT.4) GO TO 19
WRITE(6,104) (LAB(L), L=1,IL)
CO TO 43
45 WRITE(6,104) (LAB(L), L=1,IL)
GO TO 44
46 DO 44 L = 1,IL
47 XLAB(L) = FLOAT(LAB(L))/YNO
MPI(15,107) (XLAB(L), L=1,IL)
48 GO TO (12,33,34,35,36,77,39) IM
49 DO 49 I=1,4

```


APPENDIX G

DIGITAL COMPUTER PROGRAM TO ANALYZE HYDRAULIC DATA

Program Listing

PROGRAM HYD (TAPE1,INPUT,OUTPUT,PUNCH,TAPES=INPUT,TAPE6=OUTPUT,TAP
*E7=PU:IGH)

ANALYSIS OF HYDRAULIC TEST DATA

DATA REPRESENTING MASS RUNOFF, RUNOFF RATE AND BED HEIGHT ARE
RECORDED IN MACHINE UNITS (1 P.U. = 10 VOLTS) CODED IN BCD FORM ON
MAGNETIC TAPE. EACH SET OF 3 VALUES REPRESENT ON-THE-SECOND
RECORDINGS WITH ONE SET PER PRU. THIS PROGRAM CONVERTS THE READINGS
TO INCH HOUR UNITS AND INCORPORATES CHECKS ON THE CALIBRATION
COEFFICIENTS AND OPERATION OF THE EQUIPMENT.

OPTIONS

OPTIONS INCLUDE PUNCHED OUTPUT IN INCH HOUR UNITS AND INPUT OF RAW
DATA IN BINARY FORM FROM THE STORAGE FILE.

INPUT CAPS

(A = ALPHANUMERIC, I = INTEGER)

COLUMNS			
1-5	N	= NUMBER OF RECORDED SFTS, I.E. SECONDS OF RECORD- ING	(I)
6-10	N1	= TIME OF FIRST SWITCH-ON OF RAINFALL AND/OR OVERLAND FLOW	(I)
11-15	N2	= TIME OF FIRST SWITCH-OFF OF RAINFALL AND/OR OVERLAND FLOW	(I)
16-20	N3	= NEGATIVE, OVERLAND FLOW ONLY APPLIED = 0, RAIN ONLY APPLIED = POSITIVE, TIME OF SWITCH-OFF OF SECOND APPLICATION FOLLOWING FIRST APPLICATION OF RAIN AND OVERLAND FLOW	(I)
21-25	SLOPE	= BED SLOPE IN FT./FT.	(I)
26-33	TN	= TEST IDENTIFICATION	(A)
34-35	LFC	= NEGATIVE, OVERLAND FLOW ONLY IN SECOND APPLICATION = 0, NO SECOND APPLICATION = POSITIVE, RAIN ONLY IN SECOND APPLICATION	(I)
36-37	IT	= 0, BCD INPUT OF RAW DATA	(I)

```

C      38-33      PUN = 0, NO PUNCHED OUTPUT (I)
C      40-41      NL = 0, LAST TEST ANALYSTS (IF 4011-7F00 ANALYSE NEXT
C                                     TEST DATA FROM CONTROL CARD FOLLOWING) (I)
C
C-----
C      DIMENSION A(402), DW(402), B(402), REJ(20)
C      INTEGER I(10), PUN, SLOPE
90     PFAO(5,100) N, N1, N2, N3, SLOPE, TN, LFC, IT, PUN, NL
C      WRITE(6,101) T1
C      .....READ IN RAW DATA.....
C      IF(IT.EQ.0) GO TO 8
C      READ(1) (W(I), I=1,400)
C      READ(1) (DW(I), I=1,400)
C      READ(1) (B(I), I=1,400)
C      GO TO 7
C      8 DO 10 I=1,N
C      10 RFAO(1,102) W(I), DW(I), B(I)
C      .....CHECK INITIAL(SATION DATA.....
C      9 CALL CHAV(W,1,1,1,NP)
C      CALL CHAV(DW,1,N1,2,NP)
C      CALL CHAV(B,1,N1,3,NP)
C      .....CONVERT WICHINE UNIT READINGS TO INCH, HOUR UNITS.....
C      AREA = 95.135
C      MW = 62.6
C      M = N + 1
C      DO 11 I=1,M
C      W(I) = (W(I) - W(401))*509.4*12./(MW*AREA)
C      DW(I) = DW(I)*101.2
C      11 B(I) = (B(I) - B(401))*346.0*12./(MW*AREA)
C      WRITE(6,103) B(401)
C      .....WRITE OUT TEST DATA IN INCH-HOUR UNITS WITH TIME ZERO AS START
C      OF RAINFALL AND OVERLAND FLOW.....
C      M = (N - N1)/1 + 1
C      DO 12 I=1,M
C      K = I*10 + N1 - 1
C      J = K - 9
C      IF(K.GT.N) GO TO 15
C      L1 = J - N1
C      DO 13 L=1,10
C      T(L) = L1
C      13 L1 = L1 + 1
C      L1 = K - J + 1
C      WRITE(6,104) (T(L), L=1,L1)
C      WRITE(6,105) (W(L), L=J,K)
C      WRITE(6,106) (DW(L), L=J,K)
C      12 WRITE(6,107) (B(L), L=J,K)
C      .....PUNCH DATA IF REQUIRED.....
C      15 IF(PUN.EQ.0) GO TO 14
C      WRITE(7,108) (W(I), I=N1,N)
C      WRITE(7,108) (DW(I), I=N1,N)
C      WRITE(7,108) (B(I), I=N1,N)
C      .....STEADY STATE VALUES.....
C      14 N5 = N2 - 10
C      N9 = N2-N1
C      N6 = 0
C      CALL CHAV(W,T,N2,4,JP)
C      DAV = DW(4,1)
C      DSE = DW(4,2)
C      WRITE(6,10) SLOPE
C      CALL CHAV(W,N5,N2,5,NP)

```

```

IF(N3) 16,17,14
16 WRITE(6,110) N4, N9
GO TO 13
17 WRITE(6,111) N4, N9
19 WRITE(6,112) D1(401), DW(402), D(401), D(402)
GO TO 20
18 WRITE(6,113) N4, N9
GO TO 13
20 IF(N3) 22,22,21
21 N6 = N3 - 19
CALL CHAV(DW,N5,N3,6,KP)
AA = FLOAT(JP-2)
PB = FLOAT(KP-2)
SED = (AA*JSE*JSE+PB*DW(402)*DW(402))/(AA+PB)
CALL CHAV(R,N6,N3,7,RP)
N6 = N6 - N1
N9 = N3 - N1
N3 = -43
IF(LFC) 16,45,17
22 IF(LFC) 33,29,14
33 RAIN = DAV - D1(401)
WRITE(6,121) RAIN, SED
GO TO 29
34 FLOW = DAV - D1(401)
WRITE(6,114) FLOW, SED
C .....APPLICATION RATES FROM SLOPE OF MASS FLOW AT STEADY STATE.....
29 L1 = N5
L2 = N2
N6 = 0
N9 = N2-N1
26 DO 24 I=L1,L2
J = I - L1 + 1
24 REJ(J) = W(I)
CALL LREC(REJ,L1,L2,C,SEC)
IF(LFC.EQ.0.OR.N3.GT.0) GO TO 25
CC = C
SED = SEC
N3 = -43
L1 = N3-19
L2 = N3
GO TO 26
25 WRITE(6,115)
IF(N3) 27,24,31
31 WRITE(6,116) N4, N9, CC, SED
N6 = L1 - N1
N9 = N1 - N1
IF(LFC) 27,45,30
27 WRITE(6,117) N4, N9, C, SEC
IF(N3.LT.0) GO TO 33
35 C = CC - C
AA = FLOAT(N2-(5-1))
BB = FLOAT(N3-(6-1)*N1)
SEC = SQRT((AA*BB*SED+BB*BB*SEC)/AA+PB)
IF(LFC) 37,45,16
36 WRITE(6,114) C, SEC
GO TO 34
37 WRITE(6,120) C, SEC
38 N6 = 0
N9 = N2-N1
C = 3C
GO TO 30

```

```

2A WRITE(4,114) N4, N9, C, SEC
  IF(LFC) 45,30,15
  .....N4S NALAICE.....
C
38 N7 = N2 - 1
  DS = 0.
  DO 32 I=N1,N7
72 DS = DS + (DW(I)+DW(I+1))/7200.
  TA = C*FLOAT(N2-N1)/3600.
  WDET = TA - W(42)
  ODET = TA - DS
  WRITE(6,119)
  WRITE(5,121) N2, N9, TA, DS, ODET, W(N2), WDET
  N7 = N-11
  DO 40 I=N2,N7
40 DS = DS+(DW(I)+DW(I+1))/7200.
  N6 = N-10
  N7 = N6-N1
  WRITE(6,122) N7, W(N6), DS
  IF(N3.GT.0) GO TO 45
  OD = O(N6)-O(N1)
  EW = TA-W(N6)-10
  WRITE(6,123) N7, EW
45 IF(NL.NF.0) GO TO 50
100 FORMAT(5I5,A8,4I2)
101 FORMAT(1H1,40X, #HYDRAULIC ANALYSIS OF TEST #,A8//)
102 FORMAT(3F6.4)
103 FORMAT(5X, #AVERAGE RATE OF DRIP PRIOR TO TEST WAS #,F8.4, # IN./HR.
  *#//20X, #TEST DATA FOLLOWS#/)
104 FORMAT(//2X, #TIME (SEC.)#,10X,10(7X,I3))
105 FORMAT(2X, #MASS RUNOFF (INS.)#,3X,10F10.4)
106 FORMAT(2X, #RUNOFF RATE (IN./HR.)#,10F10.4)
107 FORMAT(2X, #DEFINITION (IN.)#,6X,10F10.4)
108 FORMAT(10F8.4)
109 FORMAT(//20X, #STEADY STATE RUNOFF VALUES ON A SLOPE OF#,I3, # FT./#
  *T. ARE AS BEL:#/)
110 FORMAT(5X, #OVERLAND FLOW ONLY DURING PERIOD#,I4, # TO#,I4, # SEC. #)
111 FORMAT(5X, #RAINFALL ONLY DURING PERIOD#,I4, # TO#,I4, # SEC. #)
112 FORMAT(5X, #FROM STEADY STATE RUNOFF RATE, RATE OF APPLICATION =#,
  *F8.4, # IN./HR. WITH RECORDED STD. ERROR OF#,F3.4, # IN./HR. #/
  *5X, #FROM STEADY STATE BED WEIGHT STEADY STATE DETENTION =#,F8.4,
  *# IN. WITH RECORDED STD. ERRGR OF#,F8.4, # IN. #/)
113 FORMAT(5X, #RAINFALL AND OVERLAND FLOW APPLIED DURING PERIOD#,I4,
  *# TO#,I4, # SEC. #)
114 FORMAT(5X, #RATE OF OVERLAND FLOW BY SUBTRACTION =#,F8.4,
  *# IN./HR. WITH STD. ERROR OF#,F8.4, # IN./HR. #)
115 FORMAT(//10X, #APPLICATION RATES FROM MASS FLOW RECORDING AT STEADY
  *STATE#/)
116 FORMAT(5X, #RATE OF APPLICATION DURING PERIOD#,I6, # TO#,I4, # SEC. #
  *FROM SLOPE OF MASS FLOW =#,F8.4, # IN./HR. WITH STD. ERROR OF#,F8.4,
  *# IN./HR. #)
117 FORMAT(5X, #RATE OF OVERLAND FLOW DURING PERIOD#,I4, # TO#,I4, # SEC.
  *# FROM SLOPE OF MASS FLOW =#,F8.4, # IN./HR. WITH STD. ERROR OF#,
  *F8.4, # IN./HR. #)
118 FORMAT(5X, #RATE OF RAINFALL DURING PERIOD#,I4, # TO#,I4, # SEC. FROM
  *# SLOPE OF MASS FLOW =#,F8.4, # IN./HR. WITH STD. ERROR OF#,F8.4,
  *# IN./HR. #)
119 FORMAT(//10X, #MASS BALANCE#)
120 FORMAT(5X, #RATE OF RAINFALL BY SUBTRACTION =#,F8.4, # IN./HR. WITH
  *# STD. ERROR OF#,F3.4, # IN./HR. #)
121 FORMAT(5X, #DURING PERIOD#,I4, # TO#,I4, # SEC. APPLICATION WAS#,
  *F8.4, # IN. (FROM SLOPE OF STEADY STATE MASS FLOW)#/5X,

```



```

*# INTEGRATED RUNOFF RATE =#,F4.4,# IN. AND DETENTION BY SUBTRACTION
*##,F8.4,# IN.*/5X,# RECORDED MASS RUNOFF =#,F4.4,# IN. AND DETENTIO
*# IN BY SUBTRACTION =#,F8.4,# IN.*/
122 FORMAT(5X,#RECORDED MASS RUNOFF FOR#,I4,# SEC. MASS#,F3.4,
*# IN. FROM MASS RECORDING AND#,F4.4,# IN. FROM INTEGRATED RUNOFF R
*ATE#)
123 FORMAT(5X,#EXCESS INFLOW OVER OUTFLOW AT TIME#,I4,# SEC. MASS#,
*F4.4,# IN.*/
END

```

C
C
C

```

SUBROUTINE CHA(I,N1,N2,IS,NN)
DIMENSION A(4,2), L(5), X(5), P(20)
DATA(P(1), I=1,20) /6%,1.86,1.91,1.96,2.00,2.04,2.07,2.10,
*2.13,2.16,2.18,2.20,2.22,2.24/
L = 1
DO 32 I=1,4
32 J(I) = 0
NN = N2 - N1 + 1
12 SUM = 0.
SS = 0.
DO 10 I=N1,N2
SUM = SUM + A(I)
10 SS = SS + A(I)*A(I)
A(4,2) = SUM/FFLOAT(NN)
A(4,2) = SORT((SS-SUM*A(4,2))/FLOAT(NN))
XUL = A(4,0) + A(4,2)*P(NN)
XLL = A(4,0) - A(4,2)*P(NN)
IF(L.NF.1) GO TO 14
DO 11 I=N1,N2
IF(A(I).GT.XLL.AND.A(I).LT.XUL) GO TO 11
J(L) = I
X(L) = A(I)
A(I) = 0.
NN = NN - 1
L = L + 1
IF(L.GE.5) GO TO 20
11 CONTINUE
IF(L.EQ.1) RETURN
GO TO 12
14 L = L - 1
DO 15 M=1,L
K = J(M)
15 A(K) = X(M)
RETURN
20 WRITE(6,101) I;
NN = NN + L - 1
GO TO 14
111 FORMAT(/2X,#EXCESSIVE INSTABILITY IN DATA SET #,I3/)
END

```

C
C
C

```

SUBROUTINE LRT(I,X1,K2,D,SEB)
DIMENSION X(20), T(20)
DO 10 I=X1,K2
J = I - X1 + 1
10 T(J) = FLOAT(I)/7680.
SX = J.
ST = 0.

```

```

SXT = 0.
ST2 = 0.
SX2 = 0.
J = K2 - K1 + 1
DO 11 I = 1, J
SX = SX + X(I)
ST = ST + T(I)
SXT = SXT + X(I)*T(I)
SX2 = SX2 + X(I)*X(I)
11 ST2 = ST2 + T(I)*T(I)
XJ = FLOAT(J)
SP = SXT-SX*ST/XJ
CST = ST2-ST*ST/XJ
B = SP/CST
RB = SP*B
CSX = SX2-SX*SY/XJ
SED = SQRT((CSX-RB)/(XJ-2.))
RETURN
END

```

SAMPLE DATA

400 10 130 275 3 BE03204 1 1

Sample Output

A sample output from the above program is presented on the following pages.

STEADY STATE RUNOFF VALUES ON A SLOPE OF 3 FT./FT. ARE AS BELOW

RAINFALL AND OVERLAND FLOW APPLIED DURING PERIOD 8 TO 120 SEC.
 FROM STEADY STATE RUNOFF RATE, RATE OF APPLICATION = 26.8596 IN./HR. WITH RECORDED STD. ERROR OF .1216 IN./HR.
 FROM STEADY STATE BED HEIGHT STEADY STATE DEFLECTION = .1191 IN. WITH RECORDED STD. ERROR OF .0916 IN.

RAINFALL ONLY DURING PERIOD 246 TO 265 SEC.
 FROM STEADY STATE RUNOFF RATE, RATE OF APPLICATION = 6.1661 IN./HR. WITH RECORDED STD. ERROR OF .0608 IN./HR.
 FROM STEADY STATE BED HEIGHT STEADY STATE DEFLECTION = .0693 IN. WITH RECORDED STD. ERROR OF .0879 IN.
 RATE OF OVERLAND FLOW BY SUBTRACTION = 17.6937 IN./HR. WITH STD. ERROR OF .0937 IN./HR.

APPLICATION RATES FROM MASS FLOW RECORDING AT STEADY STATE

RATE OF APPLICATION DURING PERIOD 8 TO 123 SEC. FROM SLOPE OF MASS FLOW = 26.1685 IN./HR. WITH STD. ERROR OF .0796 IN./HR.
 RATE OF RAINFALL DURING PERIOD 246 TO 265 SEC. FROM SLOPE OF MASS FLOW = 6.1533 IN./HR. WITH STD. ERROR OF .0862 IN./HR.
 RATE OF OVERLAND FLOW BY SUBTRACTION = 19.9952 IN./HR. WITH STD. ERROR OF .0894 IN./HR.

MASS BALANCE DURING PERIOD 8 TO 120 SEC. APPLICATION WAS .0956 IN. FROM SLOPE OF STEADY STATE MASS FLOW
 DURING PERIOD 8 TO 123 SEC. APPLICATION WAS .0775 IN. AND DEFLECTION BY SUBTRACTION = .1433 IN.
 INTER. STD. RUNOFF RATE = .068 IN. AND DEFLECTION BY SUBTRACTION = .1432 IN.
 RECORDED MASS RUNOFF FOR 308 SEC. WAS 1.6470 IN. FROM MASS RECORDING AND 1.0418 IN. FROM INTEGRATED RUNOFF RATE

VITA

VITA

Born: Jack Rider Burney, Durban, South Africa,
March 4, 1939.

Parents: Laurence Ernest Burney and Dorothy Ellen Burney.

Marital Status: Married to Cynthia Rose Burney. Two daughters.

Education: Northlands Boys High School, Durban, South Africa,
1956; Natal University, Pietermaritzburg, South
Africa, B.Sc.Eng.(Agric.), 1961; M.Sc.Eng., 1968.
Purdue University, West Lafayette, Indiana, U.S.A.,
Ph.D., May, 1973.

Professional Experience:

Lecturer, Department of Agricultural Engineering,
Natal University, South Africa, Feb., 1962-present.
On study leave Jan., 1970-Feb., 1973.

Graduate Research Assistant, Agricultural Engineer-
ing Department, Purdue University, Jan., 1970-Feb.,
1973.

Professional Societies:

South African Institute of Agricultural Engineers.
American Society of Agricultural Engineers.

Professional Qualification:

Registered Professional Engineer (South Africa).

Honorary: Alpha Epsilon.